

CHIRAL SYMMETRY AND THE
NUCLEON-NUCLEON INTERACTION.



THE UNIVERSITY
of MANCHESTER

A thesis submitted to the University of Manchester
for the degree of Doctor of Philosophy
in the Faculty of Science

By

Keith George Richardson

Department of Physics

September 1999

Contents

List of Figures	5
List of Tables	7
Abstract	8
Declaration and Copyright Notice	10
The Author	11
Acknowledgements	12
1 Introduction	13
2 QCD and Chiral Symmetry	16
2.1 Introduction	16
2.2 Chiral Symmetry	16
2.3 Chiral Perturbation Theory: scattering	20
2.4 Heavy Baryons	24
2.5 NN Scattering at tree level	27
3 Low Energy S-wave NN Scattering	30
3.1 Introduction	30
3.2 The Scattering Equation	32
3.3 Regularisation Schemes	33

3.4	The Renormalisation Group	36
3.5	Summary	44
4	Including Pions	45
4.1	Introduction	45
4.2	Regularisation	49
4.3	Static One Pion Exchange	52
4.4	Non-Static OPE and TPE	54
4.5	Distorted Wave Born Approximation	60
4.6	S-wave Scattering With Pions.	60
5	Results	65
5.1	Introduction.	65
5.2	The Nijmegen Phase Shift Analyses	68
5.3	General Discussion	69
5.4	Spin Singlet Partial Waves.	71
5.4.1	1D_2	71
5.4.2	1F_3	72
5.4.3	1G_4	74
5.5	Spin Triplet Uncoupled Partial Waves	75
5.5.1	3D_2	75
5.5.2	3F_3	75
5.5.3	3G_4	75
5.6	Spin Triplet Coupled Partial Waves	76
5.6.1	$^3P_2 - ^3F_2, (2)$	76
5.6.2	$^3D_3 - ^3G_3, (3)$	77
5.6.3	$^3F_4 - ^3H_4, (4)$	77
5.6.4	$^3G_5 - ^3I_5, (5)$	78
5.7	Summary	78
6	Conclusion	97

Contents	4
----------	---

A The Nijmegen OPE Potential.	100
-------------------------------	-----

References	100
------------	-----

List of Figures

2.1	The Pseudoscalar Meson Octet.	19
2.2	The Tree Level and One Loop contributions to the scattering amplitude.	23
2.3	The Feynman Diagrams for NN scattering at tree level.	28
3.1	The RG flow of the first two terms of the rescaled potential in powers of energy.	41
4.1	The Feynman Diagram for OPE.	53
4.2	The Two Pion Exchange Feynman Diagrams which contribute to NN scattering at order Λ^{-3}	55
5.1	The 1D_2 Phase Shift for four cut-off radii.	80
5.2	The 1D_2 Phase Shift near $A = 0$ for $R = 1.4$ fm.	81
5.3	The 1F_3 phase shifts for three cut-off radii.	82
5.4	The 1F_3 phase shifts near $A = 0$ for $R = 1.4$ fm.	83
5.5	The 1G_4 phase shift for four cut-off radii.	84
5.6	The 1G_4 phase shift near $A = 0$ for $R = 1.4$ fm.	85
5.7	An enlarged portion of the 1G_4 phase shifts near $A = 0$ for $R = 1.4$ fm.	86
5.8	The 1G_4 phase shift for adjusted values of A at $R = 1.4$ fm.	87
5.9	The 3F_3 phase shift at $A = 0$ for four cut-off radii.	88
5.10	The 3F_3 phase shifts near $A = 0$ for $R = 1.4$ fm.	89
5.11	An enlarged section of the 3F_3 phase shift near $A = 0$ for $R = 1.4$ fm.	90
5.12	The 3F_2 phase shift at $A = 0$ for four cut-off radii.	91

5.13 The 3F_2 phase shifts near $A = 0$ for $R = 1.4$ fm	92
5.14 The 3F_4 phase shift at $A = 0$ for four cut-off radii	93
5.15 The 3F_4 phase shifts near $A = 0$ for $R = 1.4$ fm	94
5.16 The 3G_5 phase shift at $A = 0$ for four cut-off radii	95
5.17 The 3G_5 phase shift near $A = 0$ for $R = 1.4$ fm	96

List of Tables

5.1	Contributions from the EFT potentials up to order $= 3$	68
5.2	Ratio of two-nucleon potentials in spin singlet partial waves for odd and even values of l	73

Abstract

UNIVERSITY OF MANCHESTER

ABSTRACT OF THESIS submitted by Keith George Richardson for the Degree of Doctor of Philosophy and entitled Chiral Symmetry and the Nucleon-Nucleon Interaction.

Month and Year of Submission: September 1999

Various aspects of the application of Effective Field Theory (EFT) to the Nucleon-Nucleon (NN) interaction are considered. We look for contributions beyond One Pion Exchange which are predicted by Chiral Symmetry.

Using the formalism of the Wilson Renormalisation Group (RG) we review power counting in a simplified EFT containing only nucleons. In the case of weak scattering at low energy, we find a natural expansion of the scattering matrix around the unique trivial fixed point of the RG.

We show that when scattering is strong at low energy, the calculation can be organised in a useful and systematic way by expanding the potential around a non-trivial fixed point corresponding to a bound state of two nucleons at threshold. The resulting expansion of the inverse of the scattering matrix reproduces the effective range expansion order by order.

The extension of this EFT to include pions in a manner consistent with chiral symmetry is discussed. By considering a modified effective range expansion, we find that the small momentum expansion in S-wave scattering converges slowly, if at all.

The NN potential is written down to third order in small momenta. This potential contains the leading order and next to leading order two-pion exchange contributions. Using the potential with a cut-off in coordinate space, we calculate phase shifts in peripheral partial waves for which the EFT predictions are parameter-free, and for which we may use the expansion around the trivial fixed point.

We find several partial waves in which the effects of two-pion exchange can be isolated, although no strong evidence is found for the convergence of the small momentum expansion at this order.

Declaration and Copyright Notice

No portion of the work referred to in this thesis has been submitted in support of an application for another degree or qualification of this or any other university or other institution of learning.

Copyright in text of this thesis rests with the Author. Copies (by any process) either in full, or of extracts, may be made only in accordance with instructions given by the Author and lodged in the John Rylands University Library of Manchester. Details may be obtained from the Librarian. This page must form part of any such copies made. Further copies (by any process) of copies made in accordance with such instructions may not be made without permission (in writing) of the Author.

The ownership of any intellectual property rights which may be described in this thesis is vested in the University of Manchester, and may not be made available for use by third parties without the written permission of the University, which will prescribe the terms and conditions of any such agreement.

Further information on the conditions under which disclosures and exploitation may take place is available from the Head of Department of Physics.

The Author

The author was born in Ayrshire in 1973. His secondary school education was undertaken in Belmont Academy, Ayr and Charleston Academy, Inverness. From 1992-1995 he attended Edinburgh University and graduated with a B.Sc. Hons. in Mathematical Physics. He is keenly interested in music, both as a listener and a participant, and at weekends may often be found exploring the Lakeland Fells with his wife Sandra.

Acknowledgements

Special thanks are due to my supervisor, Dr. Mike Birse, for patient and thoughtful teaching, constant support and guidance, and also for invaluable editorial comment during the preparation of this thesis.

The work presented in Chapter 3 is the result of a collaborative effort involving Mike Birse, Judith McGovern and myself.

Grateful thanks are due to S. Richardson, A. Munro and E. Munro for final proof reading of this thesis. I have also benefited greatly from many informal and enjoyable discussions with N. Evanson, S. Jones, R. Davidson, N. Petropoulos, G. Kerley and A. Sabio Vera. D. Thompson has provided much appreciated computer support.

This work was funded by PPARC to whom I am grateful.

My wife, Sandra Richardson, has provided limitless moral and almost limitless financial support over the last three years. Without her encouragement, and that of my parents, none of the work which went into the writing of this thesis would have been possible.

This thesis is dedicated to Mum, Dad and Sandra.

Chapter 1

Introduction

The history of theoretical attempts to calculate the Nucleon-Nucleon (NN) interaction from field theory is long and painful. Yukawa's early success, the prediction of the pion in 1935, led to the investigation of meson exchange potentials, and has culminated in the many phenomenological models available today, such as One Boson Exchange (OBE) potentials [1].

Of course, for a long time, the aim of meson theory was to emulate the description of electromagnetic interactions allowed by QED. Potentials such as those mentioned above fall a long way short of this sort of success. While they have in common the model independent tail contributed by One Pion Exchange (OPE), they contain many free parameters which must be fitted to experimental data. OBE potentials contain the nucleon-meson and form factors which are not known theoretically. Furthermore, such models tend to ignore irreducible contributions to the potential from the exchange of two or more mesons. Most importantly, they do not provide a systematic approach to NN interactions.

QCD has long supplanted meson theory as the theory of the strong interaction. Quantum Chromodynamics (QCD) is an SU(3) gauge theory describing the interactions of coloured spin-half quarks as mediated by spin-one gluons.

Gluons themselves carry colour charge, and the resulting interactions among gluons cause the quark-gluon coupling constant to become small for large energies, and zero in the high energy limit. This phenomenon is known as asymptotic freedom.

In this regime, the coupling constant provides a natural small expansion parameter, allowing use of perturbation theory in, for example, studies of deep inelastic scattering.

The situation at low energies is very different. Here the coupling constant is large, and causes quarks to become bound into the observed colour-neutral hadrons such as nucleons and pions. Despite our improved understanding of the strong interaction, the non-perturbative physics involved in the confinement of quarks makes the calculation of the low energy interactions of these hadrons directly from QCD extremely difficult.

Many QCD motivated models of the nucleon exist [2, 3], but where these have been used to calculate NN interactions, the long range contributions usually still come from pion and ρ exchange. In a model with both QCD and hadronic degrees of freedom, it is difficult to avoid double counting.

Fortunately, we can exploit QCD without trying to solve it directly. The QCD Lagrangian has certain symmetries in the limit of vanishing quark masses. Although these symmetries are explicitly broken or disguised by a variety of mechanisms, they have important implications for the spectrum of particles and their interactions.

Chiral Perturbation Theory (CHPT), which is introduced in Chapter 2, is an Effective Field Theory (EFT) which makes use of the fact that the up and down (and to a lesser extent strange) quark masses are small compared to typical hadronic scales. CHPT has been very successful in the pion and single-nucleon sectors. (For references and a recent introduction to EFT and CHPT techniques, see [4]).

Recently, much attention has been focussed on the extension of these ideas to the many-nucleon systems of interest in nuclear physics, and the two-nucleon interaction in particular. Chiral dynamics predicts in a natural way that the long distance, or low-energy, part of the two-nucleon interaction should be given by OPE but, more interestingly, it also predicts that there should be pieces with a two-pion range.

Various complications arise which are related to the large attraction in S-wave NN scattering which gives rise to the deuteron and the unnaturally large spin singlet scattering length. To take account of strong, low-energy scattering, it is necessary to modify the structure of the effective theory. These problems and some solutions which have been suggested will be discussed in Chapter 3.

The resulting expansion of the NN interaction involves the exchange of pions and contributions from an infinite number of contact interactions arranged according to the number of powers of momentum and pion masses which they contain. In Chapter 4, the NN potential is calculated up to third order in this expansion. This potential includes irreducible two-pion exchange which introduces three low-energy constants. We use values of these constants which have been obtained from NN scattering.

In Chapter 5, we examine the resulting phase shifts in peripheral partial waves ($l > 1$). These phase shifts are the best place to look for the effects of two-pion exchange because they receive no contributions from undetermined low energy constants to the order at which we shall be working. For high angular momenta, the centrifugal barrier also tends to obscure the effects of any regularisation procedure used to remove unphysical singularities.

The conclusions are presented in Chapter 6 where we discuss evidence for two-pion exchange.

Chapter 2

QCD and Chiral Symmetry

2.1 Introduction

Detailed reviews of chiral symmetry in nuclei are given by Birse [5] and by Bernard, Kaiser and Meißner [6]. The aim of this chapter is to give an overview of the ideas which will be most relevant in the context of NN scattering. We shall consider the implications of approximate chiral symmetry for the interactions of pions and up to one nucleon.

Extra complications arise when two (or more) nucleons are included. The discussion of these is deferred to Chapters 3 and 4.

2.2 Chiral Symmetry

Consider a simplified two flavour theory of massless non-interacting quarks given by the Lagrangian

$$L = i\bar{\psi} \not{\partial} \psi ; \tag{2.1}$$

where ψ is a two component isospinor containing the four component up and down quark spinors. It is easy to check that this Lagrangian is invariant under the SU(2) isospin and axial isospin rotations

$$U = e^{i\vec{\tau} \cdot \vec{\alpha}} = \left(1 + \frac{i}{2} \vec{\tau} \cdot \vec{\alpha} \right) ; \tag{2.2}$$

$$U(1) = e^{i\alpha \tau_3} = \left(1 + \frac{i\alpha}{2} \tau_3\right);$$

with isospin Pauli matrices τ_i and infinitesimal vectors α_i and β_i . Associated with this symmetry are the conserved vector and axial-vector Noether currents:

$$J = \frac{1}{2} \tau_3 \quad \text{and} \quad A = \frac{1}{2} \tau_1 \tau_2 \tau_3; \quad (2.3)$$

This invariance is referred to as chiral symmetry because the Lagrangian (2.1) can be decomposed into left and right-handed parts,

$$L = L_L + L_R; \quad (2.4)$$

containing fields which are helicity eigenstates,

$$L_L = \frac{1}{2}(1 + \tau_3) \quad \text{and} \quad L_R = \frac{1}{2}(1 - \tau_3); \quad (2.5)$$

whose isospin can be rotated independently using combinations of the transformations (2.2). The symmetry group can therefore be written as $SU(2)_L \times SU(2)_R$, and the associated conserved left-handed and right-handed currents are J_L and J_R . These are related to the currents (2.3) by,

$$V = J_L + J_R; \quad \text{and} \quad A = J_L - J_R; \quad (2.6)$$

The corresponding conserved charges Q and Q_5 are obtained by integrating the zero components of the currents over all space.

The Lagrangian (2.1), which has the same structure as the quark kinetic energy term in QCD, remains chirally symmetric if interactions with vector fields are included, but structures such as $\bar{\psi}\psi$ and therefore fermion mass terms and couplings to scalar fields explicitly break the symmetry.

The relevance of chiral symmetry to the real world follows from the fact that typical upper values for the current quark masses¹ are [7] 5 MeV for the up quark and 9 MeV for the down quark at a renormalisation scale of 2 GeV. These masses carry large errors since they must be extracted non-perturbatively, but they are certainly small compared to typical hadronic scales such as the pion mass (770 MeV). The chiral

¹The masses which appear in the QCD Lagrangian.

limit ($m_q \rightarrow 0$) is therefore a useful place to start when constructing effective field theories to describe low energy QCD.

In the real world, the small quark masses cause the axial and vector currents (2.6) to have a small but non-zero divergence. This is the starting point for PCAC (Partial Conservation of the Axial Current) current algebra calculations [8], an application of chiral symmetry which predates QCD. As we shall see in the case of N scattering, chiral effective field theories reproduce current algebra predictions of matrix elements at tree level but chiral perturbation theory allows systematic progress to one loop order and beyond.

The relevant part of the QCD Lagrangian can be written as follows:

$$L_{\text{QCD}} = \frac{1}{4} F_a^{\mu\nu} F_a^{\mu\nu} + \bar{\psi} (i \not{D} - M) \psi ; \quad (2.7)$$

where M is a matrix containing the quark masses, \not{D} is the gauge covariant derivative and the first term contains only gluonic degrees of freedom.

In the chiral limit, $M \rightarrow 0$, L_{QCD} is invariant under global $SU(N_f)_L \times SU(N_f)_R \times U(1)_V \times U(1)_A$ transformations, where N_f is the number of quark flavours. The charge associated with $U(1)_V$ invariance (quark number) is conserved, but $U(1)_A$ is broken by an anomaly.

If exact chiral symmetry was realised in the particle spectrum (the linear or Wigner-Weyl mode) then, experimentally, we should observe degenerate multiplets of hadrons with opposite parity and also some massless baryons [9]. No such pattern is observed.

Instead, a striking feature of the hadron spectrum is the hierarchy of meson masses. The pions, which have approximately equal masses and are abnormally light in hadronic terms, belong to a pseudoscalar meson octet whose members are the eight lightest physically observed hadrons. These are shown in Figure 2.1.

This pattern of masses is a strong indication that, in addition to the explicit symmetry breaking caused by the quark masses, the large classical symmetry group is somehow reduced dynamically.

From now on we shall focus on the case of two flavour chiral symmetry in which only the masses of the up and down quarks are treated as small quantities. The next

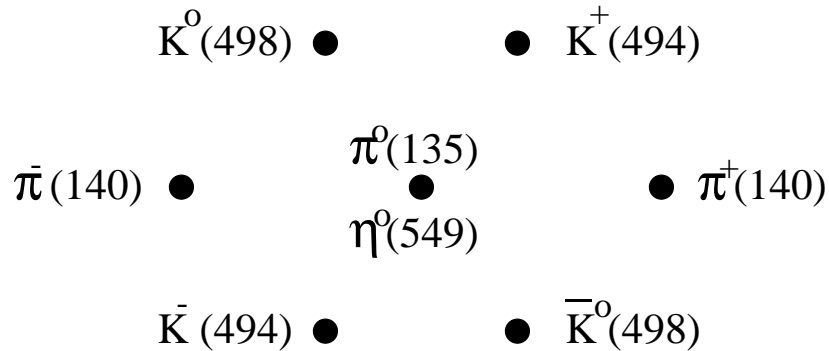


Figure 2.1: The 0 Pseudoscalar Meson Octet with masses in MeV.

lightest (strange) quark ($m_s \approx 90 - 170 \text{ MeV}$) is considerably more massive and this leads to much stronger explicit symmetry breaking which is reflected in the Kaon masses. We shall also ignore effects produced by the mass difference $m_u - m_d$ which means that we ignore the divergence of the vector current.

Examination of the particle spectrum suggests that only the $SU(2)_V \times SO(3)$ part of the $SU(2)_L \times SU(2)_R \times SO(4)$ symmetry of the massless Lagrangian is preserved by the vacuum. This is known as the non-linear or Nambu-Goldstone mode. Goldstone's Theorem [10] states that when a continuous symmetry of the Lagrangian is not respected by the vacuum, then the particle spectrum should contain one massless boson corresponding to each broken generator of the original symmetry group. In the case of massless two flavour QCD, there would be a triplet of massless pseudoscalar bosons belonging to the three-sphere $SO(4) = SO(3)$. Attributing their small masses to the explicit symmetry breaking associated with the current quark masses, and observing that they have the correct quantum numbers, we identify the pions with these Goldstone bosons.

The relationship between the small masses associated with the pseudo-Goldstone bosons and the non-zero current quark masses is made explicit by the Gell-Mann-Oakes-Renner relation [11]:

$$m_{\pi^0}^2 = \frac{1}{2}(m_u + m_d) \langle \bar{\psi}\psi \rangle + f^2 m^2; \quad (2.8)$$

where $\frac{1}{2}(m_u + m_d) \langle \bar{\psi}\psi \rangle$ is the value of the quark condensate in the QCD vacuum and $m = \frac{1}{2}(m_u + m_d)$ is the average light quark mass.

The current matrix element which occurs in pion decay is,

$$\langle 0 | \bar{A}_i(x) j_j(q) | i \rangle = i f q e^{iqx} \delta_{ij}; \quad (2.9)$$

which defines the pion decay constant $f = 92.5 \pm 0.2 \text{ MeV}$. This quantity can be measured in the charged pion decay process $\pi^+ \rightarrow \ell^+ + \nu_\ell$. Taking the divergence of (2.9) we find,

$$\langle 0 | \partial_\mu \bar{A}_i(x) j_j(q) | i \rangle = f m^2 e^{iqx} \delta_{ij}. \quad (2.10)$$

The field $\partial_\mu \bar{A} = f m^2$ clearly has the same behaviour as a canonically normalised pion field close to a single pion pole, $q^2 \rightarrow m^2$. In PCAC calculations, it is assumed that matrix elements of the field are smooth functions of q^2 between $q^2 = 0$ and $q^2 = m^2$.

In the effective theory which is introduced in the next section, the fact that pions interact weakly at low energies is crucial. In fact, if pions were true Goldstone Bosons, their interactions would vanish at zero energy. This is because, in the chiral limit, global chiral rotations are equivalent to the creation of zero energy pions. Since the vacuum would be invariant under such rotations, observable consequences of the interactions of pions with each other, and with other particles, would vanish at threshold.

Since pions are only approximate Goldstone bosons, such amplitudes have residues proportional to powers of the pion mass at zero energy.

2.3 Chiral Perturbation Theory: scattering.

Although the mechanism which causes chiral symmetry to be hidden is not yet understood, using the ideas outlined in the previous section, we can still deduce much about the interactions of the particles which constitute the asymptotic spectrum of QCD. To make this approach to hadronic interactions systematic, we first appeal to an unproved but plausible 'theorem' of Weinberg [12] which states that:

For a given set of asymptotic states, perturbation theory with the most general Lagrangian containing all terms allowed by the assumed symmetries

will yield the most general S-matrix elements consistent with analyticity, perturbative unitarity, cluster decomposition and the assumed symmetries.

In QCD, the asymptotic states are the hadrons, and at lowest energies we may simply consider the pions. The above theorem indicates that if we build a Lagrangian involving pion fields, and we carefully include in it all terms consistent with unitarity, charge conjugation symmetry, parity and approximate chiral symmetry, then we will have an effective theory describing their interactions equivalent to that given by the low energy limit of QCD. It will become clear however, that the effective Lagrangian contains many terms whose coefficients are not constrained by the imposed symmetry. These 'low energy constants' must be determined experimentally.

It was shown some time ago that, at tree level, this approach was equivalent to current algebra methods at lowest order, although an unambiguous continuation to one loop order and beyond had to wait for the work of Weinberg [12].

Going beyond tree level involves deciding which of the Feynman diagrams generated by the infinite number of terms in the Lagrangian should be kept. It might seem at first that four momentum integrals could mix up terms with any number of loops. However, Weinberg showed that there is a consistent way to order the loop contributions. His scheme consists of a power counting rule according to which one assigns an order to each diagram. This chiral power depends on the number of derivative interactions, vertices of various types, and loops contained in the diagram.

Since the addition of baryons to Weinberg's scheme complicates the discussion somewhat, it is instructive to see how the theory works in their absence. The lowest order chiral perturbation theory (CHPT) Lagrangian is presented below. To this order CHPT coincides exactly with the non-linear sigma model [13]. In the absence of external currents, the Lagrangian can be constructed using the following choice of chiral covariant derivative,

$$\partial_\mu U \quad \text{where} \quad U = e^{i\sqrt{2}\pi/f} \quad (2.11)$$

and takes the form

$$\mathcal{L}^{(2)} = \frac{f^2}{4} \text{Tr} (\partial_\mu U \partial^\mu U^\dagger) + \frac{f^2 m^2}{4} \text{Tr} (U + U^\dagger) \quad (2.12)$$

The first term is chirally invariant, whereas the second term, whose coefficient has been fixed to give the correct pion mass, provides explicit breaking of chiral symmetry. This choice of U is known as the exponential parameterisation. The Lagrangian is used by expanding in powers of the pion fields. Keeping only terms with up to four pion fields,

$$\mathcal{L}^{(2)} = \frac{1}{2} \partial_\mu \vec{\phi} \cdot \partial_\mu \vec{\phi} + \frac{1}{6f^2} (\vec{\phi} \cdot \partial_\mu \vec{\phi})^2 - \frac{m^2}{2} (\vec{\phi} \cdot \vec{\phi}) - \frac{m^2}{48f^2} \vec{\phi}^4; \quad (2.13)$$

It is important to note that chiral Lagrangians are not unique, but they will always give the same predictions for on-shell observables. Differing off-shell predictions are a consequence of using different interpolating pion fields.

From the Lagrangian, we infer the following Feynman rules. The relativistic propagator for a pion with four-momentum l is given by

$$\frac{i}{l^2 - m^2 + i\epsilon}; \quad (2.14)$$

and the four pion vertex with incoming pion four-momenta $q_{1,2}$ and outgoing four-momenta $q_{3,4}$ by

$$\frac{i}{f^2} (\eta_{12} \eta_{34} - \eta_{13} \eta_{24} + \eta_{14} \eta_{23}) - m^2 + \text{permutations}; \quad (2.15)$$

where isospin factors have been omitted for simplicity.

Dimensional analysis indicates that factors of m or q in the Lagrangian must always be paired with inverse powers of f . Furthermore, it is found in actual calculations that f typically appears multiplied by factors of 4, which are generated by loop integrals. The scale $4f$ is also roughly the scale at which the theory is expected to break down due to the exclusion of heavy particles.

This suggests an expansion of the amplitude in powers of $(q^2 - m^2)/(4f)^2$. Counting powers of small momenta $Q \ll m$, a propagator is clearly $O(Q^{-2})$ and the vertex $O(Q^2)$. Loops, involving an integral over one four-momentum variable, count as $O(Q^4)$. The total chiral power is then given by

$$= \sum_i V_i d_i - 2I + 4L; \quad (2.16)$$

In the above expression, V_i is the number of vertices of type i , d_i is the number of derivatives or pion masses at a type i vertex, I is the number of internal pion lines

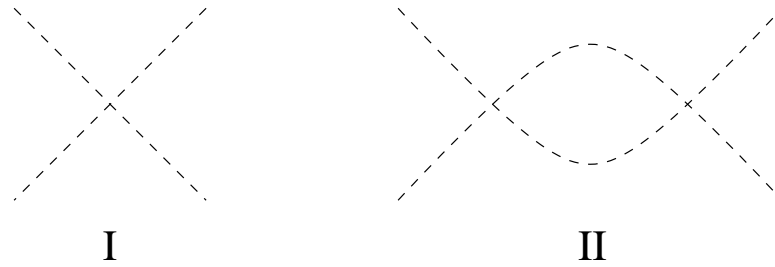


Figure 2.2: The (I) Tree Level and (II) One Loop contributions to the $\pi\pi \rightarrow \pi\pi$ scattering amplitude. The dashed lines represent pion fields.

and L is the number of loops. For example, the four pion vertex (2.15) has $d_i = 2$. Using Euler's topological identity relating the number of vertices, edges and faces on a planar graph, I can be eliminated to give:

$$I = \sum_i (d_i - 2)V_i + 2L + 2; \quad (2.17)$$

This result is known as Weinberg's power counting theorem.

Consider the $\pi\pi \rightarrow \pi\pi$ scattering diagrams in Figure 2.2. The four pion vertex from (2.12) contains two derivatives. In Figure 2.2 (I), there is one vertex with two derivatives. This gives a total chiral power of $D = 2$. Now consider Figure 2.2 (II). This diagram includes two vertices with two derivatives each and one loop. The corresponding chiral power is $D = 4$ which means that the one-loop contribution to $\pi\pi \rightarrow \pi\pi$ scattering is suppressed by two chiral powers relative to the tree level amplitude.

Calculation of this loop diagram leads to a divergence multiplying a $D = 4$ term. Infinities of this type are removed by renormalising the relevant counterterm. By construction, all appropriate counterterms with four derivatives are already included in the Lagrangian. In the present example, the necessary term is part of $\mathcal{L}^{(4)}$. Contact terms from $\mathcal{L}^{(4)}$ will contribute at tree level when working to $\mathcal{O}(Q^4)$.

Using these techniques to calculate $\pi\pi$ scattering lengths [9], one obtains values consistent with those extracted from experiment. The procedure of renormalising the theory order by order is characteristic of effective field theories, and is perfectly systematic despite the non-renormalisability (in the strict sense) of the non-linear sigma model Lagrangian (2.12).

The price to be paid is a large number of undetermined constants and new interactions every time we go to higher order in the calculation of a given quantity. Once these constants are determined however, they may be used in the calculation of more processes giving the theory predictive power.

Ultimately, it may even be possible to calculate these numbers directly using, for example, lattice QCD, but estimates of their sizes can be obtained using resonance saturation, the large N_c limit and extended NJL models.

2.4 Heavy Baryons

A problem arises when one tries to include relativistic heavy baryons, such as nucleons, in the theory. Since these are not massless in the chiral limit, they introduce a new energy scale, and upset the neat counting scheme mentioned above. The solution, borrowed from heavy quark effective field theory [14], is to consider perturbations around the limit in which the nucleon is considered as a static source. It is then possible to recover a consistent power counting scheme, although we now have a dual expansion in Q and $1/M$. This technique is known as heavy baryon chiral perturbation theory (HBCHPT).

In HBCHPT, the fully relativistic N Lagrangian is reduced by splitting the nucleon spinors into upper (light) and lower (heavy) components, and integrating out the latter [6]. The resulting nucleon propagator is independent of the nucleon mass M . The terms involving M which would arise in the expansion of the denominator of a relativistic propagator are now generated by terms in the reduced Lagrangian.

In the present context, we are only interested in contributions involving two nucleons and up to two pions. These will allow us to calculate N scattering lengths up to order Q^2 in section 2.5. Using a common notation, the corresponding lowest order ($\mathcal{O}(1)$) chirally invariant two-nucleon Lagrangian is written:

$$L_N^{(1)} = N \left[i \not{D} - \frac{g_A}{2} \not{\alpha} \cdot \nabla \right] N ; \quad (2.18)$$

defining the vector and axial vector quantities:

$$D = \partial + \frac{1}{2} u^\dagger \partial u \quad \text{and} \quad u = i f u^Y \partial u g \quad (2.19)$$

D is a chirally covariant derivative and u , which contains the pion fields, is defined in the following way:

$$u^2 = U = e^{i \vec{\tau} \cdot \vec{\pi} / f} \quad (2.20)$$

This Lagrangian is used by expanding the above matrices in powers of the pion fields. The part we require is obtained by keeping terms with up to two pion fields,

$$\mathcal{L}_N^{(1)} = N^\dagger i \partial_0 \frac{1}{4f^2} (\vec{\tau} \cdot \vec{\pi}) \frac{g_A}{2f} \vec{\tau} \cdot \vec{\pi} N + \dots \quad (2.21)$$

As usual, $\vec{\tau}$ and $\vec{\pi}$ are the Pauli spin and isospin matrices.

Chiral symmetry can be realised in the Lagrangian formalism in many ways, and there are several popular conventions. Weinberg [15] and O'Connell et al. [16] prefer to parameterise the pion three sphere using stereographic coordinates. This leads to a Lagrangian which looks quite different from the expression (2.18). As may be checked by expanding in powers of the pion field, it contains the same structures as (2.21) to the order considered here. Any differences which occur at higher orders will, of course, disappear in the calculation of physical observables.

An important feature of (2.21) is the appearance, in the final term, of pseudovector N coupling. In this representation of chiral symmetry, all pion nucleon interactions contain at least one derivative.

In time ordered perturbation theory calculations of N scattering using Lagrangians with pseudoscalar N coupling, there are large contributions from nucleon pair terms. Before the implications of chiral symmetry for the pion nucleon interaction were realised, these unnaturally large contributions had to be removed by hand.

In contrast, when all terms consistent with chiral symmetry are included in the Lagrangian, as demanded by the philosophy of EFT, the resulting amplitude is naturally small. For example, in the linear sigma model a neat cancellation occurs between the pair terms and the contribution where the two pions couple first to a field which then couples to the nucleon. The advantage of using the Lagrangian (2.21) is that all

amplitudes involving Goldstone bosons vanish term by term at threshold in the chiral limit.

The last term in this Lagrangian is independently chirally invariant, and its coefficient must therefore be fixed independently of the effective theory. It can be shown that $g_A = 1.26$ is the axial-vector beta decay constant, and the pion nucleon coupling then obeys the Goldberger-Treiman relation for on-shell nucleons:

$$g_N = \frac{M g_A}{f} ; \quad (2.22)$$

The propagator for a nucleon with a four-velocity v and small on-shell momentum l satisfying $v \cdot l = Q$ may be written in the following way:

$$\frac{i}{v \cdot l + i} ; \quad (2.23)$$

so that it is clearly $O(1=Q)$. We are now in a position to extend the power counting rule (2.17) to include nucleons. Again denoting the total chiral power by Δ ,

$$\Delta = \sum_i V_i d_i - 2I - I_N + 4L ; \quad (2.24)$$

where I_N is the number of internal nucleon lines. This expression may be recast in a more useful form using Euler's identity as before, and another topological identity

$$\sum_i V_i n_i = 2I_N + E_N ; \quad (2.25)$$

with n_i equal to the number of nucleon fields appearing in a type i vertex, and E_N the number of external nucleon lines. This leads to

$$\Delta = \sum_i V_i \left(d_i + \frac{n_i}{2} \right) - 2 + 2L - E_N + 2 ; \quad (2.26)$$

This form is particularly useful since the expression in brackets is always greater than or equal to zero.

We shall also require the two-nucleon part of the second-order Lagrangian which contains four terms whose coefficients are not determined by chiral symmetry:

$$\begin{aligned} L_N^{(2)} = N & \left[\frac{1}{2M} \bar{D} \not{D} D + i \frac{g_A}{4M} \bar{D} \not{v} D + c_2 \bar{D} \not{v} u u + 2c_1 m^2 (U + U^\dagger) \right] \\ & + c_2 \frac{g_A^2}{8M} (\bar{D} \not{v} u)^2 + c_3 \bar{D} u u + i \frac{1}{2} c_4 + \frac{1}{4M} \bar{D} \not{v} D ; \end{aligned} \quad (2.27)$$

using the definitions (2.19, 2.20). Notice the appearance of terms in this Lagrangian which are proportional to the inverse nucleon mass. The coefficients of these terms are fixed to ensure that Lorentz invariance is recovered order by order in the energy expansion.

If the quark mass splitting is taken into account, the Lagrangian contains an extra isospin violating term whose coefficient is c_5 . After expanding in powers of the pion field, (2.27) becomes:

$$\begin{aligned} L_N^{(2)} = & N \frac{r^2}{2M} N \frac{2c_1}{f^2} m^2 N N \sim^2 & (2.28) \\ & + c_2 \frac{g_A^2}{8M} \frac{1}{f^2} N N \partial_0 \sim \partial_0 \sim \frac{c_3}{f^2} N N^h (r \sim)^2 (\partial_0 \sim)^i \\ & + 4c_4 + \frac{1}{M} \frac{1}{8f^2} \epsilon_{ijk} \epsilon_{abc} N_k \epsilon N \partial_i \epsilon_j \epsilon_b + \dots \end{aligned}$$

As already mentioned, O'Connell et al. [16] employ a different representation of chiral symmetry. In this language, the low energy constants corresponding to the c_i are $B_{1,2,3}$. Since their primary interest is NN scattering, they only consider the three terms which give rise to non-zero contributions to that amplitude. Comparing their Lagrangian with (2.28), we can read off the relationships

$$B_1 = 4c_3; \quad B_2 = 4c_4 + \frac{1}{M} \quad \text{and} \quad B_3 = 8c_1: \quad (2.29)$$

2.5 NN Scattering at tree level.

To demonstrate the usefulness of the field theory defined by (2.21) and (2.28), we shall compare the calculation of the NN S-wave scattering lengths up to order $\epsilon = 2$ with their experimental values. The three possible diagrams containing vertices from $L_N^{(1)}$ and $L_N^{(2)}$ are shown in Figure 2.3.

The amplitudes corresponding to the two diagrams with an intermediate nucleon vanish at threshold because the NN vertex in (2.21) contains a spatial derivative acting on a pion field:

$$T_I^{ba} = T_{II}^{ba} = 0: \quad (2.30)$$

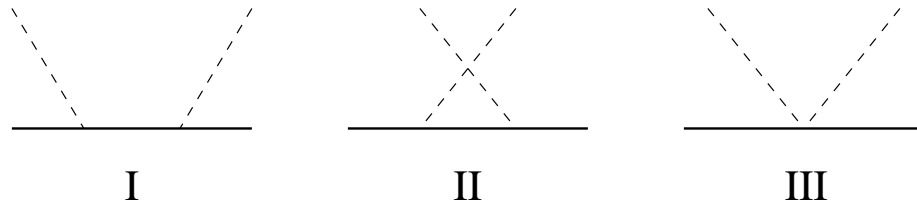


Figure 2.3: The Feynman diagrams for NN scattering at tree level. Dashed and solid lines represent pion and nucleon fields respectively.

a and b label the isospin of incoming and outgoing pions. The seagull diagram, Figure 2.3 III, with a vertex from $L_N^{(1)}$ produces:

$$T_{\text{III}}^{ba} = \frac{m}{2f^2} i_{bac} c; \quad (2.31)$$

Together, (2.30) and (2.31) constitute the entire $\mathcal{O}(1)$ calculation:

$$T_1^{ba} = \frac{m}{2f^2} i_{bac} c; \quad (2.32)$$

The $\mathcal{O}(2)$ contributions also come from the seagull diagram, but now with insertions from $L_N^{(2)}$. The sum of these is given by

$$T_2^{ba} = \frac{2m^2}{f^2} c_2 + c_3 - 2c_1 - \frac{g_A^2}{8M} i_{ba}; \quad (2.33)$$

Notice that there is no contribution from c_4 at threshold since the corresponding vertex contains two spatial derivatives. Decomposing the total amplitude into isospin even and odd parts,

$$T^{ab} = T_+^{ab} + T_-^{iabc}; \quad (2.34)$$

where

$$T_+ = \frac{2m^2}{f^2} c_2 + c_3 - 2c_1 - \frac{g_A^2}{8M} \quad \text{and} \quad T_- = \frac{m}{2f^2}; \quad (2.35)$$

T_+ contains one term with a fixed coefficient proportional to $1/M$ which would arise in the expansion of the intermediate nucleon propagators in Figure 2.3 I, II in a fully relativistic calculation.

The even and odd scattering lengths are defined by

$$a_{\pm} = \frac{1}{4} \left(1 + \frac{m}{M}\right)^{-1} T_{\pm}; \quad (2.36)$$

The S-wave scattering lengths which are normally quoted are labelled by total isospin and are related to a_{\pm} as follows:

$$a_{\frac{1}{2}} = a_{+} + 2a_{-} \quad a_{\frac{3}{2}} = a_{+} - a_{-} \quad (2.37)$$

To order m^2 these are given by

$$a_{\frac{1}{2}} = \frac{m}{4f^2} + \frac{m^2}{2f^2} (c_2 + c_3 - 2c_1) + \frac{4 + g_A^2}{8M} m^2; \quad (2.38)$$

$$a_{\frac{3}{2}} = \frac{m}{8f^2} + \frac{m^2}{2f^2} (c_2 + c_3 - 2c_1) + \frac{2 - g_A^2}{8M} m^2; \quad (2.39)$$

The order m results were originally obtained by Weinberg using current algebra [17]:

$$a_{\frac{1}{2}} = 2a_{\frac{3}{2}} = \frac{1}{4} \frac{m}{f^2} = 0.175m^{-1}; \quad (2.40)$$

and compare very favourably with the empirically determined values [18],

$$a_{\frac{1}{2}} = (0.173 \pm 0.003)m^{-1} \quad \text{and} \quad a_{\frac{3}{2}} = (0.101 \pm 0.004)m^{-1}; \quad (2.41)$$

Notice that (2.40) provides a natural explanation for the smallness of the experimentally measured isospin averaged amplitude $a_{\frac{1}{2}} + 2a_{\frac{3}{2}}$.

The determination of the c_i from N scattering observables is discussed by Buttiker and Meiner [19]. In Chapter 5 we shall use the central values from the work of Bernard et al. [20]. These are listed below in units of GeV^{-1} along with the quoted uncertainties:

$$\begin{aligned} c_1 &= 0.93 \pm 0.10 & c_2 &= 3.34 \pm 0.20 \\ c_3 &= 5.29 \pm 0.25 & c_4 &= 3.63 \pm 0.10; \end{aligned} \quad (2.42)$$

The $O(m^2)$ contributions to N scattering at threshold using these values do not lead to a marked improvement of the results (2.40). This can be explained by the relative importance of the one loop contribution which enters alongside vertices from $L_N^{(3)}$ at order m^3 .

The $O(m^3)$ calculation of a_{\pm} is given by Bernard et al. [6]. It is interesting to note that the $O(m^4)$ contribution to the dominant scattering length, $a_{\frac{1}{2}}$, is exactly zero [21].

Chapter 3

Low Energy S-wave NN Scattering

3.1 Introduction

The success of effective chiral Lagrangians in the pion and pion-nucleon sectors does not carry over easily to the two-nucleon case. There are several interrelated reasons for this which will be addressed in due course. The most obvious problem is that NN scattering is, empirically, not weak at low energies in $l=0$ partial waves. In the 1S_0 channel, the scattering length $a' \approx 24$ fm is unnaturally large indicating a nearly bound state, and there is a bound state in the coupled 3S_1 - 3D_1 channels. These features indicate that a naive perturbative expansion of the corresponding partial wave amplitudes will fail.

Weinberg [15] argued that the techniques of effective field theory should still be applicable, so long as power counting rules are applied to the irreducible potential rather than the amplitude. Solving the Lippmann-Schwinger or Schrödinger equation would sum up large contributions from intermediate, nearly on-shell nucleons.

According to the rules of effective field theory, the Lagrangian must now include appropriate four-nucleon contact interactions which have the form [15];

$$L_{NN} = \frac{1}{2}C_S (NN)(NN) + \frac{1}{2}C_T (N \sim N)(N \sim N) + \dots \quad (3.1)$$

Omitted terms contain derivatives acting on nucleon fields which lead to a momentum and energy dependent potential. In the approach to power counting explained in the

previous chapter, dimensional counting was used to assign a chiral order to each term in the Lagrangian. Such an ordering is clearly possible here, although it is not obvious that it is useful when an infinite number of diagrams must be summed.

There is a more immediate, but not unrelated, complication; the potential obtained from (3.1) is highly singular. Singular potentials are an unavoidable consequence of using local meson-nucleon and nucleon-nucleon couplings in the Lagrangian, and one must therefore specify a regularisation and renormalisation scheme in order to obtain finite physical quantities. Many such schemes have been proposed [22, 23, 24, 25, 26, 27, 28, 29, 30, 31, 32, 33], but the inconsistencies in the results obtained when the potential must describe strong scattering have led to the conclusion that Weinberg's power counting fails in such systems. (For more details and references see [34, 35] and Section 3.3).

A different approach to power counting has recently been suggested by Kaplan, Savage and Wise (KSW) [30] in the framework of the Power Divergence Subtraction scheme (PDS). It has also been obtained by van Kolck [32] in a scheme independent approach. Although this power counting seems to avoid the problems just mentioned, its basis and relation to more familiar schemes is not immediately obvious.

In this chapter, to understand the failure of Weinberg's power counting and the apparent success of modified power counting, we shall use the method of the Wilson (or 'exact') renormalisation group [36] applied to a potential which is allowed to have a cut-off dependence [37]. This is implemented by imposing a momentum cut-off on the integrals encountered when iterating the potential, and demanding that observables calculated in this way are cut-off independent.

For simplicity, we restrict our attention to the field theory containing only nucleons with interactions given by (3.1). This theory can be obtained by integrating pions out of the full HBCHPT which was described in the previous chapter. We therefore expect that it should be valid up to momenta of the order of the pion mass.

From (3.1) we obtain a potential with an infinite number of terms. The potential is rewritten in units of the cut-off. If Λ is allowed to vary, the potential must change to ensure that the theory still has the correct long-range behaviour. The variation

of the potential with Λ is given by a renormalisation group (RG) equation. As the cut-off is lowered to zero, all finite ranged physics is integrated out of the theory, and physical masses and energy scales no longer appear explicitly. In the limit, the (dimensionless) rescaled potential must therefore become independent of Λ , the only remaining scale. The many possible limiting values of the potential are fixed points of the renormalisation group equation.

We shall find two kinds of fixed point: the first is trivial, corresponding to an identically zero potential (no scattering), and the second corresponds to potentials producing a bound state exactly at threshold.

By looking at perturbations of the potential around the single fixed point of the first type, we find that it is stable and the scaling behaviour of the perturbations leads to Weinberg's power counting. This organisation of the potential is systematic in a natural situation where perturbation theory is applicable, but not in the case of interest (low energy S-wave NN scattering).

The simplest fixed point of the second type is unstable, and the power counting found here closely matches the power counting which was found by KSW using the framework of PDS. Perturbations around this fixed point systematically generate terms in the effective range expansion, which has been used to parameterise low energy S-wave NN data for many years.

3.2 The Scattering Equation

The irreducible potential obtained from (3.1) only receives contributions from tree level graphs, and has the following simple expansion in S-wave scattering:

$$V(k^0; k, p) = C_{00} + C_{20}(k^2 + k^0) + C_{02}p^2 \quad ; \quad (3.2)$$

where k and k^0 are relative momenta and $p = \sqrt{ME}$ is the corresponding on-shell value at centre of mass energy E . The coefficients in this potential are combinations of those in the Lagrangian (3.1): $C_{00} = C_S - 3C_T$ etc.

We shall work with the reactance matrix K since it has a simpler relationship to the effective range expansion than the scattering matrix T . The Lippmann-Schwinger

(LS) equation for the on-shell K matrix corresponding to the potential (3.2) is given by

$$K(k^0; k; p) = V(k^0; k; p) + \frac{M}{2} P \int_0^{\infty} dq \frac{V(k^0; q; p) K(q; k; p)}{p^2 - q^2}; \quad (3.3)$$

where P denotes a principal value integral. The reactance matrix consequently satisfies standing wave boundary conditions.

The inverse of the on-shell K matrix differs from that of the on-shell T matrix by a term $iM p^{-4}$, which ensures that T is unitary if K is Hermitian. Observables are obtained from K by expanding the inverse of its on-shell value in powers of energy:

$$\frac{1}{K(p; p; p)} = \frac{M}{4} \left[\frac{1}{a} + \frac{1}{2} r_e p^2 + \dots \right]; \quad (3.4)$$

This is just the familiar effective range expansion where a is the scattering length and r_e is the effective range. For weak scattering at threshold, $a < 0$ corresponds to attraction and $a > 0$ to repulsion. $a \rightarrow 0^-$ signals a zero energy bound state approached from above or below.

3.3 Regularisation Schemes

A natural approach to regularising this theory is to impose a momentum space cut-off at $\Lambda < \Lambda_0$ where Λ_0 is a scale corresponding to underlying physics which has been integrated out of the effective theory [24, 25]. This can be done either by introducing a form factor in the potential reflecting the non-zero range of the interaction, or a cut-off on the momenta of intermediate virtual nucleon states. In the case of a sharp momentum cut-off, the divergent integrals which arise in solving the scattering equation (3.3) are of the form

$$I_n = \frac{M}{2} P \int_0^{\Lambda} dq \frac{q^{2n+2}}{p^2 - q^2}; \quad (3.5)$$

where extra factors of q^2 in the numerator of the integrand occur in loop integrals with insertions of momentum dependent factors from the potential.

Expanding this integral in powers of energy, we see that it has $n + 1$ power law

divergences,

$$I_n = \frac{M}{2} \left[\frac{p^{2n+1}}{2n+1} - \frac{p^{2n-1}}{2n-1} \right] + \dots + p^{2n} + p^{2n} I(p); \quad (3.6)$$

where $I(p)$ is a function of p which is finite as $p \rightarrow 0$;

$$I(p) = \frac{p}{2} \ln \frac{p+a}{p-a}; \quad (3.7)$$

A sharp cut-off is used here to avoid unnecessary complications. If a different choice was made, the divergences in the I_n would appear with different numerical coefficients, and the structure of $I(p)$ would change. Neither of these modifications would affect the conclusions below.

If the potential (3.2) is truncated at a given order in the energy/momentum expansion it has an n -term separable form, and we can obtain an explicit expression for the K -matrix and thence the observables in the effective range expansion. The undetermined coefficients in the potential may then be fixed by demanding that they reproduce the observed effective range expansion up to the same order.

In this way, by including more and more terms in the potential, it is possible to determine whether the calculation is systematic. By systematic we mean that the inclusion of extra terms in the potential should not result in large changes to the coefficients which have already been fitted. Satisfying this condition ensures that the resulting Lagrangian is meaningful outside the process in which it is determined.

Two distinct cases have been identified. When the coefficients in the effective range expansion are natural the cut-off can be chosen in such a way that the calculation is systematic. As long as

$$ka \ll \frac{1}{a} - \frac{1}{r_e}; \quad (3.8)$$

the requirements given above are satisfied. In this weak scattering regime, perturbation theory is valid for $p < \dots$, and Weinberg's power counting rules apply.

The scattering length a is unnaturally large in S-wave NN scattering however:

$$a \approx 24 \text{ fm} \gg \frac{1}{\mu}; \quad (3.9)$$

where the scale of excluded physics $\Lambda_0 \sim m$. In this case choosing $\Lambda_0 \ll 1/a$ would lead to a (systematic) theory with an extremely limited range of validity. One might hope that choosing the cut-off between the energy scales set by the inverse scattering length and effective range could be useful:

$$\frac{1}{a} \ll \Lambda_0 \ll \frac{1}{r_e}; \quad (3.10)$$

but now corrections to the coefficients in the potential resulting from the addition of extra terms will contain powers of both $1/a$ and r_e . This choice does not lead to a systematic expansion in either Λ_0 or $1/a$.

An alternative approach is to use Dimensional Regularisation (DR) in which the loop integrals, I_n , are continued to D dimensions. In the commonly employed minimal subtraction scheme (\overline{MS}) [23], any logarithmic divergence (pole at $D = 4$) is subtracted and power law divergences do not appear. Since no logarithmic divergences appear in (3.6), the loop integrals I_n are set to zero and the K -matrix is simply given by the first Born approximation,

$$K(k^0; k; p) = V(k^0; k; p); \quad (3.11)$$

From the on-shell version of this identity we can obtain the effective range expansion which is found to converge only in the region $p < \sqrt{2}ar_e$. As in the case of a cut-off $\Lambda_0 \ll 1/a$, this scheme is always systematic, but useless when a is large.

In the PDS scheme, linear divergences (corresponding to poles at $D = 3$) are subtracted so that the I_n do not vanish. The resulting K -matrix now has a dependence on the subtraction scale μ , and choosing

$$\frac{1}{a} < \mu < p \ll \frac{1}{r_e}; \quad (3.12)$$

where p is the momentum scale of interest, a systematic power counting scheme emerges which appears to be useful. The coefficient of the leading order counterterm scales like $1/a$, and this term must therefore be treated non-perturbatively.

Note that the subtracted term μ , which is linear in μ , is the only divergence which occurs when the potential is momentum independent ($C_{2i;0} = 0$ in (3.2)). PDS must

therefore be interpreted as a momentum independent scheme. Gegelia [31] has obtained a similar result by performing a momentum subtraction at the unphysical point $p = i$.

The results obtained using these schemes agree with those of van Kolck (in a scheme independent approach) [32] and more recently Cohen and Hansen [33] (in coordinate space).

The relationship between cut-off regularisation in coordinate space and the many possible DR schemes has been clarified by Phillips, Beane and Birse [38]. They start from the general expression for the I_n continued to the entire complex dimension and energy planes. These functions have poles at odd values of D corresponding to infrared divergences for $D = 1 - 2n$ and ultraviolet divergences for $D = 3 - 2n$.

Subtracting the $n + 1$ UV divergences between $D = 3 - 2n$ and $D = 4$ recovers the power law divergences in (3.6) with Λ replaced by the DR scale μ . Subtracting the infinite number of remaining UV poles ($D > 4$) reproduces the function $I(p)$ which is defined in (3.7). Cut-off regularisation is, therefore, exactly equivalent to DR in the 'uvPDS' scheme where all UV divergences are subtracted.

In the original form of PDS [30], only the $D = 3$ divergence is subtracted. This is therefore the simplest of an infinite number of equivalent schemes.

In the next section, we shall see that PDS power counting can be understood in terms of an expansion around a fixed point of the renormalisation group (RG) equation which we derive for the potential. We shall also make clear that it is, at least to all orders considered so far, equivalent to an effective range expansion (as suggested by van Kolck [32]).

3.4 The Renormalisation Group

The starting point for the derivation of the RG equation is the LS equation (3.3) where all quantities are now allowed to depend on μ . V is the potential required to reproduce the observed K -matrix to all orders, and it will therefore be μ dependent after renormalisation in a cut-off scheme. The μ dependence of the free Green's

function G_0 regulates divergent loop integrals. As above, we use a sharp cut-off on loop momenta. This choice will simplify the discussion but, as before, our results apply equally well to any reasonable choice of momentum space cut-off.

To proceed, it is helpful to demand that the entire on-shell K -matrix is independent of Λ . Note that this is a stronger requirement than is necessary simply to ensure cut-off independence of the resulting observables. After differentiating the LS-equation with respect to Λ and setting $\partial K / \partial \Lambda = 0$, the RG-equation for $V(k^0; k; p;)$ can be obtained by operating on the resulting expression from the right with $(1 + G_0 K)^{-1}$ to produce

$$\frac{\partial V}{\partial \Lambda} = \frac{M}{2} V(k^0; k; p;) - \frac{2}{p^2} V(k^0; k; p;) \quad (3.13)$$

In the derivations which follow, we shall impose the boundary condition that V should have an expansion in powers of p^2 , k^2 and k^0 . This means that it can be obtained from the type of Lagrangian proposed by Weinberg [15] and written in the form (3.2).

To bring out the interesting features of this approach, it is useful to introduce the dimensionless momentum variables, $\hat{k} = k/\Lambda$ etc., and the scaled potential

$$\hat{V}(\hat{k}^0; \hat{k}; \hat{p};) = \frac{M}{2} V(k^0; k; p;) \quad (3.14)$$

where the overall factor of $M/2$ comes from the LS-equation (3.3). Finally, we rewrite the RG-equation in terms of these new variables:

$$\frac{\partial \hat{V}}{\partial \Lambda} = \hat{k}^0 \frac{\partial \hat{V}}{\partial \hat{k}^0} + \hat{k} \frac{\partial \hat{V}}{\partial \hat{k}} + \hat{p} \frac{\partial \hat{V}}{\partial \hat{p}} + \hat{V} + \hat{V}(\hat{k}^0; 1; \hat{p};) \frac{1}{1 - \hat{p}^2} \hat{V}(1; \hat{k}; \hat{p};) \quad (3.15)$$

In the following, the idea of a fixed point will be important. As Λ varies, the RG-equation (3.15) describes how the rescaled potential must flow to ensure that the long range behaviour of the theory does not change. As the cut-off is taken to zero, more and more physics is integrated out of the theory. In the limit, the cut-off is the only remaining energy scale and the rescaled potential, being dimensionless, must become independent of Λ . The many possible limiting values of the potential are fixed points of the renormalisation group equation. To find fixed points, we look for solutions of (3.15) which satisfy

$$\frac{\partial \hat{V}}{\partial \Lambda} = 0: \quad (3.16)$$

Near a fixed point, all physical energies and masses are large compared to the cut-off and power counting becomes possible.

The simplest example is the trivial fixed point $\hat{V}(\hat{k}^0; \hat{k}; \hat{p};) = 0$. It is easy to see that the K-matrix calculated from this potential is also zero, corresponding to no scattering. It is necessary to know how perturbations around the fixed point potential scale if we are to use it as the basis of a power counting scheme. This can be done by linearising the RG-equation by looking for eigenfunctions which scale as an integer power of μ ,

$$\hat{V}(\hat{k}^0; \hat{k}; \hat{p};) = C \mu^{\lambda} (\hat{k}^0; \hat{k}; \hat{p};) \quad (3.17)$$

Substituting this back into (3.15), the linear eigenvalue equation for λ is found to be

$$\hat{k}^0 \frac{\partial}{\partial \hat{k}^0} + \hat{k} \frac{\partial}{\partial \hat{k}} + \hat{p} \frac{\partial}{\partial \hat{p}} + \lambda = 0 \quad (3.18)$$

The solutions of this equation which satisfy the boundary conditions specified above are easily found to be

$$(\hat{k}^0; \hat{k}; \hat{p};) = \hat{k}^{0\lambda} \hat{k}^m \hat{p}^n \quad (3.19)$$

with RG eigenvalues $\lambda = 1 + m + n + 1$, where l, m and n are non-negative even integers. The momentum expansion of the rescaled potential around the trivial fixed point is therefore given by

$$\hat{V}(\hat{k}^0; \hat{k}; \hat{p};) = \sum_{l, m, n} \mathcal{C}_{lmn} \frac{\hat{k}^{0\lambda} \hat{k}^m \hat{p}^n}{\mu^{\lambda}} \quad (3.20)$$

(For a Hermitian potential one must take $\mathcal{C}_{lmn} = \mathcal{C}_{mln}$.) The coefficients \mathcal{C}_{lmn} have been made dimensionless by taking out a factor $1 = \mu_0^{\lambda}$ where, as before, μ_0 is a scale corresponding to underlying (integrated out) physics.

Since all of the allowed eigenvalues are positive, this potential vanishes as $\mu \rightarrow 0$! 0, and the trivial fixed point is stable. The power counting scheme associated with this fixed point can be made explicit by considering the unscaled potential:

$$V(k^0; k; p;) = \frac{2^{-2}}{M^0} \sum_{l, m, n} \mathcal{C}_{lmn} \frac{k^{0\lambda} k^m p^n}{\mu_0^{1+m+n}} \quad (3.21)$$

As long as the \mathcal{C}_{lmn} are natural, the contributions of energy and momentum dependent terms to the potential are suppressed by powers of $1 = \mu_0$. Assigning an order $d = 1$

to these perturbations leads to a scheme which is exactly equivalent to that originally suggested by Weinberg [15].

In Section 3.3, we saw that power counting in this way is useful in the case where scattering is weak at low energies, and either dimensional regularisation with minimal subtraction or a cut-off may be used. When the scattering length is unnaturally large however, we are forced to choose Λ to be so small that the theory becomes essentially useless. To find a useful expansion of a potential which describes low-energy S-wave scattering, it is necessary to look for a non-trivial fixed point which describes strong scattering at low energies.

The simplest fixed point of this kind can be found by looking for a momentum independent potential, $\hat{V} = \hat{V}_0(p)$, which satisfies the full RG-equation. This becomes

$$p \frac{\partial \hat{V}_0}{\partial p} + \hat{V}_0(p) + \frac{\hat{V}_0(p)^2}{1 - p^2} = 0: \quad (3.22)$$

Solving this equation subject to the boundary condition that the potential be analytic in p^2 as $p^2 \rightarrow 0$ we obtain

$$\hat{V}_0(p) = \frac{1}{2} \ln \frac{1+p}{1-p}: \quad (3.23)$$

The corresponding unscaled potential is

$$V_0(p; \Lambda) = \frac{2^{-2}}{M} \ln \frac{1+p}{1-p} = \frac{2^{-2}}{M} [I(p)]^{-1}; \quad (3.24)$$

where $I(p)$ is the same function that was defined in (3.7). The RG-equation (3.15) was derived using a sharp cut-off, and this form for the fixed point potential is a consequence of that choice. Choosing another type of cut-off would change the second (p dependent) term in the square brackets, but the $1=$ behaviour as $p \rightarrow 0$ is independent of the form of cut-off used.

Inserting the potential (3.24) in the LS-equation, we find $1=K = 0$. This fixed point therefore corresponds to a zero energy bound state (i.e. the scattering length is infinite). Not surprisingly, this fixed point has properties which are quite different from those we found in the trivial case. As before, we look at perturbations around the fixed point which scale as an integer power of Λ :

$$\hat{V}(\hat{k}^0; \hat{k}; p; \Lambda) = \hat{V}_0(p) + C(\hat{k}^0; \hat{k}; p); \quad (3.25)$$

where \hat{V}_0 is a function which is well behaved for small momenta and energy and satisfies the linearised RG equation:

$$\hat{k}^0 \frac{\partial}{\partial \hat{k}^0} + \hat{k} \frac{\partial}{\partial \hat{k}} + \hat{p} \frac{\partial}{\partial \hat{p}} + \frac{\hat{V}_0(\hat{p})}{1 - \hat{p}^2} (\hat{k}^0; 1; \hat{p}) + (1; \hat{k}; \hat{p})^i = 0 \quad (3.26)$$

The general case $\hat{V}_0 = \hat{V}_0(\hat{k}; \hat{k}; \hat{p})$ can be tackled by breaking it down into simpler types of perturbations. Perturbations which depend only on energy $\hat{V}_0 = \hat{V}_0(\hat{p})$ turn out to be particularly important, so we shall consider these first. Equation (3.26) can be integrated subject to the same boundary conditions as before, and the result is simply

$$\hat{V}_0(\hat{p}) = \hat{p}^{-1} \hat{V}_0(\hat{p})^2; \quad (3.27)$$

with eigenvalues $\lambda = 1; 3; 5; \dots$.

The first of these eigenvalues is negative, and is associated with an unstable perturbation since it gives rise to a term in the potential which scales like \hat{p}^{-1} as $\hat{p} \rightarrow 0$.

Figure 3.4 shows the renormalisation group flow of the first two coefficients in the expansion of the potential in powers of energy:

$$\hat{V}_0(\hat{p}) = b_0 + b_2 \hat{p}^2 + \dots \quad (3.28)$$

The trivial fixed point is at the origin, and the non-trivial one is at $b_0 = b_2 = 1$. Although the position of the fixed point is determined by our choice of regulator, the pattern of RG flow is general. The arrows show the direction of flow as $\hat{p} \rightarrow 0$.

Potentials which start on the critical surface $b_0 = 1$ flow towards the trivial fixed point in this limit. A potential that starts with a small perturbation away from this surface, however, initially flows towards the unstable fixed point for large \hat{p} , but approaches either the trivial fixed point or infinity as $\hat{p} \rightarrow 0$.

We must also consider perturbations which are momentum dependent. This time we look for a function of the form

$$\hat{V}_0(\hat{k}; \hat{k}; \hat{p}) = \hat{k}^n \hat{V}_1(\hat{p}) + \hat{V}_2(\hat{p}) \quad (3.29)$$

which satisfies (3.26). The solutions are given by

$$\hat{V}_0(\hat{k}; \hat{k}; \hat{p}) = \hat{k}^n \hat{p}^n + \frac{1}{n+1} + \frac{\hat{p}^2}{n-1} + \frac{\hat{p}^{n-2}}{4} \hat{V}_1(\hat{p}) \hat{V}_2(\hat{p}); \quad (3.30)$$

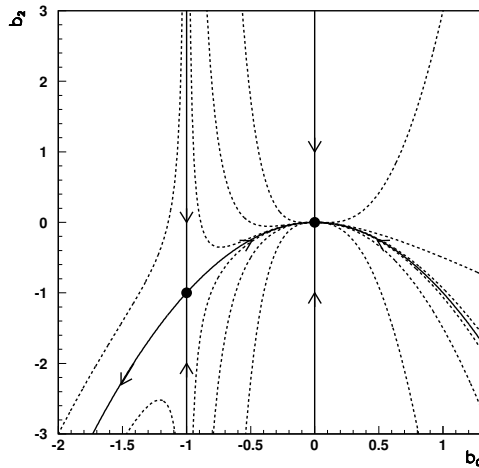


Figure 3.1: The RG flow of the first two terms of the rescaled potential in powers of energy. The fixed points are indicated by the black dots. The solid lines are flow lines that approach one of the fixed points along a direction corresponding to an RG eigenfunction; the dashed lines are more general flow lines. The arrows indicate the direction of the flow as $\mu \rightarrow 0$.

If a Hermitian potential is required, a matching perturbation of this form should be added with k replaced by k^0 . As usual, the eigenvalues are given by the condition that the potential be a well behaved function of energy and squared momenta. In this case they are $\lambda = n = 2; 4; 6; \dots$.

In general, new solutions to the linearised RG-equation (3.26) can be obtained by multiplying existing ones by p^m where m is a positive even integer. Applying this to the functions in equation (3.30) results in a new set of eigenfunctions with corresponding eigenvalues $\lambda = n + m$.

An important point to note is that the momentum dependent eigenfunctions have different eigenvalues from the corresponding purely energy dependent ones and so they scale differently with μ . This is quite unlike the more familiar case of perturbations around the trivial fixed point where, for example, the p^2 and k^2 terms in the potential are both of the same order, $\lambda = 3$. It means that, in the vicinity of the non-trivial fixed point, one cannot use the usual equations of motion to eliminate energy dependence from the potential in favour of momentum dependence.

One more kind of perturbation is possible: a product of two factors of the type given in equation (3.30), where one is a function of \hat{k} and the other is a function of \hat{k}^0 , is a solution of the linearised RG-equation with eigenvalues $\lambda = 5; 7; 9; \dots$. These solutions can also be multiplied by powers of p^2 to give eigenfunctions with higher eigenvalues.

Any perturbation which solves equation (3.26) subject to the given boundary conditions can be expressed as a sum of those given above, so we are in a position to expand a general potential around this fixed point. Near the fixed point we need only consider the perturbations with the lowest eigenvalues. Including the unstable perturbation, the first two give the following unscaled potential:

$$V(k^0; k; p;) = V_0(p;) + \frac{M_0}{2^2} \chi^1 \mathcal{C}_1 \frac{p}{0}^{+1} V_0(p;)^2 + \mathcal{C}_2 k^0 + k^2 \left(2p^2 + \frac{2M_0^3}{3 \cdot 2^2} V_0 \frac{V_0(p;)}{0} \right); \quad (3.31)$$

Although this potential looks complicated, it has a two-term separable structure, and we can obtain an exact expression for the K -matrix [25, 27]. Expanding the inverse of the on-shell K -matrix, we find the following effective range expansion

$$\frac{1}{K(p; p; p)} = \frac{M_0}{2^2} \chi^1 \mathcal{C}_1 \frac{p}{0}^{+1} + \dots \quad (3.32)$$

to first order in the \mathcal{C}_1 .

To this order, the potential is determined uniquely by comparing equation (3.32) with the effective range expansion (3.4):

$$\mathcal{C}_1 = \frac{1}{2 a_0}; \quad \mathcal{C}_1 = \frac{0 r_e}{4} \quad \dots \quad (3.33)$$

The identification of the terms in the potential and the effective range expansion is straightforward at this order because only energy dependent perturbations contribute to the scattering. It is not clear that this equivalence persists to higher order in the \mathcal{C}_1 . To illustrate the situation, we have calculated corrections to the unscaled potential (3.31) up to order $\mathcal{C}_1 \mathcal{C}_2$. We find the following extra contributions:

$$\frac{M_0}{2^2} \mathcal{C}_1 \mathcal{C}_2 k^0 + k^2 + A p^2 + \frac{4M_0^3}{3 \cdot 2^2} V_0 \frac{V_0(p;)}{0}; \quad (3.34)$$

where A is a constant of integration which is not fixed by the boundary conditions. This unfixed term arises from the solution of the homogeneous part of the linearised RG equations, and has exactly the same structure as the $\ell = 1$ term in (3.31).

Both of these perturbations contribute to the effective range. To avoid spoiling the one to one correspondence between observables and terms in the potential, we are free to choose $A = -2$ which ensures that the contribution of $\mathcal{C}_1 \mathcal{C}_2$ to the effective range vanishes.

So long as analogous procedures can be carried out to all orders, the effective theory defined by an expansion around this fixed point is systematic and completely equivalent to the effective range expansion. This corresponds to the fact that the parts of our potential which now contribute to observables act like a quasipotential: an energy-dependent boundary condition on the logarithmic derivative of the wave function at the origin. Such an equivalence has previously been suggested by van Kolck [32].

As has already been pointed out, the form of the fixed point potential (3.24) depends on the type of cut-off used, but for small p it always behaves like $1/a$. We can therefore compare the terms that appear in the expansion of our potential (3.31) with those of KSW [30]. The subtraction scale in PDS acts as a resolution scale, and plays a similar role to Λ in a cut-off scheme. To first order in $1/a$ and p^2 , their potential can be written in the form

$$V(p; \mu) = \frac{4}{M} \left[1 - \frac{1}{a} + \frac{r_e}{2} p^2 + \dots \right] \quad (3.35)$$

The leading order term in this expansion scales like $1/a$ which agrees with the $1/a$ dependence of the fixed point potential (3.24), and the factors of $1/a^2$ in the second and third terms match the $1/a^2$ factors in the energy dependent perturbations of (3.31). The power counting for perturbations around the non-trivial fixed point agrees with that of KSW if, as before, we assign them an order $d = 1$.

The fixed point is unstable and, since $1/a \neq 0$, as $\mu \rightarrow 0$ the potential will either flow to the non-trivial fixed point or diverge to infinity. As long as it is possible to choose the cut-off so that $1/a \ll \mu \ll \Lambda_0$ however, the behaviour of the potential is dominated by the flow towards the non-trivial fixed point, and the eigenfunctions

found above still define a systematic expansion of the potential, as noted in [30].

The approach of van Kolck [32] is equivalent to starting at the trivial fixed point, and following the flow line corresponding to the physical K -matrix back to the region $1/a \ll \mu$ where the power counting around the non-trivial fixed point is again useful. This procedure involves solving the RG equation to all orders in the scattering length, resumming terms involving powers of $1/a$.

3.5 Summary

In the case of weak scattering, the effective field theory originally suggested by Weinberg [15] to describe NN scattering is systematic, and gives predictions which are independent of the regularisation scheme used (coordinate space or momentum space cut-off, dimensional regularisation (\overline{MS}), etc.). This can be understood in terms of an expansion of the potential around the trivial fixed point of the RG equation. This is the expansion used in the next chapter to describe NN scattering in higher partial waves.

In the presence of a resonance or bound state close to threshold, conventional regularisation schemes do not lead to power counting schemes which are both systematic and useful. Recently, several equivalent power counting schemes based on new regularisation or subtraction schemes have been proposed which appear to avoid the problems mentioned above. We have demonstrated that these correspond to an expansion of the potential around the simplest non-trivial fixed point of the RG. Terms in this potential have a one to one correspondence with on-shell scattering observables in the effective range expansion to all orders considered so far. The success of the effective range expansion [39, 40] can therefore be understood in terms of an effective field theory based around this non-trivial fixed point [28, 29, 30].

Chapter 4

Including Pions

4.1 Introduction

The low energy effective field theory without pions, which was considered in the previous chapter, is not constrained by chiral symmetry – all information about the interaction is contained in the values of coefficients of contact interactions.

While it is important to understand how power counting works in the restricted EFT, the inclusion of pions should significantly add to its usefulness since it is well known, and understood from chiral dynamics, that they provide the longest range part of the interaction between nucleons. The first success of HB χ PT, which is constrained by chiral dynamics, is that the leading order, finite range contribution is the crucial One Pion Exchange (OPE) potential.

In this chapter, we consider the predictions of the effective field theory up to third order in small momenta. This involves calculating the one loop, two pion exchange (TPE) graphs. Adding higher order terms to the interaction potential allows us to test the convergence of the chiral expansion in the two-nucleon sector.

As in the nucleon-only theory, naive power counting rules must be modified for reducible loop diagrams; those loops which involve pure two-nucleon intermediate states are enhanced by a factor of $M = Q$. To a given order in the chiral expansion, this effect increases the number of diagrams which must be summed. To avoid calculating these extra diagrams explicitly, we follow Weinberg's prescription [15] and define an

effective potential to be used in a Schrodinger equation.

As well as testing for convergence of predictions for observables as more terms are added to the potential, we shall compare the results obtained when corrections to OPE are treated both perturbatively and non-perturbatively. If the expansion is under control, then iterating the TPE potential should generate only higher order contributions and should not result in a qualitatively different fit to experimental measurements.

The potentials which are presented in this chapter will be of most interest in those partial waves for which four-nucleon contact interactions do not contribute at the order to which we will be working ($\ell = 3$). In partial waves which exhibit weak scattering at low energies, Weinberg power counting is valid, and contact interactions contribute at orders $\ell = 0; 2; 4; \dots$. The $\ell = 2$ counterterms contribute to P-wave scattering, and so the D-waves are the first in which we do not have the freedom to tune short distance physics.

Since the low energy constants required for a complete calculation to order $\ell = 3$ have already been determined from NN scattering, the EFT makes parameter-free predictions in partial waves for which $\ell > 1$. Of course, our decision to stop calculating at order $\ell = 3$ is purely arbitrary. A $\ell = 4$ counterterm would allow a free parameter in D-waves, but counterterm contributions to F-wave scattering do not enter until $\ell = 6$. For this reason we expect that F-waves and above will provide the best opportunity to test the EFT expansion.

Furthermore, potentials derived from low energy effective theories are not expected to be reliable at short distances. In fact, as we shall see, parts of the chiral TPE potential are substantially more singular at the origin than the centrifugal barrier term in the Schrodinger equation. In a useful EFT, it is expected that the range of these singularities will be set by the a priori unknown high energy scale Λ_0 . Provided the separation between low and high energy scales is large enough, the insensitivity of observables to the core of the potential as ℓ becomes large, and at low energies, should obscure the effects of whatever procedure is used to regularise these singularities.

On the other hand, as l becomes large the longest range interaction, OPE, becomes dominant. To find evidence for chiral TPE, it is necessary to search for a window in energy and angular momentum in which NN observables are not sensitive to short distance behaviour of the potential, but are still not completely explained by OPE.

In $l > 1$ partial waves, scattering is weak at low energies and Weinberg's simple power counting in m and p ought to be valid. In the language of Chapter 3 we can expand around the trivial fixed point of the potential.

The new EFT is expected to break down at the high energy scale which is set by the mass of the lightest relevant degree of freedom not included. For the purpose of comparison, One Boson Exchange (OBE) potentials provide a good description of the on-shell NN interaction. The most important contributions to OBE potentials are OPE, the scalar (σ 550) exchange and vector (ρ 770) and ω (783) exchange. Other mesons such as the relatively light pseudoscalar (η 549) are sometimes included, but they couple weakly to nucleons and can be safely ignored in the present discussion. Although the ω does not correspond to an observed narrow resonance in $\pi\pi$ scattering, it is included to obtain the correct amount of intermediate range attraction.

It is a well established fact that ω exchange is a parameterisation of the exchange of two correlated pions in a relative S-wave state. In particular, the Paris [41] and Stony Brook [42] potentials successfully replace ω exchange by TPE derived by dispersion relations from $\pi\pi$ and N scattering. The relationship between this and the chiral partner of the pion is discussed by Birse [5].

One of the aims of this investigation is to decide whether the TPE to be derived from the effective field theory is able to reproduce this important contribution. If it is, then one might expect the breakdown scale to be set by the ω mass (770 MeV).

In practice, at least to the order in the chiral expansion considered here, the breakdown occurs at a much lower energy except in the partial waves which are well described by OPE alone.

The potentials which will be presented in this chapter constitute a complete calculation up to third order in small masses and momenta. This requires vertices taken

from $L_N^{(1)}$ and $L_N^{(2)}$. Contributions from the pion only Lagrangian L_N involve two loops and enter at order ϵ^4 , so correlated TPE diagrams with two loops are not included explicitly here. A complete calculation to order ϵ^4 introduces many other two loop graphs which have not yet been evaluated.

The most general coordinate space potential that we will obtain from the effective Lagrangian may be decomposed into four radial functions multiplying different combinations of spin factors:

$$U(r) = U_C(r) + U_S(r) \boldsymbol{\tau}_1 \cdot \boldsymbol{\tau}_2 + U_T(r) S_{12} + U_{LS}(r) \boldsymbol{L} \cdot \boldsymbol{S}; \quad (4.1)$$

with the further isospin decompositions $U_C = V_C(r) + W_C(r) \boldsymbol{\tau}_1 \cdot \boldsymbol{\tau}_2$ and so on. $\boldsymbol{\tau}$ and $\boldsymbol{\sigma}$ are the usual spin and isospin Pauli matrices and the subscripts C;S;T and LS label the central, spin, tensor and spin orbit contributions respectively. The tensor operator S_{12} is given by

$$S_{12} = 3 \frac{(\boldsymbol{\sigma}_1 \cdot \boldsymbol{r})(\boldsymbol{\sigma}_2 \cdot \boldsymbol{r})}{r^2} - \boldsymbol{\sigma}_1 \cdot \boldsymbol{\sigma}_2 \quad (4.2)$$

For given values of total spin S and orbital angular momentum l , the spin and isospin dot products evaluate to numbers: $\boldsymbol{\tau}_1 \cdot \boldsymbol{\tau}_2 = 2 \frac{h}{2} S(S+1) - \frac{3}{2} I$, and for isospin, $\boldsymbol{\tau}_1 \cdot \boldsymbol{\tau}_2 = 2 \frac{h}{2} I(I+1) - \frac{3}{2} I = (l+S+1) \pmod{2}$ for neutron-proton scattering.

In singlet spin states ($S=0$), the matrix elements of the tensor S_{12} and spin-orbit $\boldsymbol{L} \cdot \boldsymbol{S}$ operators vanish. In triplet states ($S=1$) S_{12} can mix together partial waves which differ by two units of orbital angular momentum l , but parity conservation implies that states with $l=j$ are decoupled. Partial waves will be labelled using the universal Russell-Saunders notation $^{2S+1}l_j$.

The potentials are to be used in non-relativistic Schrodinger equations which may be reduced by the usual methods to linear one dimensional differential equations in the radial variable r . In uncoupled channels ($l=j$) the radial wavefunctions $u_j(p;r)$ satisfy

$$\frac{d^2}{dr^2} + p^2 - \frac{j(j+1)}{r^2} - M U(r) u_j(p;r) = 0; \quad (4.3)$$

In coupled channels we must consider two wavefunctions, which we shall label $u_j(p;r)$ and $w_j(p;r)$, together. In the limit of vanishing tensor potential these correspond to the $l=j-1$ and $l=j+1$ wavefunctions and they satisfy the coupled

differential equations

$$\begin{aligned} \frac{d^2}{dr^2} + p^2 - \frac{j(j-1)}{r^2} M U_-(r) + \frac{2(j-1)}{2j+1} M U_T(r) u_j(p;r) & \\ = \frac{6}{2j+1} \frac{j(j+1)}{6} M U_T(r) w_j(p;r) & \end{aligned} \quad (4.4)$$

and

$$\begin{aligned} \frac{d^2}{dr^2} + p^2 - \frac{(j+1)(j+2)}{r^2} M U_+(r) + \frac{2(j+2)}{2j+1} M U_T(r) w_j(p;r) & \\ = \frac{6}{2j+1} \frac{j(j+1)}{6} M U_T(r) u_j(p;r); & \end{aligned} \quad (4.5)$$

with $U_{\pm}(r)$ given by the appropriate spin and isospin matrix elements of (4.1) excluding the tensor piece. In these expressions M is twice the reduced mass of the nucleons. In np scattering, $M = 938.9M \text{ eV}$ and this quantity will hereafter be referred to simply as the nucleon mass.

Since the potentials will be iterated to ensure that all $\ell = 3$ contributions are included, it is important that they are derived from irreducible Feynman diagrams. This issue arises in relation to iterated OPE and the TPE box diagrams.

4.2 Regularisation

In general, the potentials obtained from the effective theory are more singular than $1/r^2$ for small r . Consequently, it is not possible to integrate (4.3), (4.4) and (4.5) without some form of regularisation. This is a natural state of affairs in a field theory; singular potentials in coordinate space are analogous to bad ultraviolet behaviour and divergent loop integrals in momentum space.

The procedure for handling such momentum space divergences within a natural power counting regime was outlined in Chapter 2. The integrals are performed using a regularisation scheme which introduces a new scale (cut-off) or (DR):

$$p, m < \Lambda, \ll \mu_0: \quad (4.6)$$

It is evident that the physical system must have a clear separation of energy scales to allow a choice of Λ satisfying (4.6). In cut-off regularisation, the ratio $\Lambda = \mu_0$ may

be left finite or taken to zero. In the former case, cut-off dependent contributions to observables are suppressed by powers of Λ^{-1} . The assumption that the separation of scales is sufficient to justify using the EFT may be checked by testing the sensitivity of observables to Λ . If the cut-off is to be removed, the divergent part of the integral is subtracted by renormalising the coefficient of the relevant counterterm.

Another way of obtaining finite observables is to perform a perturbative expansion of the amplitude in momentum space counting chiral powers. This approach is used by Kaiser et al. [43] who perform a partial calculation of the amplitude to third order in small momenta. In this calculation, no infinities occur for finite momenta.

In the present work, the potential is calculated in momentum space and Fourier transformed into coordinate space before any loop integrals are performed. The resulting potentials are as singular as $1/r^6$ for small r . Many approaches to regularisation are possible in coordinate space. The connection to power counting is, in general, more difficult to expose than in momentum space.

For example, Oudenez et al. [16] use a Gaussian form factor in the momentum space potential which leads to unwieldy expressions in coordinate space, especially when TPE is included.

Here we shall choose to avoid the singular region by solving the Schrodinger equation for $r > R$ and imposing a boundary condition on the logarithmic derivative of the wave function at $r = R$. Coordinate space cut-offs have also been used by Cohen and Hansen [33] in an EFT context. Interestingly, they were used by Feshbach and Lomon [44] to investigate TPE potentials in the 1960's.

We have already stated however, that the effective field theory is parameter-free in $l > 1$ partial waves. Ideally, R should be chosen to be small enough that the desired long distance physics predicted by the effective theory is included, but large enough that any unphysical singularities do not dominate the centrifugal barrier term in the Schrodinger equation. This is analogous to the choice (4.6) of cut-off in momentum space with the intermediate scale replaced by $1/R$.

If this condition is met, then the value of the logarithmic derivative may be expanded in powers of energy, and it is possible to determine how its value should

scale with R in order for observables to remain unchanged. This type of analysis is closely related to the renormalisation group treatment of the previous chapter. In what follows we shall use an energy independent boundary condition.

Because, as will be explained, the lowest order pionic (static OPE) contribution is ubiquitous and uniquely defined, it will be included in all of our potentials. We wish to examine corrections to the corresponding phase shifts.

To begin, it is possible to define two solutions, f_+ and f_- , to the uncoupled Schrodinger equation (4.3) with $U(r)$ equal to the OPE potential such that their asymptotic values satisfy [45]

$$f_{\pm}(p;r) \sim e^{\pm ipr} \text{ as } r \rightarrow \infty; \quad (4.7)$$

suppressing angular momentum labels. In general, both of these functions will be irregular at the origin:

$$f_{\pm}(p;r) \sim (pr)^{\pm 1} \text{ as } pr \rightarrow 0; \quad (4.8)$$

The 'physical wavefunction' in the l 'th partial wave, $\psi_l(r)$, is obtained by choosing a linear combination of these functions which is regular at the origin:

$$\psi_l(p;r) \sim (pr)^{l+1} \text{ as } pr \rightarrow 0; \quad (4.9)$$

$$\psi_l(p;r) \sim \sin(pr + \delta_l) \text{ as } r \rightarrow \infty$$

defining δ_l as the phase shift due to the OPE potential alone. We also define a corresponding irregular function

$$f_{l+}(p;r) \sim (pr)^{l+1} \text{ as } pr \rightarrow 0; \quad (4.10)$$

$$f_{l+}(p;r) \sim \cos(pr + \delta_l) \text{ as } r \rightarrow \infty;$$

It is then straightforward to demonstrate that the physical wavefunction $\psi_l(r)$, corresponding to OPE modified by the addition of an extra short-range interaction, will satisfy

$$\psi_l(r) = \sin(\delta_l + \delta_l') f_{l+}(p;r) + \cos(\delta_l + \delta_l') \psi_l(p;r); \quad (4.11)$$

where $\delta_l + \delta_l'$ is the total phase shift.

Now consider the case of interest – imposing a boundary condition on the wavefunction's logarithmic derivative at $r = R$:

$$R \frac{d}{dr} \ln \psi_l(p; r) \Big|_{r=R} = 1 + 1 + \dots \quad (4.12)$$

Notice that, in the case $\ell = 0$, the small pR behaviour of the wavefunction is not modified by the boundary condition.

Using the limiting behaviour given in (4.9) and (4.10), we obtain the following expression for the tangent of the change in the phase shift due to the boundary condition as $pR \rightarrow 0$:

$$\tan(\delta_\ell) \sim (pR)^{2\ell+1} \frac{1}{2\ell+1} \quad (4.13)$$

The case $\ell = 0$ corresponds to the EFT prediction in partial waves with $l > 1$; for small enough pR , phase shifts are not affected by the boundary condition. Note that, if we fix δ_ℓ at a particular (sufficiently low) energy, on dimensional grounds, δ_ℓ must scale like:

$$\delta_\ell \sim (2\ell+1) \frac{1}{R} \quad (4.14)$$

where \mathcal{C}_ℓ is a dimensionless number. The leading order perturbation around the trivial RG fixed point which contributes to scattering in the l 'th partial wave scales in the same way, but with the inverse cut-off radius R replaced by $1 = \Lambda$.

4.3 Static One Pion Exchange

At next to leading order ($\ell = 0$), we must introduce OPE. Since it is well known that OPE accounts for the longest range part of the NN interaction, it is not surprising that it dominates the predictions for phase shifts in higher partial waves ($l > 4$).

The static OPE potential may be obtained in momentum space by calculating the diagram in Figure 4.1. It is of order $\ell = 0$ and requires two single derivative vertices taken from $L_N^{(1)}$:

$$\frac{g_A}{2f} \frac{1}{q^2 + m^2} \vec{q}_1 \cdot \vec{q}_2 \quad (4.15)$$

with centre of mass three momentum transfer $\vec{q} = \vec{k} - \vec{k}'$. Non-static corrections to this, proportional to $1 = M$, do not enter until order $\ell = 3$ in the momentum expansion.

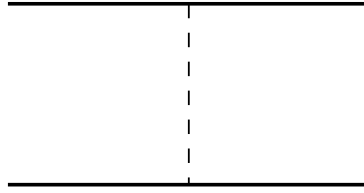


Figure 4.1: The Feynman Diagram for OPE. The solid lines represent nucleons and the dotted line represents a pion propagator.

Fourier transforming this potential leads to the familiar Yukawa potential in coordinate space plus a delta function piece which may be absorbed by a redefinition of the coupling constants C_S and C_T multiplying the four nucleon contact terms considered in Chapter 3. The remainder produces the following contributions:

$$W_S^{(0)}(r) = \frac{m^2 g_A^2}{48 f^2} \frac{e^{-x}}{r} \quad (4.16)$$

$$W_T^{(0)}(r) = \frac{m^2 g_A^2}{48 f^2} \frac{3 + 3x + x^2}{x^2} \frac{e^{-x}}{r}$$

where, from now on, x will represent $m r$ and the superscript indicates that this potential is of order $\epsilon = 0$.

The central part of the OPE potential behaves like $1/r$ for small r , and it is therefore possible, for $S = 0$, to obtain regular and irregular solutions of the corresponding Schrodinger equation in the usual way without regularisation. However, the singular behaviour leads to a term proportional to $r \ln m r$ in the expansion of the irregular $l = 0$ partial wave solution. This term becomes important when the Yukawa potential is used alongside zero range potentials as in Section 4.6.

The spin and isospin structure of the central OPE potential means that it is alternately attractive and repulsive for spin singlet even and odd partial waves respectively. Taken on its own, the OPE potential is too weak to produce the strong scattering observed in S-waves. The strength of the central potential is about a third of the size necessary to produce a bound state [18].

An impressive feature of OPE is the tensor contribution proportional to S_{12} . This causes mixing between triplet partial waves. Without mixing of this form the deuteron would not be bound, as the pure 3S_1 interaction is not strong enough to support a

bound state. In fact, OPE produces the bulk of the mixing required in most coupled channels as will be obvious from the phase shifts plotted in Chapter 5.

The $1=r^3$ behaviour of the tensor term in (4.16) for small r means that the potential must be regularised if it is to be iterated to obtain the corresponding spin triplet phase shifts. Although the central part of OPE is relatively well behaved for small r , from an EFT point of view it is no more reliable here than the highly singular TPE contributions.

When comparing the predictions of these potentials to partial wave analyses, it is necessary to remember that the latter are essentially phenomenological potential models. The good agreement we shall find between OPE and the higher Nijmegen partial waves at low energies is simply due to the fact that the potentials have the same content for large r . In fact, to facilitate comparison at higher energies, we choose to use their form for the OPE potential. This form of the potential includes effects due to the small pion mass splitting which is usually ignored in chiral effective field theory treatments since the scale of the mass differences is set by the π structure constant. This OPE is given in the Appendix, and is equivalent to (4.16) when the pion masses are made equal.

Isospin violation in NN scattering is discussed by Epelbaum and Meißner [46] in the context of PDS. Although we use the Nijmegen expression for OPE, we shall ignore all other contributions which are $O(\epsilon)$.

The deviation of phase shifts from static OPE, at energies where phenomenological potentials begin to differ, is therefore of most interest to us since we hope to look for the effect of model independent non-static OPE and TPE contributions constrained by chiral symmetry.

4.4 Non-Static OPE and TPE

The non-static corrections to OPE, and the leading order TPE contributions both enter at order $\epsilon = 2$. Non-static corrections to TPE start at order $\epsilon = 3$ along with the leading seagull counterterms from $L_N^{(2)}$.

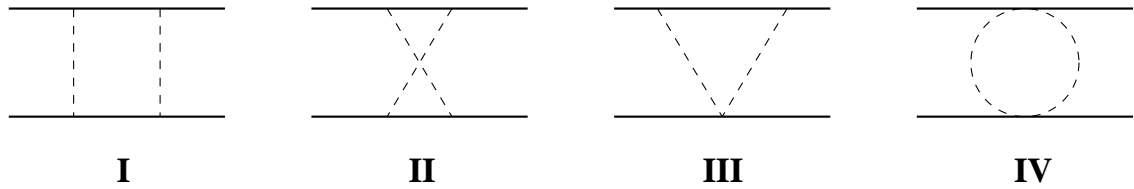


Figure 4.2: The Two Pion Exchange Feynman Diagrams which contribute to NN scattering at order $\epsilon = 3$.

The Feynman diagrams which contribute to two pion exchange up to order $\epsilon = 3$ are shown in Figure 4.2. Vertex corrections to OPE and contact interactions only lead to coupling constant and wave function renormalisation [47].

Non-static contributions proportional to $1/M$ arise in a calculation of the Feynman diagram in Figure 4.1 to order $\epsilon = 2$. This leads to an energy dependent potential. Ordóñez et al. [16] use the energy dependent form of OPE directly, but to keep the present calculation as simple as possible, we choose to transform away this energy dependence analytically using a redefinition of the wavefunction. For this reason, our TPE potential is not the same as that of Ordóñez et al. (in the point coupling limit).

Iterating the OPE potential once produces a reducible TPE interaction with the same structure as that obtained from Figure 4.2 I and II involving four vertices from $L_N^{(1)}$ and two nucleon propagators. Changing the definition of OPE alters which parts of the interaction derived from these diagrams must be subtracted to make it irreducible. This ambiguity, along with o -shell ambiguities, has historically been the source of a great deal of confusion regarding the correct form of the two pion exchange potential [48, 49].

To obtain the correct potentials, it is useful in practice to use time-ordered (or old-fashioned) perturbation theory to calculate the diagrams of Figures 4.1 and 4.2 [15, 16]. In this approach, it is straightforward to separate reducible TPE graphs (which contain pure two-nucleon intermediate states) from genuine TPE contributions to the potential.

The correct form of the static TPE potential to be used with an energy independent static OPE interaction has been obtained by Coon and Friar [50, 51]. They show

how to remove iterated static OPE from their TPE potential by adding and subtracting it from the non-pionic part of the two nucleon Hamiltonian. The former piece is implicitly included in the two nucleon Green's function, and the latter part is treated as a counterterm. Energy dependence in the resulting potential is then removed by a wave function redefinition.

A different method of removing energy dependence is considered by Epelbaum et. al. [47], but they use equations of motion which involve trading off energy dependence and momentum dependence. As we found in the previous chapter, energy and momentum dependent perturbations scale differently around the non-trivial RG fixed point. This method must therefore be applied to S-wave scattering with care.

There are two remaining TPE diagrams which contribute at order ϵ^2 . The double seagull or 'bubble' diagram (Figure 4.2 IV) has one loop and two vertices from $L_N^{(1)}$, and the 'triangle' diagram (Figure 4.2 III) has three vertices from $L_N^{(1)}$ and one nucleon propagator.

The contributions from Figure 4.2 III and IV are spin independent because both single pion vertices connect to the same nucleon leg. Since these diagrams are obviously irreducible, they may be calculated without further ado. A few intermediate steps are given to illustrate the techniques used. More details may be found in [51].

In momentum space, discarding $O(1/M)$ corrections for the moment, the contribution from the bubble diagram, Figure 4.2 IV, can be written as

$$\frac{1}{128f^4} \int \frac{d^3l}{(2\pi)^3} \frac{1}{l_+^2} \frac{(!_+ !_+)^2}{(!_+ + !_+)^2}; \quad (4.17)$$

with $!_+ = \frac{q}{(q_+^2 + 4m^2)}$.

This expression can be obtained either by calculating the Feynman diagram and integrating over l_0 , or by summing contributions from the corresponding two time ordered diagrams. Making several changes of variable and performing a Fourier transform it is possible to obtain the following symmetric form for the potential in coordinate space:

$$V_{IV}(r) = \frac{1}{8f^4} \int \frac{d^3q}{(2\pi)^3} \int \frac{d^3l}{(2\pi)^3} e^{i(q+l)r} \frac{(!_q !_l)^2}{!_q !_l (!_q + !_l)^2}; \quad (4.18)$$

using the notation $!_q = \frac{q}{q^2 + m^2}$. The integrand may be simplified by discarding

two divergent (zero range) contributions and made separable at the cost of introducing an integral over a new variable :

$$V_{IV}(r) = \frac{1}{4f^4} \int_0^\infty d^3q e^{iq \cdot r} \frac{1}{q^2 + m_\pi^2} \quad (4.19)$$

$$= \frac{m}{32f^4} \int_0^\infty \frac{dr^2}{dr^2} 4m^2 K_1(2mr) :$$

Using the properties of the modified Bessel functions K_n , we arrive at the final form of the potential:

$$V_{IV}(r) = \frac{m}{128 f^4 r^4} [xK_0(2x) + K_1(2x)] : \quad (4.20)$$

Note that this spin independent isovector contribution has no important counterpart in OBE potentials.

The single seagull or 'triangle' diagram leads to

$$\frac{g_A^2}{16f^4} \int_0^\infty \frac{d^3q}{(2)^3} \frac{q^2 r^2}{(q^2 + m_\pi^2)^2} ; \quad (4.21)$$

which becomes, in coordinate space,

$$V_{III}(r) = \frac{g_A^2}{f^4} \int_0^\infty \frac{d^3q}{(2)^3} \frac{d^3q}{(2)^3} e^{i(q+1)r} \frac{q \cdot 1}{(q^2 + m_\pi^2)^2} : \quad (4.22)$$

To remove the dot product we differentiate under the integrals and separate as before:

$$V_{III}(r) = \frac{2g_A^2}{f^4} \lim_{r_1, r_2 \rightarrow r} \int_0^\infty \int_0^\infty d^3q \frac{e^{iq \cdot r_1}}{(q^2 + m_\pi^2)^2} \int_0^\infty d^3q \frac{e^{iq \cdot r_2}}{(q^2 + m_\pi^2)^2} \quad (4.23)$$

which can be evaluated and simplified to give

$$V_{III}(r) = \frac{m g_A^2}{64 f^4 r^4} (2x^2 + 5)K_1(2x) + 5xK_0(2x) ; \quad (4.24)$$

after performing the derivatives and taking the limit.

The total of the contributions mentioned above constitutes the static part of the π - π TPE potential. This is presented below in coordinate space decomposed according to (4.1). Only the non-zero contributions are shown.

$$W_c^{(2)} = \frac{m}{128 f^4 r^4} [1 + 2g_A^2(5 + 2x^2) + g_A^4(23 + 12x^2)] K_1(2x) \quad (4.25)$$

$$+ \frac{1}{x} [1 + 10g_A^2 + g_A^4(23 + 4x^2)] K_0(2x)$$

$$V_S^{(2)} = \frac{g_A^4 m^h}{32^3 f^4 r^4} 3xK_0(2x) + (3 + 2x^2)K_1(2x)^i$$

$$V_T^{(2)} = \frac{g_A^4 m^h}{128^3 f^4 r^4} 12xK_0(2x) + (15 + 4x^2)K_1(2x)^i$$

For small r , all of the above potentials behave like r^{-5} . For comparison, the longest range part of each of these potentials is listed below :

$$W_C^{(2)} = \frac{m^{7=2} g_A^4}{64^{5=2} f^4} \frac{e^{-2x}}{r^{3=2}}; \quad V_S^{(2)} = \frac{m^{5=2} g_A^4}{32^{5=2} f^4} \frac{e^{-2x}}{r^{5=2}}; \quad (4.26)$$

$$V_T^{(2)} = \frac{m^{5=2} g_A^4}{32^{5=2} f^4} \frac{e^{-2x}}{r^{5=2}};$$

In each case the long-range contribution is from a box diagram .

The $= 3$ contributions to the TPE potential are now introduced. These potentials arise from diagrams of the form Figure 4.2 III with the seagull vertex taken from $L_N^{(2)}$ and may be calculated straightforwardly using methods similar to those described above. There is no contribution from the term in the Lagrangian proportional to the low energy constant c_2 . This was checked by calculating the diagram explicitly, but it is related to the fact that the momentum transfer vanishes in the centre of mass [43]. In contrast, the vanishing contribution in N scattering was proportional to c_4 .

$$V_C^{(3)} = \frac{3g_A^2}{32^2 f^4} \frac{e^{-2x} h}{r^6} 2c_1 x^2 (1+x)^2 + c_3 (6 + 12x + 10x^2 + 4x^3 + x^4)^i \quad (4.27)$$

$$W_S^{(3)} = \frac{g_A^2}{48^2 f^4} \frac{e^{-2x}}{r^6} c_4 (1+x)(3+3x+x^2)$$

$$W_T^{(3)} = W_S^{(3)}$$

These potentials are more singular than the $= 2$ potentials; they all behave like r^{-6} near $r = 0$. At large distances, the dominant terms are:

$$V_C^{(3)} = \frac{3g_A^2 m^4}{32^2 f^4} (2c_1 + c_3) \frac{e^{-2x}}{r^2} \quad \text{and} \quad W_S^{(3)} = \frac{g_A^2 m^3}{48^2 f^4} c_4 \frac{e^{-2x}}{r^3}; \quad (4.28)$$

Notice that these central, spin and tensor potentials have shorter ranges than their $= 2$ counterparts.

The $1=M$ corrections must be calculated with care. In a relativistic calculation these arise when retardation in intermediate propagators is taken into account. In the

calculation of N scattering we saw that, in HBCHPT, they come from terms in the $\mathcal{L} = 2$ Lagrangian with fixed coefficients. The correct form of these contributions for the energy independent potential used here is given by Friar [52]. For completeness, they are listed below.

$$\begin{aligned}
 V_C^{(M)} &= \frac{1}{32M} \frac{3g_A^4}{32^2 f^4} \frac{e^{2x} h}{r^6} (6 + 12x + 16x^2 + 16x^3 + 7x^4 + x^5) \quad (4.29) \\
 W_C^{(M)} &= \frac{1}{32M} \frac{g_A^2}{4^2 f^4} \frac{e^{2x} h}{r^6} (6 + 12x + 10x^2 + 4x^3 + x^4) \\
 &\quad + \frac{1}{32M} \frac{g_A^4}{16^2 f^4} \frac{e^{2x} h}{r^6} (36 + 72x + 62x^2 + 28x^3 + 8x^4 + 3x^5) \\
 V_S^{(M)} &= \frac{1}{32M} \frac{g_A^4}{16^2 f^4} \frac{e^{2x} h}{r^6} (6 + 12x + 11x^2 + 6x^3 + 2x^4) \\
 W_S^{(M)} &= \frac{1}{32M} \frac{g_A^2}{6^2 f^4} \frac{e^{2x}}{r^6} (1 + x)(3 + 3x + 2x^2) \\
 &\quad + \frac{1}{32M} \frac{g_A^4}{24^2 f^4} \frac{e^{2x} h}{r^6} (18 + 36x + 31x^2 + 14x^3 + 2x^4) \\
 V_T^{(M)} &= \frac{1}{32M} \frac{3g_A^4}{32^2 f^4} \frac{e^{2x} h}{r^6} (12 + 24x + 20x^2 + 9x^3 + 2x^4) \\
 W_T^{(M)} &= \frac{1}{32M} \frac{g_A^2}{6^2 f^4} \frac{e^{2x}}{r^6} (1 + x)(3 + 3x + x^2) \\
 &\quad + \frac{1}{32M} \frac{g_A^4}{48^2 f^4} \frac{e^{2x} h}{r^6} (36 + 72x + 52x^2 + 17x^3 + 2x^4) \\
 V_{SO}^{(M)} &= \frac{1}{32M} \frac{3g_A^4}{2^2 f^4} \frac{e^{2x}}{r^6} (1 + x)(2 + 2x + x^2) \\
 W_{SO}^{(M)} &= \frac{1}{32M} \frac{g_A^2 (g_A^2 - 1)}{2^2 f^4} \frac{e^{2x}}{r^6} (1 + x)^2
 \end{aligned}$$

Taken together, (4.16), (4.25), (4.27) and (4.29) constitute the entire potential to order $\mathcal{L} = 3$ in the chiral expansion and next to leading order in the expansion of the inverse nucleon mass.

This potential has been used in several other calculations. Friar [52] has demonstrated that it is one of a class of infinitely many equivalent potentials. The Nijmegen group [53] have recently used it as part of a new proton-proton partial wave analysis, and Kaiser et al. [43] originally wrote down this form after taking the Fourier transform of their perturbatively derived on-shell scattering amplitude, but not in the context of a particular iteration scheme.

4.5 Distorted Wave Born Approximation

The Distorted Wave Born Approximation (DWBA) will be used in two ways. In the next section we shall use it to examine the effect of perturbatively removing OPE from the phase shifts produced by a strong, short-range potential.

Secondly, it will allow us to consider treating TPE perturbatively and non-perturbatively while keeping OPE to all orders in Chapter 5.

The DWBA can be derived from the well known and exact two-potential formula,

$$\tan \delta_1^{(1)} - \tan \delta_1^{(2)} = \frac{1}{p} \int_0^Z u_1^{(1)}(r) U^{(1)}(r) U^{(2)*}(r) u_1^{(2)}(r) dr \quad (4.30)$$

by writing $U^{(1)}(r) = U^S(r)$ and $U^{(2)}(r) = U^S(r) + U^W(r)$. U^S is a strong potential to be treated to all orders, while U^W is an additional weak potential for which we expect first order perturbation theory to be accurate. The substitution results in an approximate expression relating the change in the scattering function to the (suitably normalised) wave function due to the potential U^S acting alone and the weak potential U^W :

$$\tan \delta_1' - \tan \delta_1^S = \frac{1}{p} \int_0^Z u_1^S(r) U^W(r) u_1^S(r) dr \quad (4.31)$$

Corrections to this expression are proportional to $(u_1 - u_1^S)U^W$. This approximation is so-called because (4.31) is essentially the Born approximation with the plane waves replaced by waves 'distorted' by the strong potential. Notice that it reduces to the Born approximation when U^S and the resulting phase shifts are zero.

4.6 S-wave Scattering With Pions.

The subtleties discussed in Chapter 3 were a consequence of the strength of the S-wave interaction at low energies. In this partial wave, convergence of the Q expansion is less obvious than in other partial waves where interactions are weak and chiral power counting indicates that pions can be included perturbatively. The question of whether or not pions can be treated perturbatively in this partial wave using a suitably modified power counting scheme has been debated recently [54, 55, 33].

One way to investigate whether including pions perturbatively is valid in the presence of strong scattering is to consider what happens to the effective range expansion (ERE) (3.4) when pions are removed. So long as the short distance potential has a simple structure, the effective range r_e can be interpreted, very roughly, as half the range of the potential [45]. We notice immediately that in np scattering, r_e is rather large ($r_e \approx 2.7$ fm) compared with typical nuclear scales. Dimensional analysis suggests that the size of the effective range due to short distance physics alone should be set by the inverse of the high energy scale $\Lambda = \Lambda_0$. Even if Λ_0 is as low as $m_\pi = 2$, then we would expect a modified effective range of the order of 0.6 fm.

It is natural to ask whether removing pions, which give rise to the long-range OPE potential, will reduce r_e to a more natural size. This gives us an opportunity to test the momentum expansion in a low partial wave. In this section we shall investigate removing OPE perturbatively and non-perturbatively and compare the results.

Consider a potential which reproduces the low energy 1S_0 np phase shifts. The subscript $l = 0$ is dropped for convenience. The potential consists of an unknown short-range piece which we take to be zero for $r > R$, plus the relevant part of the OPE potential:

$$U^1(r) = \frac{e^{-m_\pi r}}{r}; \quad \text{where} \quad g_A^2 = \frac{g_A^2 m_\pi^2}{16 f^2}; \quad (4.32)$$

is of order Q^2 . We are implicitly making the assumption that there is sufficient separation between long and short distance scales to allow a suitable choice of R . The wave function due to the short range potential acting alone is

$$u^S(r) = \frac{\sin(pr + \delta_s)}{p \cos \delta_s} \quad (4.33)$$

for $r > R$. $u^S(r)$ has been normalised so that it is suitable for use in (4.31) which now reads,

$$\tan \delta_s' - \tan \delta_s + \frac{M}{p \cos^2 \delta_s} \int_R^{\infty} \sin^2(pr + \delta_s) \frac{e^{-m_\pi r}}{r} dr; \quad (4.34)$$

The short distance potential cannot be made truly zero-range in S-wave scattering since the presence at the origin of the irregular solution, along with the $1/r$ singularity in the OPE potential, causes the integral in (4.34) to diverge logarithmically as $R \rightarrow 0$.

As has already been discussed in Chapter 3, low energy S-wave scattering is well described by the effective range expansion truncated at order p^2 . If the power counting derived earlier is valid, then it should be possible to obtain a 'modified effective range expansion' with the effects of one pion exchange removed perturbatively. Inverting both sides of (4.34), multiplying by p and expanding to first order in ϵ we find

$$p \cot \delta' - p \cot \delta_s = M \frac{(p \cot \delta_s)^2}{p^2 \cos^2 \delta_s} (p) + O(\epsilon^2); \quad (4.35)$$

where (p) represents the integral in (4.34). Integrating, expanding in powers of mR and discarding $O(mR)$, (p) may be written,

$$\begin{aligned} (p) = & \frac{1}{2} (\gamma + \ln(mR)) \\ & + \frac{1}{2} \cos 2\delta_s + \ln(mR) + \frac{1}{2} \ln \left(1 + \frac{4p^2}{m^2}\right) \\ & + \frac{1}{2} \sin 2\delta_s \tan^{-1} \frac{2p}{m} + O(mR); \end{aligned} \quad (4.36)$$

is Euler's constant. Notice that it is necessary to keep terms up to order p^4 in (p) to obtain the modified effective range expansion to order p^2 :

$$\begin{aligned} \frac{1}{a} + \frac{r_e}{2} p^2 = & \frac{1}{a_s} + \frac{r_s}{2} p^2 + M \left(\gamma + \ln mR \right) \frac{1}{a_s^2 m^2} + \frac{2}{a_s m} \\ & + M \left(\frac{1}{m^2} + \frac{2}{a_s^2 m^4} - \frac{8}{3a_s m^3} + \frac{r_s}{a_s m^2} - \frac{r_s}{m} \right) p^2; \end{aligned} \quad (4.37)$$

The above expression gives the physical quantities $a; r_e$ in terms of the modified quantities $a_s; r_s$. Taking coefficients of p^0 and p^2 , and solving for the modified coefficients,

$$\frac{1}{a_s} = \frac{1}{a} + M \left(\gamma + \ln mR \right) + \frac{2M}{m a} - \frac{M}{m^2 a^2} \quad (4.38)$$

$$r_s = r_e + 2M \left(\frac{1}{m^2} + \frac{8}{3am^3} - \frac{2}{a^2 m^4} + \frac{1}{m} r_e - \frac{1}{am^2} r_e \right); \quad (4.39)$$

ignoring corrections $O(\epsilon^2)$. Notice that a_s is not uniquely defined due to the logarithm in (4.38). Cohen and Hansen [33] find equivalent expressions which are also obtained in coordinate space, but using a rather different approach.

As well as expanding in powers of ϵ , to make the approach systematic we must count powers of small momenta in other quantities. The power counting scheme

obtained around the non-trivial fixed point in the previous chapter implies that we should treat $1/a$ as order Q .

We assume that other coefficients in the modified effective range expansion scale according to their dimension. The modified effective range should therefore scale like $Q^0 = a_0$.

Using these assignments, we find that the last two terms in the square brackets are suppressed relative to the first three by a factor $Q = a_0$, and should be ignored to leading order in small momenta. Omitting these terms, we find $r_S = 1.0 \text{ fm}$, while including them, $r_S = 4.0 \text{ fm}$ (the dominant correction comes from the fourth term in the square brackets in (4.39)).

Clearly the expansion in Q is converging at best slowly.

We investigate this further by considering a distorted wave modified ERE [56], which is obtained without expanding in powers of Q . This is obtained using techniques similar to those used to define an ERE in the presence of the Coulomb potential where the usual expansion fails due to the potential's infinite range (see for example [42]).

The calculation requires the solutions to the Schrodinger equation in the presence of the OPE potential, f_0 and f_0 , which were defined in (4.9) and (4.10). Solving the Schrodinger equation using a series expansion, they are found to have the following behaviour for small r :

$$\begin{aligned} f_0(r) &= C_0(p) r - \frac{M}{2} r^2 + O(r^3) \\ f_0(r) &= \frac{1}{C_0(p)} \frac{\hbar}{M} r \ln(p)r + O(r^2 \ln r)^i : \end{aligned} \quad (4.40)$$

$C_0(p)$ and $\delta(p)$ are functions which must be determined numerically.

From these, we construct a comparison function $\tilde{f}_0(r)$ which is a solution to the same Schrodinger equation, but satisfying $\tilde{f}_0(0) = 1$ and

$$\tilde{f}_0(r) = \sin(pr + \delta) \quad (4.41)$$

for large r . δ is the phase shift obtained from the Schrodinger equation for a potential containing OPE and an unknown short range piece as before. Writing $\delta = \delta_0 + \delta^i$,

$$\tilde{f}_0(r) = C_0(p) \frac{\hbar}{M} f_0(r) + f_0(r) \cot \delta^i : \quad (4.42)$$

The calculation now proceeds by analogy with the usual derivation of the ERE in which $\psi(r)$ is a free wave solution. The resulting modified ERE is given by

$$p \cot \delta_s = M \ln \left(\frac{p}{p_0} \right) + C_0^2(p) p \cot \delta_s^0 : \quad (4.43)$$

$C_0^2(p)$ is an arbitrary constant which is present due to the presence of the logarithmic term in the expansion of f_0 . This, in turn, is due to the $1/r$ singularity in the OPE potential. Because of this arbitrariness in the zero energy part of the modified ERE, it is again not possible to uniquely define a modified scattering length. By expanding $p \cot \delta_s^0$, and using numerically obtained values for the scattering length and effective range due to OPE alone, we find an increased effective range $r_s = 4.4 \text{ fm}$. Again, this disagrees with the result obtained in the momentum expansion. The similarity to the result including higher order terms is presumably accidental.

Steele and Fumstahl [54] have also found an increased effective range ($r_s = 3.1 \text{ fm}$) in a modified effective range expansion, but using a cut-off pion Yukawa.

The fact that the effective range remains large when OPE is removed might indicate that there is other important long-range physics. The modified effective range is certainly more natural expressed in units of $1/(2m_\pi)$ than units of $1/m_\pi$.

These problems have also been discussed by Kaplan and Steele [55] who apply effective field theory techniques to a range of toy models. The EFT expansion succeeds for simple short range potentials where a small modified effective range is found. The expansion fails, however, when the model of the short distance physics is given by two Yukawa functions with different ranges and opposite signs. In the latter case, the coupling constants were adjusted to reproduce the physical scattering length and effective range.

This suggests that the problem with the momentum expansion found in the above calculations might be due to complexities in the real short distance NN interaction rather than the perturbative treatment of OPE.

Chapter 5

Results

5.1 Introduction.

In Chapter 4, the two nucleon potential as calculated to third order ($\alpha = 3$) in small momenta and masses was presented. There are many questions which we can ask about these potentials. Some can be answered quite generally, while others will be addressed in the context of individual partial waves.

The first calculation of NN scattering to this order was performed by Ordóñez et al., although it differed in several respects from the calculation described here. Most importantly, Delta resonances were included and g_A , f and the low energy constants B_i were treated as free parameters in a fit to the VPI [57] partial wave analysis (PWA). Since the determination of the low energy constants from NN scattering does not include Delta's, the B_i found by these authors cannot be compared with empirically determined values¹.

Ideally, the potentials should be used to calculate cross-sections which can be compared directly with experimental data. Such an analysis has been performed by Rentmeester et al. [53] who use the same potential as model-independent input to a new multi-energy PWA of the 1998 Nijmegen proton-proton database [58]. As in the present work, the potential is regularised by excluding the region $r < R$ and imposing

¹The relationship between the B_i and the c_i in the absence of Delta's is given by Equation (2.29) on page 27.

a boundary condition at the cut-off radius in each partial wave considered.

In the PWA the boundary condition is allowed to be an analytic function of energy and this energy dependence is controlled by a variable number of parameters which are adjusted to minimise χ^2 in a fit to the chosen data set for $R = 1.4$ fm and $R = 1.8$ fm. The c_i are treated as free parameters, and the values found are reasonably close to those obtained from NN scattering data. At both radii a systematic reduction in χ^2_{min} and the number of necessary boundary condition parameters is found as the leading order TPE and then next to leading order TPE potentials are added.

Nevertheless, their optimum fit including the $\ell = 3$ potential requires 23 boundary conditions. Although this procedure seems to provide evidence for the importance of the long range part of the TPE potential, adjusting boundary conditions in $\ell > 1$ partial waves is not in keeping with a consistent EFT treatment to order $\ell = 3$ for the reasons discussed in Chapter 4; the first contact interaction which contributes to D-wave scattering ($\ell = 2$) enters at order $\ell = 4$, and contributions to higher partial waves are suppressed by larger chiral powers.

Since the EFT predictions are parameter-free in D-waves and higher, we restrict our attention to $\ell > 1$ partial waves. We shall investigate the EFT predictions in these partial waves by imposing an energy independent boundary condition on the wavefunctions at $r = R$ in such a way that, for small enough pr , they match on to free wavefunctions at the cut-off radius (see Chapter 4). In addition, we can explore deviations from the EFT prediction by allowing the boundary condition parameter to be non-zero:

$$R \frac{d}{dr} \ln u_1(p; r) \Big|_{r=R} = 1 + 1 + \quad (5.1)$$

in uncoupled waves, and the 2×2 boundary condition matrix A ,

$$R \frac{d}{dr} \alpha_j(p; r) \Big|_{r=R} = [\text{Diag}(j; j+2) + A] \alpha_j(p; r) \quad (5.2)$$

in the coupled waves. We shall want to vary the boundary condition parameters for two reasons. Firstly, letting α and A vary over a fixed range allows us to demonstrate explicitly how dependence on the boundary condition changes as angular momentum ℓ and laboratory energy T_{lab} vary. Secondly, it is interesting to test whether the addition

of a single free parameter allows us to compensate for omitted higher order physics. By doing this, we make contact with the new PWA of Rentmeester et al. [53] who allow several free parameters in each partial wave.

In a contrasting approach, Kaiser et al. [43] calculated the graphs of Figure 4.2 (including iterated OPE) at next to leading order in the expansion of the inverse nucleon mass and obtained phase shifts by projecting the amplitude into the appropriate partial wave. Although not intended for use in a particular Schrodinger equation, the irreducible part of their interaction transformed into coordinate space is the same as the potential used in the present work and also by the Nijmegen group [53].

This perturbative calculation leads to finite predictions at finite momenta and contains no free parameters. It is not, however, a complete calculation of the interaction to order ϵ^3 because of the enhancement of reducible loop graphs. A full perturbative calculation to this order would require the tedious evaluation of the reducible two and three-loop diagrams which contribute at order ϵ^2 and ϵ^3 respectively. We shall sum these diagrams automatically by solving the Schrodinger equations.

In a further paper, Kaiser et al. [59] add vector meson exchange to the ϵ^3 potential. While the addition of ρ and ω exchange clearly permits a better description of the data, the inclusion of heavy mesons cannot be reconciled with chiral power counting. In particular, the low energy constants c_i are no longer related in any simple way to those obtained from analyses of NN scattering, and they must be refitted to NN scattering data.

More recently, Meiner has considered iterating the interaction calculated to order ϵ^3 in momentum space [60]. This work is performed in a similar spirit to the calculation presented here. The potential is regularised with exponential and sharp cut-offs. He finds evidence for ϵ^3 TPE in several partial waves.

To test the full TPE predictions, we attempt to identify the partial waves, energies and cut-off radii for which phase shifts are simultaneously insensitive to non-perturbative effects and variation of R . In these regions, the TPE potential can be studied as unambiguously as possible.

	V_C	V_S	V_T	V_{SO}	V_Q	W_C	W_S	W_T	W_{SO}	W_Q
OPE		p	p			p	p	p		
TPE ($\ell = 2$)	p						p	p		
TPE ($\ell = 3$)	p		p	p		p		p	p	
TPE ($\ell = M$)	p				p					
exchange							p	p	p	p
! exchange	p			p						

Table 5.1: Contributions from the EFT potentials up to order $\ell = 3$ compared with the most important OBE contributions [18]. V_Q and W_Q are isoscalar and isovector quadratic spin-orbit potentials. The remaining notation was defined in Chapter 4.

In one partial wave in which TPE seems to be too strong, we shall demonstrate that adjusting the single parameter α to allow for neglected higher order effects allows reasonably good global fits over similar energy ranges to those considered in [59] when the full TPE potential is included.

5.2 The Nijmegen Phase Shift Analyses

We do not attempt to compare our results directly with NN scattering data. Instead we consider the three most up-to-date potentials of the Nijmegen group [61], and the 1993 partial wave analysis PWA93 [62]. Since the three potentials were determined in fits to the same data set as the PWA93 [58], and all have a χ^2 per datum of around 1, they may be considered as independent PWA's and we shall refer to them as such.

Since these analyses have different characteristics, the spread in the corresponding phase shifts gives an indication of the systematic errors involved in choosing a particular PWA. All four PWA's include the OPE interaction given in the Appendix. To aid comparison, we also use this form which takes account of pion mass differences. In our results (Figure 5.1 to 5.17) we show the full range of phase shifts produced by the PWA's as a striped band. A short description of each follows.

Reid93 is an update of the well known Reid68 potential [63]. Apart from the explicit appearance of the OPE interaction, the potential consists of a sum

of regularised Yukawa functions with arbitrarily chosen masses and coefficients adjusted separately in each partial wave (up to $j = 4$) to optimise the total χ^2 . It should be noted that the potentials for $j \geq 5$ are set equal to potentials from lower partial waves, and are not allowed to vary independently. A total of 50 parameters are used in the fit.

The N_{ij}^I potential was constructed using an updated version of the N_{ij}^I eigen soft core potential [64] as a starting point. χ^2 was then minimised by unfixing certain parameters in the potential and fitting them separately in each partial wave. A total of 41 adjustable parameters were required.

The N_{ij}^{II} potential was obtained in the same manner as N_{ij}^I , but with all non-local contributions removed. In this case, the fit made use of 47 parameters.

The PWA 93 parameterisation of the NN interaction consists of a potential tail including OPE and heavy meson exchange contributions. The remaining energy dependence of phase shifts is reproduced using an energy dependent boundary condition at $R = 1.4 \text{ fm}$.

5.3 General Discussion

The OPE phase shifts are obtained by solving the Schrodinger equations (4.3 – 4.5) in the region $r > R$. Four values of the cut-off radius R are used: $R = 0.8 \text{ fm}$, 1.0 fm , 1.4 fm and 1.8 fm . In uncoupled partial waves, the TPE phase shifts are calculated both perturbatively using the DWBA (4.31) with OPE wavefunctions as input, and non-perturbatively by solving the Schrodinger equation for the sum of OPE and TPE interactions. In coupled partial waves, only the non-perturbative calculation is performed.

In general, we find that as R is increased the agreement between perturbative and non-perturbative treatments of the TPE parts of the potential improves. This can be understood from an RG point of view as discussed in Chapter 4. The inverse of the cut-off radius $1/R$ plays the role of the low cut-off scale. As $1/R \rightarrow 0$ the expansion

parameter of the EFT, $\mu = \mu_0$, becomes very small and the convergence properties of the theory improve. In terms of the potential, the large non-perturbative effects when R is small are caused by the strong singularities encountered in the short distance part of potential. When R is made large enough, these singularities are removed.

On the other hand, sensitivity to the boundary condition parameter increases as R becomes larger, and eventually the phase shifts acquire a rapid energy dependence which is an artefact of the sharp cut-off. An example of how such energy dependence can arise is given by the non-trivial fixed point potential (3.24) found in the RG analysis of Chapter 3. The cut-off dependent part of this potential contains a logarithm which blows up for a fixed momentum p as μ approaches p from above, causing rapid variation of the potential with energy.

In the RG treatment, the energy dependence compensates for the effects of a sharp momentum space cut-off. Since we have not solved an exact RG equation for μ , the energy dependence caused by the boundary condition is still present in phase shifts and becomes important for high enough energies.

Sensitivity to the boundary condition decreases for small R and low energies where its effect becomes small compared to the potential (or centrifugal barrier in regions where the potential is sufficiently weak). As would be expected, sensitivity to non-perturbative effects and the regularisation procedure is delayed to higher energies as l becomes large because of the centrifugal barrier.

In each partial wave we look for a region of R and T_{lab} where non-perturbative and perturbative predictions agree and are insensitive to the cut-off. If the phase shift in this window is sufficiently different from the OPE prediction, then we can interpret the difference as a prediction of chiral TPE.

For each partial wave, we first show the full TPE prediction as R is varied (Figure 5.1, 5.3 etc.). In uncoupled waves both perturbative and non-perturbative results are shown. In general, we find that near $R = 1.8$ fm phase shifts are very sensitive to R in the regions of energy where TPE contributions are important and insensitive to μ . For $R = 1.4$ fm inwards, insensitivity to R persists to higher energies. $R = 1.4$ fm is one of the cut-off radii used by Rentmeester et al. [53] in their analysis of the $\mu = 2$

and $\ell = 3$ potentials. For this reason we show the results obtained using this value of R in each partial wave considered here (Figure 5.2, 5.4 etc.). In these plots, the effect of adding first leading order TPE contributions, and then the full TPE potential is shown. Sensitivity (or insensitivity) to the boundary condition parameter is also shown on this plot by allowing $0.5 < \alpha < 0.5$ for the full TPE result in uncoupled waves, and $1/2 < A_{ij} < 1/2$ in coupled waves.

The effects of the $1=M$ potential in peripheral waves are quite small compared with rest of the $\ell = 3$ potential. This suggests that the $1=M$ expansion is under control. For example, in the 3G_5 wave at 150M eV where we see good evidence for chiral TPE, the $1=M$ effects are responsible for a 4% reduction in the phase shift. In lower partial waves, they are more important, causing an 8% increase in the 1D_2 phase shift at 100M eV.

In addition, phase shifts are not overly sensitive to fairly generous variations of the c_i around their central values. Allowing for twice the quoted uncertainties [20], we find a maximum variation of 4% in the 3G_5 partial wave at 150M eV. The size of this change is comparable with the size of the shaded areas on the plot corresponding to variation of A . Similar sized effects are found in other partial waves in the regions of energy in which TPE is important.

5.4 Spin Singlet Partial Waves.

5.4.1 1D_2

The first counterterm which contributes to D-wave scattering enters the EFT at order $\ell = 4$. Since this is only one order higher than the effects we are looking for, it is not surprising that R dependence and α dependence are significant for energies above about 20M eV. At $R = 0.8$ fm, non-perturbative effects cannot be ignored at any reasonable energy.

The full TPE phase shifts are plotted in Figure 5.1 for four values of R and for $\alpha = 0$. Two curves are shown for each radius, corresponding to perturbative and non-perturbative treatments of TPE contributions. The full range of Nijmegen phase

shifts is also shown for comparison.

This figure illustrates quite nicely some of the general features discussed in the previous section. At the smallest cut-off radius, non-perturbative effects are very large, while at $R = 1.8$ fm sensitivity to R controls the phase shift. Between $R = 1.0$ fm and $R = 1.4$ fm dependence on R is less severe, and non-perturbative TPE effects do not overwhelm the results below about 20 MeV.

At our chosen value of the cut-off radius ($R = 1.4$ fm), the full TPE predictions lie almost on top of the Nijmegen values. No conclusions should be drawn from this accident since in this partial wave there is no region of R and T_{lab} in which TPE contributions can be isolated unambiguously.

In Figure 5.2, the OPE, leading order TPE and full TPE phase shifts are shown. In this plot, TPE effects are included perturbatively. For all of these cases, the line $\delta = 0$ is shown, and for full TPE the shaded band indicates how phase shifts vary for $0.5 < \lambda < 0.5$.

A pattern which is seen in most other partial waves is evident in Figure 5.2; the leading order ($\ell = 2$) TPE contributions are smaller than the next to leading order ($\ell = 3$) contributions. In this partial wave, despite problems with non-perturbative effects and cut-off dependence we can, at least, conclude that TPE contributes with the correct sign and roughly the correct strength.

5.4.2 1F_3

As angular momentum ℓ increases, the F -wave phase shifts are the first for which we expect insensitivity to the contact interactions which are produced by the low energy effective theory up to order $\ell = 3$ in the momentum expansion. The first contact interaction which contributes to F -wave scattering would enter at order $\ell = 6$.

Figure 5.3 shows the perturbative and non-perturbative $\ell = 3$ TPE predictions for three cut-off radii. The difference between iterated and DWBA curves is only visible at $R = 1.0$ fm. The curves for $R = 0.8$ fm are not shown because they lie nearly on top of the $R = 1.0$ fm curves.

Again, R dependence is large near $R = 1.8$ fm and small for R below about 1.4 fm

r (fm)	0:8	1:0	1:4	1:8
$U_{\text{odd}}=U_{\text{even}}$	0:25	0:21	$3:10^{-2}$	0:32

Table 5.2: Ratio of two-nucleon potentials in spin singlet partial waves for odd and even values of l .

and T_{lab} less than about 120 MeV. Comparison with the 1D_2 case seems to indicate that our power counting expectations are justified.

More surprising is the almost exact agreement between perturbative and non-perturbative calculations of TPE. Examination of the potential provides an explanation. In spin singlet partial waves with even angular momentum l , all contributions to the potential are attractive. For odd angular momentum, OPE and isovector parts of the asymptotic TPE potential (4.26, 4.28) are repulsive. In the latter case, the cancellation between repulsive and attractive parts of the potential cuts its size significantly, allowing the cut-off radius to be reduced without introducing parts of the potential which need to be treated non-perturbatively.

The ratio between $U_{\text{even}}(r)$ and $U_{\text{odd}}(r)$ for four values of r is shown in Table 5.2. The very small ratio at $r = 1.4$ fm is caused by a change in sign of the odd l potential near this radius from repulsive at large radii to attractive for small radii. The even l potential is always attractive.

In Figure 5.4, the OPE, leading order TPE and full TPE results are shown for $R = 1.4$ fm. TPE is included perturbatively. Once again, the $\ell = 3$ contributions are the dominant part of the chiral TPE potential. The leading order TPE potential is small and repulsive in the range of energy shown. The $\ell = 3$ contribution is larger and attractive, and closes the gap between OPE predictions and the phase shifts of the Nijmegen potentials. As expected from power counting, the phase shifts are considerably less sensitive to the same variation of Λ at a given energy than in the 1D_2 partial wave.

5.4.3 1G_4

The 1G_4 phase shift is an important place to look for the effects of TPE. In Figure 5.6, it is clear that OPE is too weak to account for the Nijmegen phase shifts. Figure 5.5 shows the perturbative and non-perturbative TPE results for four cut-off radii. As usual, R dependence is particularly strong around $R = 1.8$ fm, but from 1.4 fm inwards the phase shifts are insensitive to R below around 170 MeV (compared with about 120 MeV in the 1F_3 wave). We therefore have a large window in which we can investigate TPE.

In Figure 5.6 the OPE, leading order TPE and full TPE results are presented. Again, leading order TPE contributions are smaller than $\ell = 3$ contributions. Over the chosen range, R dependence is very small. The region from 62 to 110 MeV is enlarged in Figure 5.7 and shows the situation clearly in a region where TPE contributions are not sensitive to R or non-perturbative effects.

In this partial wave, TPE is clearly too attractive at all energies, although it contributes with the correct sign. This indicates that there are important higher order contributions missing. It may be worth noting that the PWA93 phase shift, (which has the lowest χ^2 of all of the Nijmegen potentials), lies at the top of the striped band for T_{lab} above about 150 MeV.

It is interesting to ask whether a single parameter introduced to compensate for this discrepancy allows good agreement with the Nijmegen results over a large energy range. The results obtained when α is adjusted by hand to produce a rough global fit to the Nijmegen results up to 300 MeV are shown in Figure 5.8. The OPE and $\ell = 2$ curves can be brought into better agreement at high energies at the cost of increasing the discrepancy at intermediate energies. The 'best' values of α were as follows:

$$\alpha_{\text{OPE}} = 3.5; \quad \alpha_{\text{TPE2}} = 2.5 \quad \text{and} \quad \alpha_{\text{TPE3}} = 1.5: \quad (5.3)$$

α_{TPE2} and α_{TPE3} are associated with $\ell = 2$ and $\ell = 3$ potentials respectively. The full TPE calculation gives the best fit overall, although it is still slightly too attractive at intermediate energies.

5.5 Spin Triplet Uncoupled Partial Waves

5.5.1 3D_2

In spin singlet partial waves, the tensor parts of the OPE and TPE potentials do not contribute. The uncoupled spin triplet waves are therefore the first in which these parts of the potential are tested. The situation in the 3D_2 partial wave is similar to the 1D_2 case, although OPE alone is much closer to the Nijmegen results in the triplet partial wave. As in the 1D_2 , the $R = 1.4$ fm results are close to the PWA's but again, dependence on R and non-perturbative TPE effects prevents us from drawing too many conclusions from this.

5.5.2 3F_3

The 3F_3 partial wave, like the 1G_4 , is a promising place to look for TPE. Figure 5.10 shows that the discrepancy between OPE and the Nijmegen results is already significant below 80 MeV. Figure 5.9 shows the full TPE prediction for four values of cut-off radius R . It is clear that for R between about 1.0 fm and 1.4 fm, sensitivity to R and non-perturbative TPE contributions is no larger than the discrepancies among the Nijmegen phase shifts.

Dependence on the cut-off radius is again large at $R = 1.8$ fm. The comparison with OPE and leading order TPE is shown for $R = 1.4$ fm in Figure 5.10. Over the entire energy range shown, the $\ell = 3$ calculation represents a substantial improvement over OPE and the leading order TPE result. The agreement with Nijmegen results for $\ell = 0$ and $R = 1.4$ fm persists to about 250 MeV, although the prediction is strongly R dependent at such a high energy. The region between 50 and 80 MeV is shown enlarged in Figure 5.11. Once again the $\ell = 3$ contribution is clearly dominant.

5.5.3 3G_4

The 3G_4 partial wave is described very well by OPE; even at 250 MeV the OPE prediction lies between the extremes of the Nijmegen PWA's. In the sense that the TPE

contributions do not spoil this agreement, they have the correct magnitude.

5.6 Spin Triplet Coupled Partial Waves

5.6.1 ${}^3P_2 - {}^3F_2, (\pi/2)$

The 3P_2 phase shift is very sensitive to short distance effects, and we do not consider it here except to verify that it has the correct behaviour at very low energies when $\delta = 0$. The mixing angle, $\pi/2$, is described well by OPE up to about 40 MeV where the results become dependent on R . Up to about 100 MeV, both parts of TPE are very small corrections to the OPE prediction for $R = 1.4$ fm.

The 3F_2 phase shift is the first observable in a coupled channel in which the opportunity to study TPE corrections presents itself. The full TPE phase shift is shown at $\delta = 0$ in Figure 5.12 for four cut-off radii. The rather unusual looking behaviour above 90 MeV as R is varied between 1.0 fm and 1.4 fm is probably caused by interference with the 3P_2 phase shift. In addition, the difference between the $R = 0.8$ fm and 1.0 fm results suggests that non-perturbative TPE effects may be important at these radii. The phase shift near $R = 1.8$ fm is sensitive to the cut-off radius as usual.

Despite the unusual features described above, the TPE phase shift lies consistently above the Nijmegen PWA's in the region of energy where dependence on R is small (below about 60 MeV).

The OPE, leading order TPE and full TPE results are shown for $R = 1.4$ fm in Figure 5.13. In this, and other coupled waves, the shaded band shows the maximum variation of the full TPE result as the three independent elements of the boundary condition matrix A are allowed to vary between $-1=2$ and $1=2$.

As is clear from the figure, the OPE results describe the Nijmegen PWA's quite well in the region of energy shown. The leading order TPE corrections are small and have the correct sign, but the full TPE corrections are much too large. It is worth noting at this point that Kaiser et al. [43] also find too much attraction in this partial wave. They also note that the VPI [57] PWA and the Nijmegen PWA 3F_2 phase

shifts are very similar. For these reasons, it is unlikely that the over-attraction is an artefact of the way the calculation has been performed, or due to the choice of a particular PWA.

5.6.2 ${}^3D_3 - {}^3G_3, ({}_3)$

The 3D_3 phase shift is very sensitive to R at all energies. As in the other two D -waves, we observe that if the cut-off is placed at $R = 1.4$ fm, the full TPE phase shift lies within the Nijmegen range over a reasonable range of energies, in this case up to about 100 MeV. The agreement may be of more significance in this partial wave than the other two D -waves because the OPE phase shift has the wrong sign.

${}_3$ is described extremely well by OPE up to around 250 MeV. As with ${}_2$ the TPE corrections are both very small for $R = 1.4$ fm and do not spoil this agreement. Kaiser et al. [43] do not find quite such good agreement with OPE at high energies. This may be an indication that the two and three loop reducible iterated OPE graphs not calculated in that work are significant for this mixing angle.

In the 3G_3 phase shift, OPE is too repulsive. As in other isoscalar partial waves, the leading order TPE potential is small and repulsive. Adding ${}_3$ TPE brings the phase shift back into agreement with the Nijmegen PWA's, particularly at $R = 1.4$ fm. The differences among the Nijmegen phase shifts are larger than the improvement however, so we do not show these results here.

5.6.3 ${}^3F_4 - {}^3H_4, ({}_4)$

The 3F_4 phase shifts for TPE at the usual four cut-off radii are shown in Figure 5.14. Dependence on R is still surprisingly large at $R = 1.4$ fm, and sets in at lower energies than in other F -waves. $R = 1.4$ fm happens to be a particularly good choice in this partial wave. This is shown alongside the OPE and leading order TPE results in Figure 5.15. As usual, for the full TPE result, sensitivity to A is shown by a shaded band.

The ${}_2$ corrections have almost no effect on the leading order predictions. The

result to order $\ell = 3$, however, represents a marked improvement over OPE. Despite sensitivity to the cut-off radius, this is true over a wide range of values of R .

δ_4 , like δ_3 and δ_2 , is dominated by OPE. TPE corrections are small enough not to spoil the agreement.

The Nijmegen PWA's are not expected to provide a good description of H-waves and higher, as the potentials used to produce the quoted phase shifts are taken from a lower partial wave. Nevertheless, there is a tendency for full TPE to be over-attractive in the 3H_4 partial wave.

5.6.4 ${}^3G_5 - {}^3I_5$, (δ_5)

Despite large differences among the PWA phase shifts, the 3G_5 partial wave shows very good evidence for the importance of chiral TPE. Figure 5.16 shows the full TPE for our four choices of cut-off radius. Disregarding the $R = 1.8$ fm case as usual, R dependence is small below around 130 MeV. Figure 5.17 shows OPE, leading order TPE and full TPE for $A = 0$. The shaded band shows variation of full TPE with A over the usual range. The OPE potential is substantially too repulsive above around 60 MeV and leading order TPE has the wrong sign, but the agreement of the full TPE result with the PWA's is quite impressive, particularly as variation with A is small.

As would be expected, δ_5 and the 3I_5 phase shift are dominated by OPE.

5.7 Summary

The D-wave phase shifts are very sensitive to the cut-off radius and effects generated by iterating the TPE potential. We note that, in all three cases, the choice $R = 1.4$ fm leads to surprisingly good agreement with the Nijmegen PWA's.

In all of the F-wave phase shifts, the results are much less sensitive to the regularisation procedure. In three of these four partial waves, the TPE results are in good agreement with the Nijmegen PWA's for $R = 1.4$ fm. The full TPE contribution to the 3F_2 potential is too large and attractive at all energies.

The G-wave phase shifts are the least sensitive to the effects of iteration of TPE

and boundary condition parameters. In the 3G_3 partial wave uncertainties in the Nijmegen PWA's prevent any firm conclusion, and the 3G_4 partial wave is very well described by OPE alone. Clean signals of TPE are seen in the 1G_4 and 3G_5 phase shifts. In the 1G_4 case, TPE is too attractive, but adjusting the boundary parameter can correct for this. Of any partial wave, the most convincing evidence for TPE is seen in the 3G_5 phase shift where OPE is much too repulsive, but including both TPE contributions leads to very good agreement with the PWA's.

The mixing angles α_2 , α_3 and α_4 are well described by iterated OPE, and the TPE corrections to these are small.

In most partial waves considered here, $\alpha = 3$ TPE corrections are much larger than $\alpha = 2$ corrections. In general, the TPE potential is slightly underattractive in isoscalar partial waves, and too attractive in isovector partial waves.

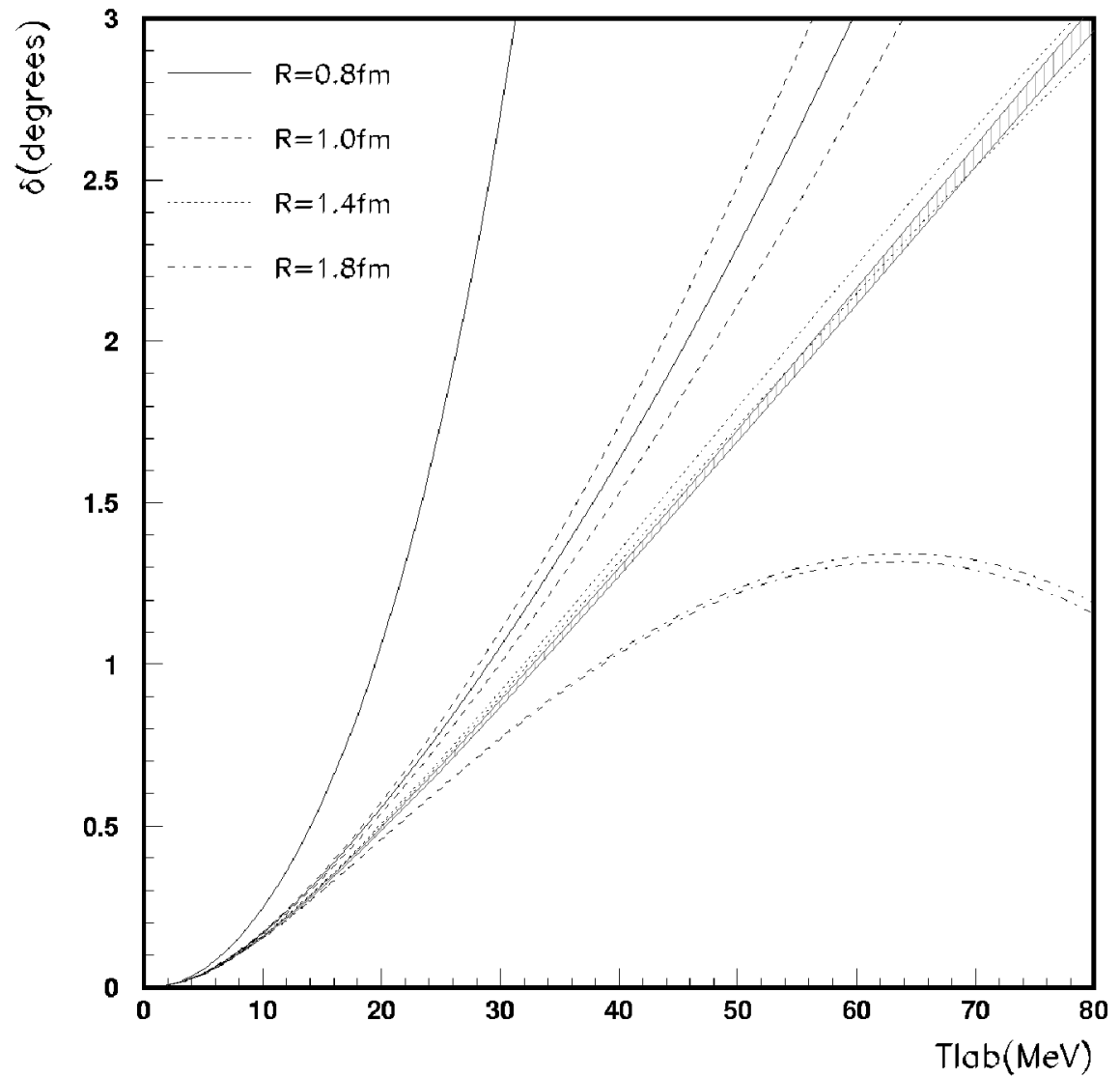


Figure 5.1: The 1D_2 phase shift at $\eta = 0$ for four cut-off radii. At each radius, the upper curve is obtained by iterating the full $\eta = 3$ potential, while for the lower curve the TPE contribution is included perturbatively. The striped band represents the Nijmegen Partial Wave Analyses (see text).

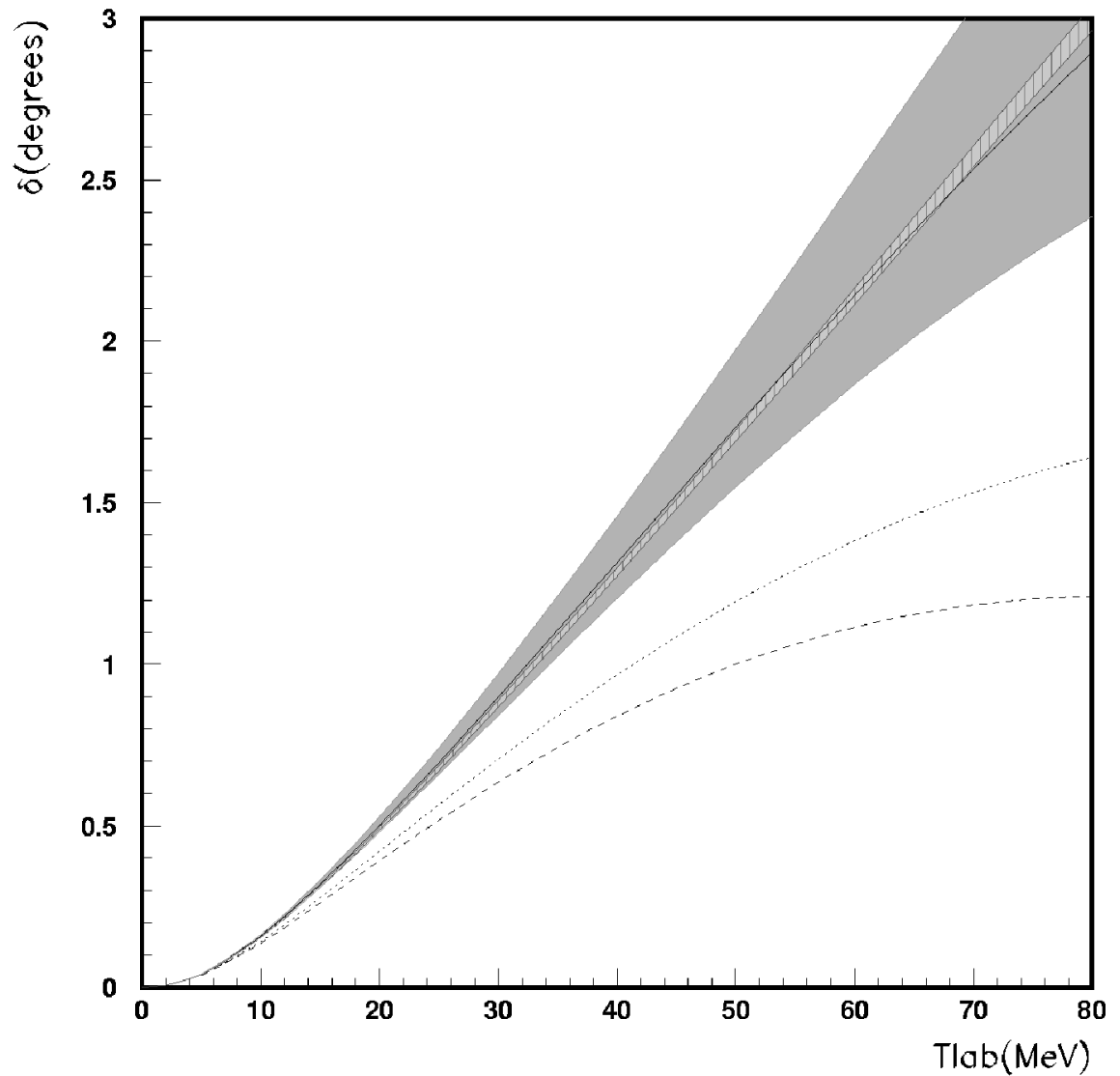


Figure 5.2: 1D_2 phase shift near $k = 0$ for cut-off radius $R = 1.4$ fm. The dashed line is iterated OPE, the dotted line includes leading order TPE ($\ell = 2$) perturbatively, and the solid line is the full calculation to order $\ell = 3$ with TPE treated perturbatively. The shaded band shows variation of the $\ell = 3$ phase shifts for $0.5 < c < 0.5$.

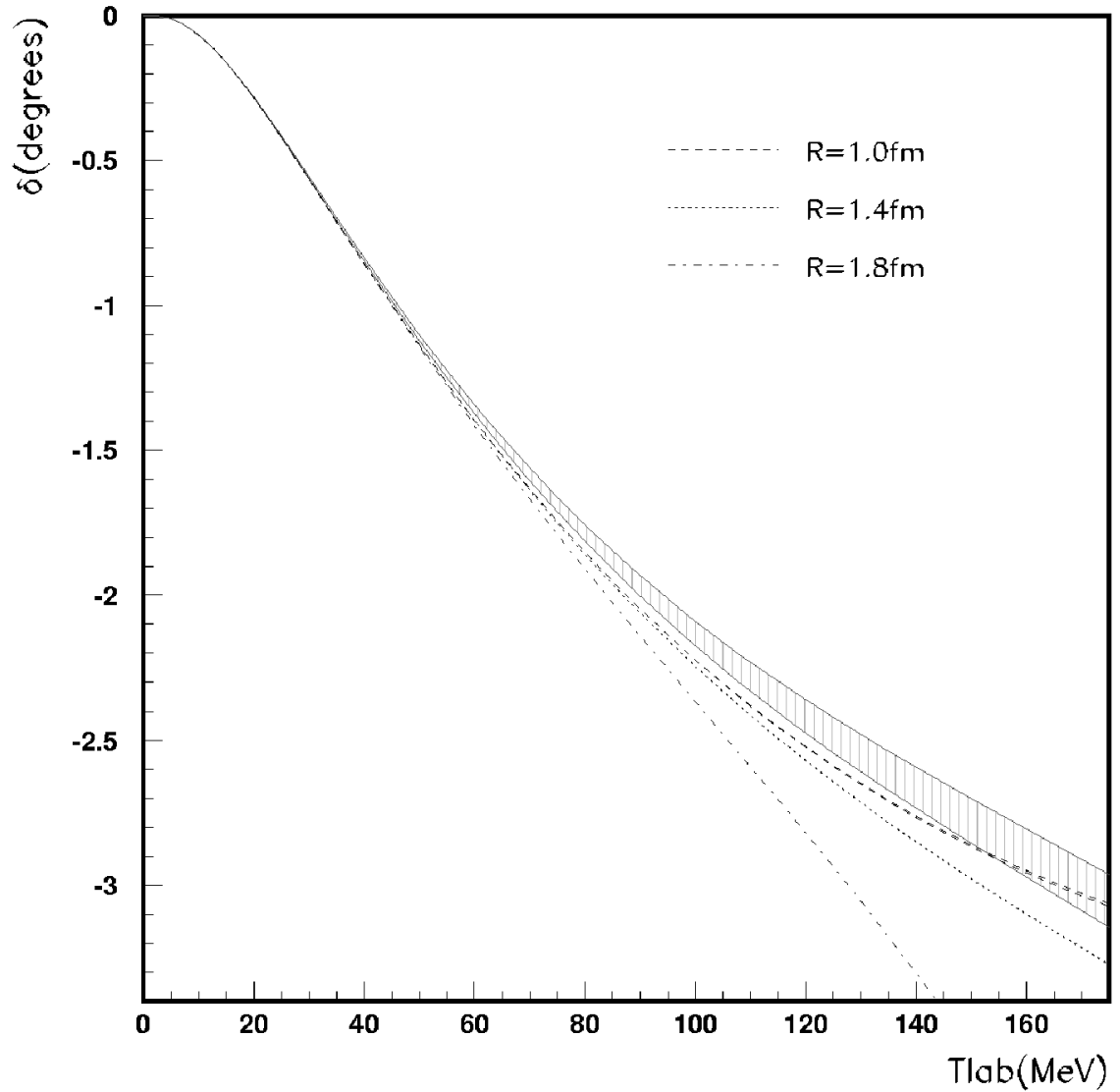


Figure 5.3: 1F_3 phase shift at $a = 0$ for three cut-off radii. At each radius, the upper curve is obtained by iterating the full 3S_1 potential, while for the lower curve the TPE contribution is included perturbatively although the difference is only visible at $R = 0.8$ fm. The phase shifts at $R = 0.8$ fm are not shown, as they lie almost exactly on top of the $R = 1.0$ fm results. The striped band represents the Nijmegen phase shifts.

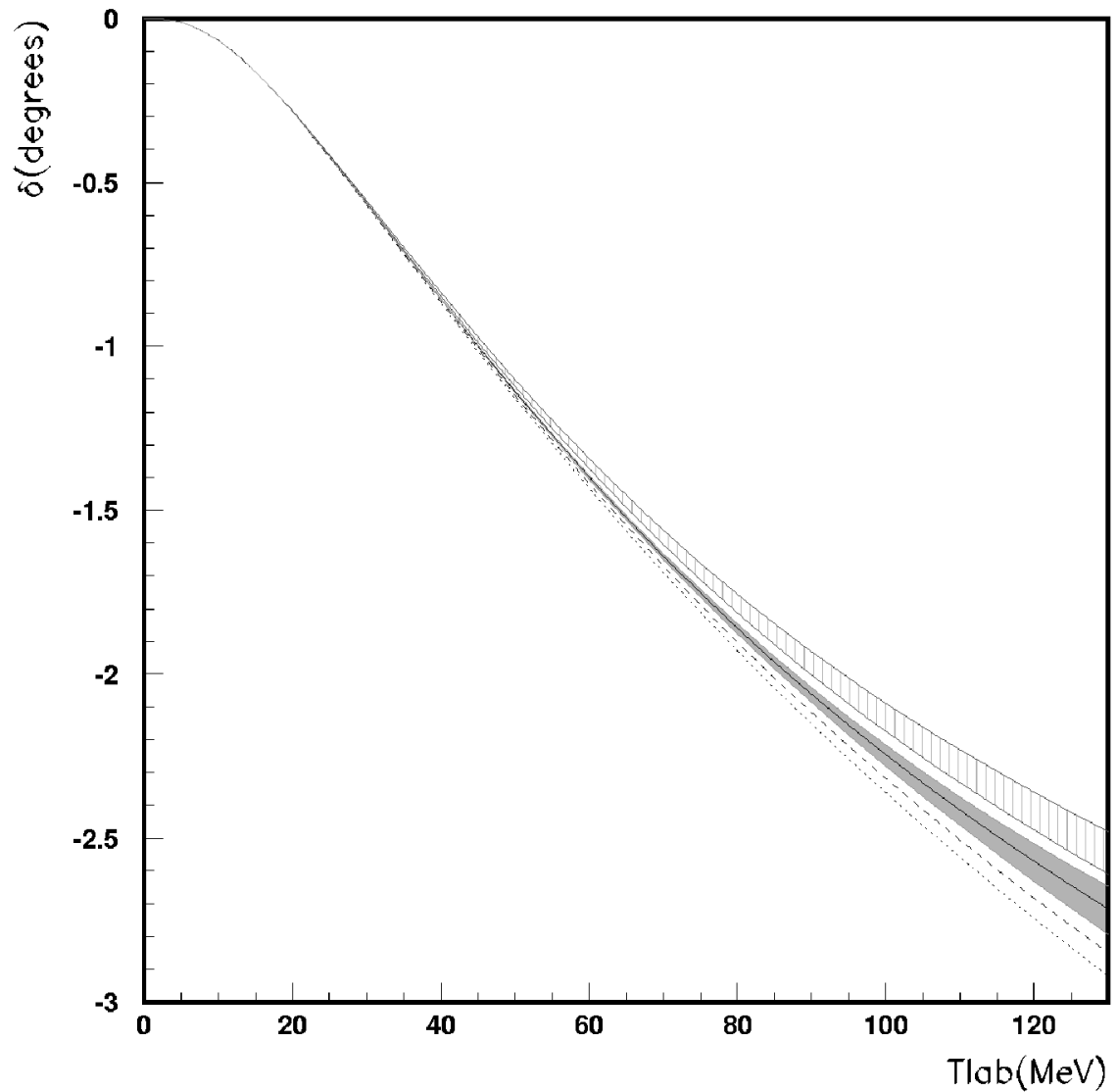


Figure 5.4: 1F_3 phase shifts near $\epsilon = 0$ for cut-off radius $R = 1.4$ fm. The dashed line is iterated OPE, the dotted line includes leading order TPE ($\ell = 2$) perturbatively, and the solid line is the full calculation to order $\ell = 3$ with TPE treated perturbatively. The shaded band shows variation of the $\ell = 3$ phase shifts for $0.5 < c < 0.5$.

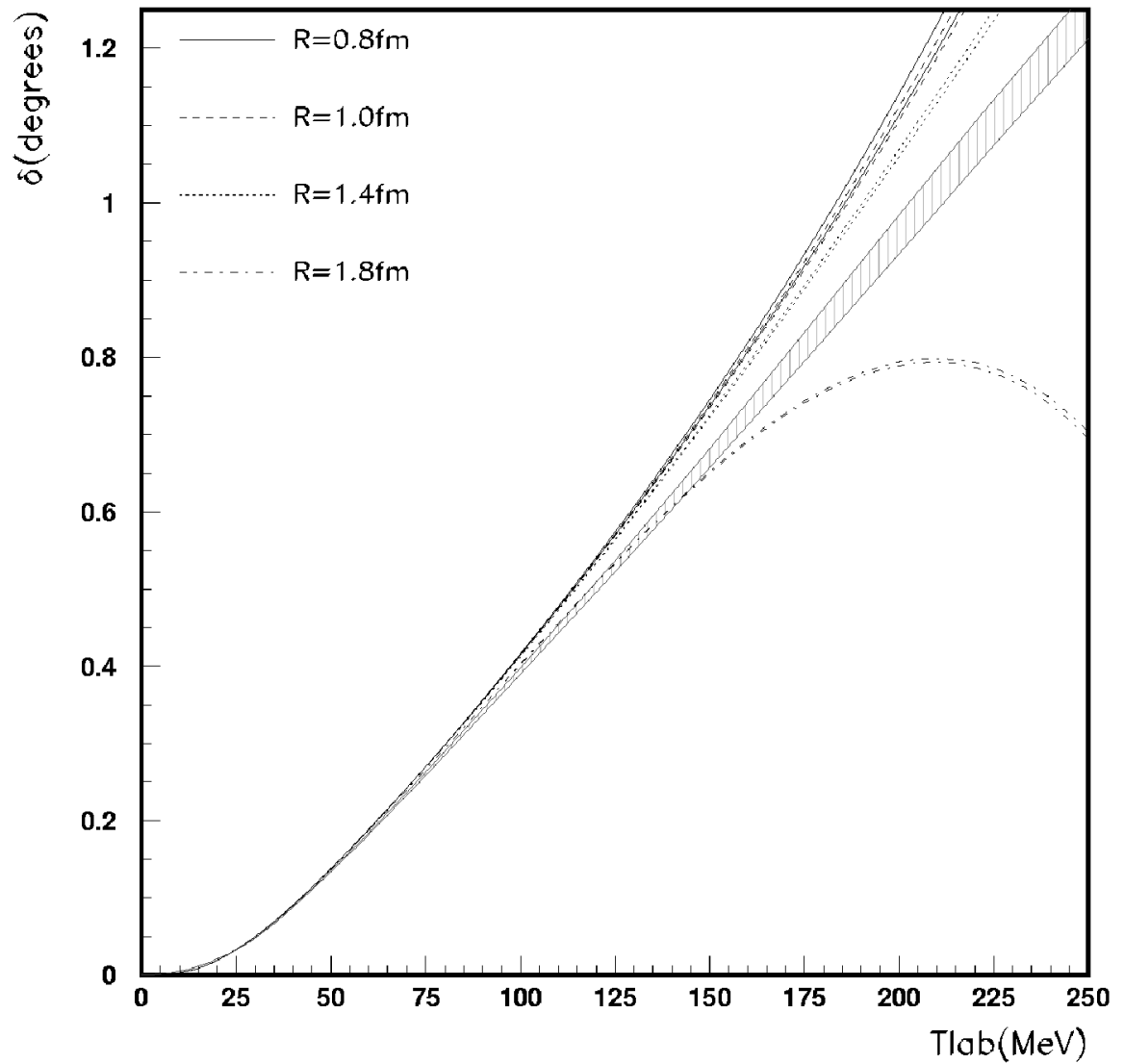


Figure 5.5: 1G_4 phase shift at $\theta = 0$ for four cut-off radii. At each radius, the upper curve is obtained by iterating the full $\mu = 3$ potential, while for the lower curve the TPE contribution is included perturbatively. The striped band represents the Nijmegen phase shifts.

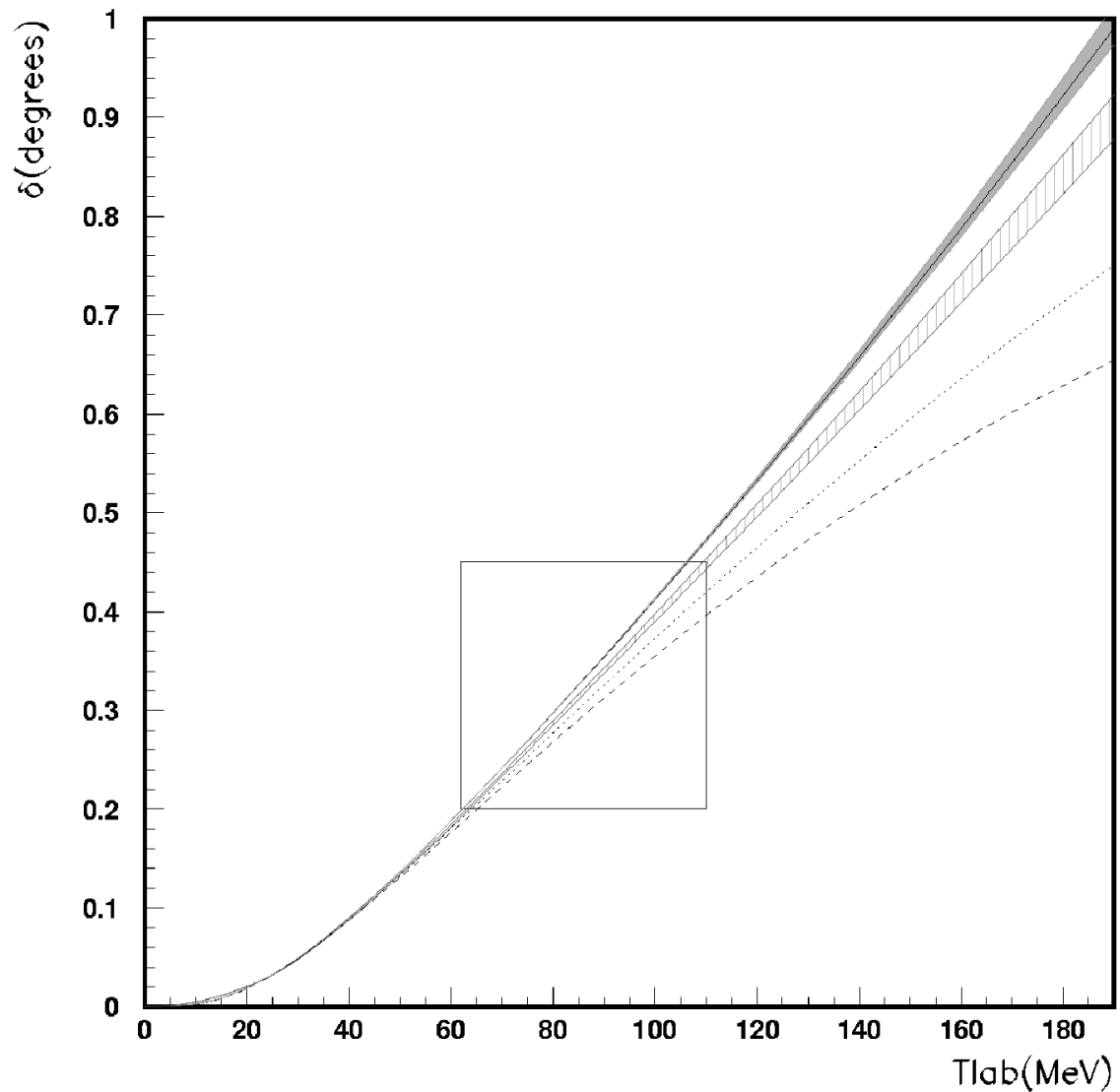


Figure 5.6: The 1G_4 phase shift near $\alpha = 0$ for cut-off radius $R = 1.4$ fm. The dashed line is iterated OPE, the dotted line includes leading order TPE ($\alpha = 2$) perturbatively, and the solid line is the full calculation to order $\alpha = 3$ with TPE treated perturbatively. The shaded band shows variation of the $\alpha = 3$ phase shifts for $0.5 < \alpha < 0.5$. The boxed area is shown enlarged in Figure 5.7.

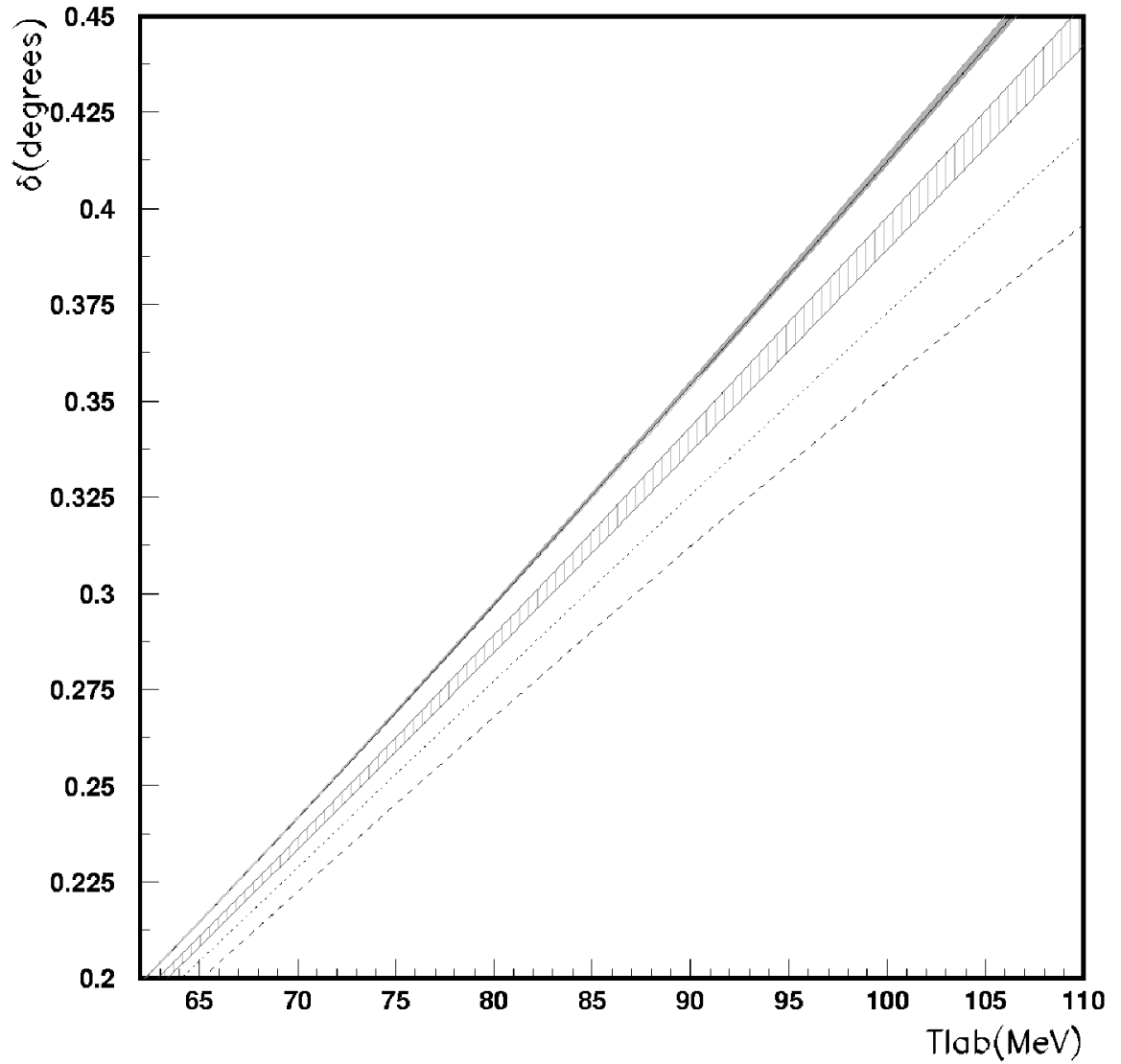


Figure 5.7: An enlarged portion of the 1G_4 phase shifts near $\delta = 0$ for cut-off radius $R = 1.4$ fm. The dashed line is iterated OPE, the dotted line includes leading order TPE ($\ell = 2$) perturbatively, and the solid line is the full calculation to order $\ell = 3$ with TPE treated perturbatively. The shaded band shows variation of the $\ell = 3$ phase shifts for $0.5 < c < 0.5$.

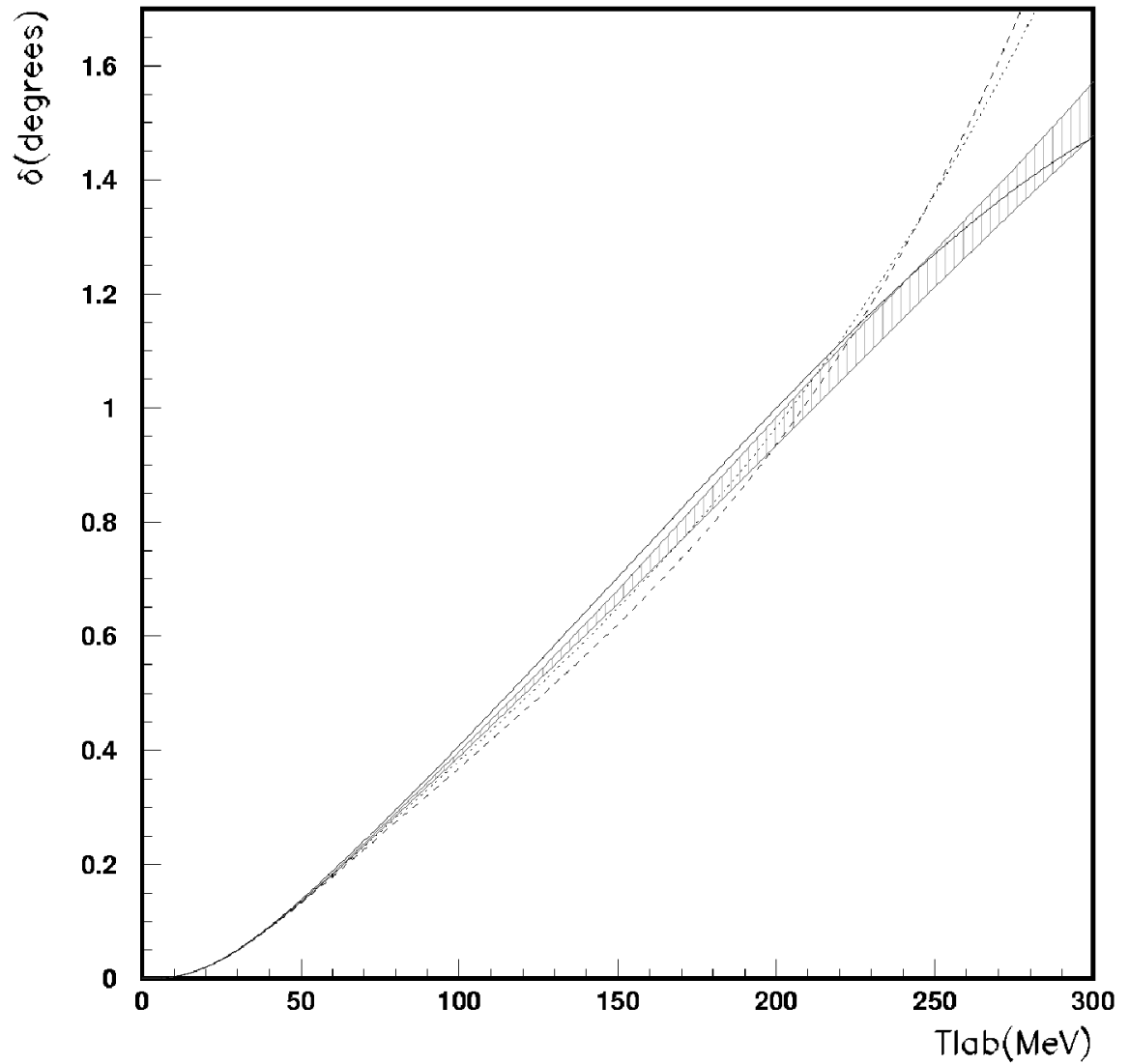


Figure 5.8: 1G_4 phase shifts for adjusted values of α at cut-off radius $R = 1.4$ fm. The dashed curve shows the OPE result for $\alpha = 3.5$, the dotted curve is the leading order TPE (DW BA) result at $\alpha = 2.5$, and the solid line is the full TPE (DW BA) result at $\alpha = 1.5$.

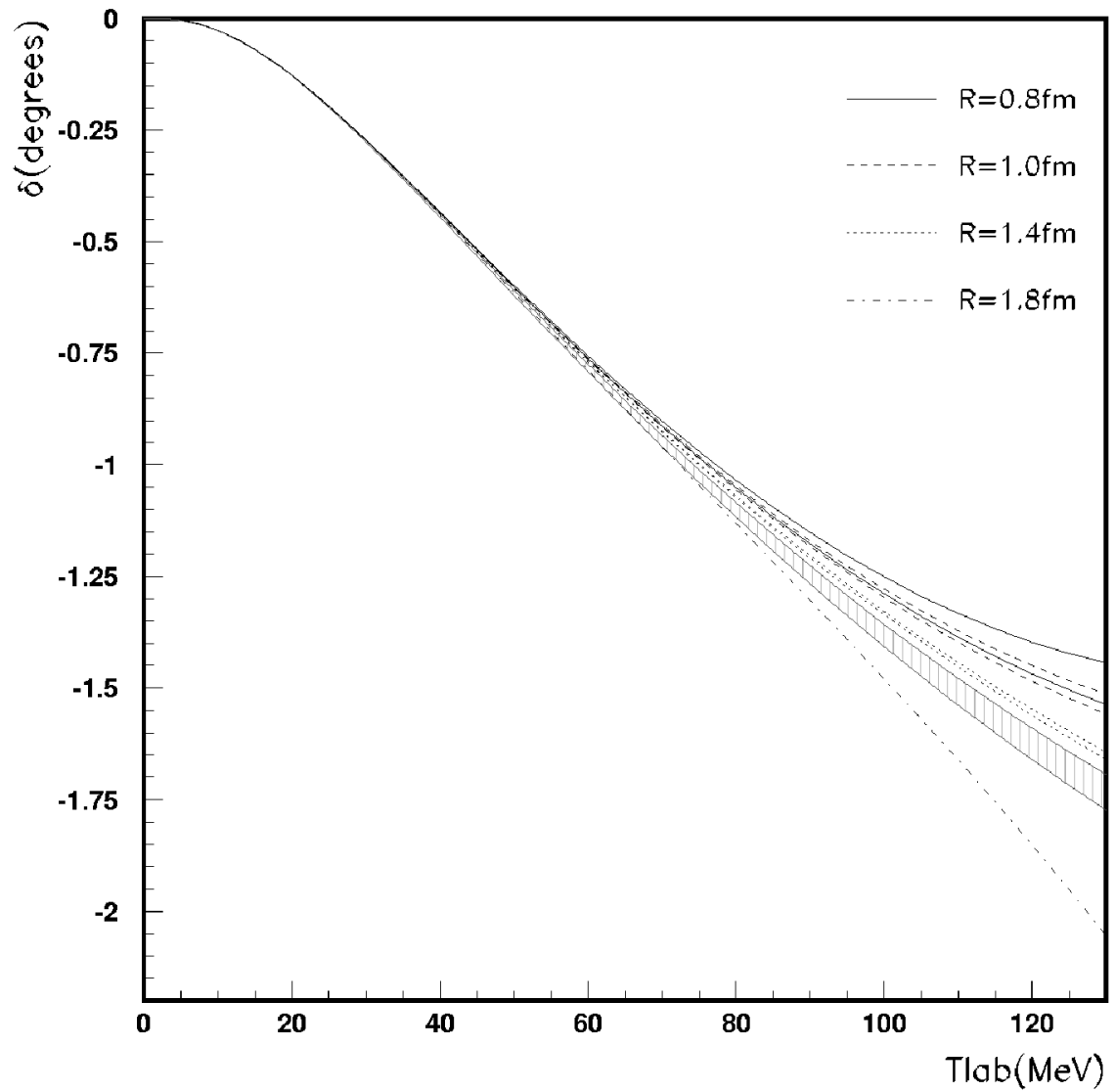


Figure 5.9: 3F_3 phase shift at $\theta = 0$ for four cut-off radii. For each value of R , the result of including full OPE + TPE results perturbatively (DW BA) and non-perturbatively is shown.

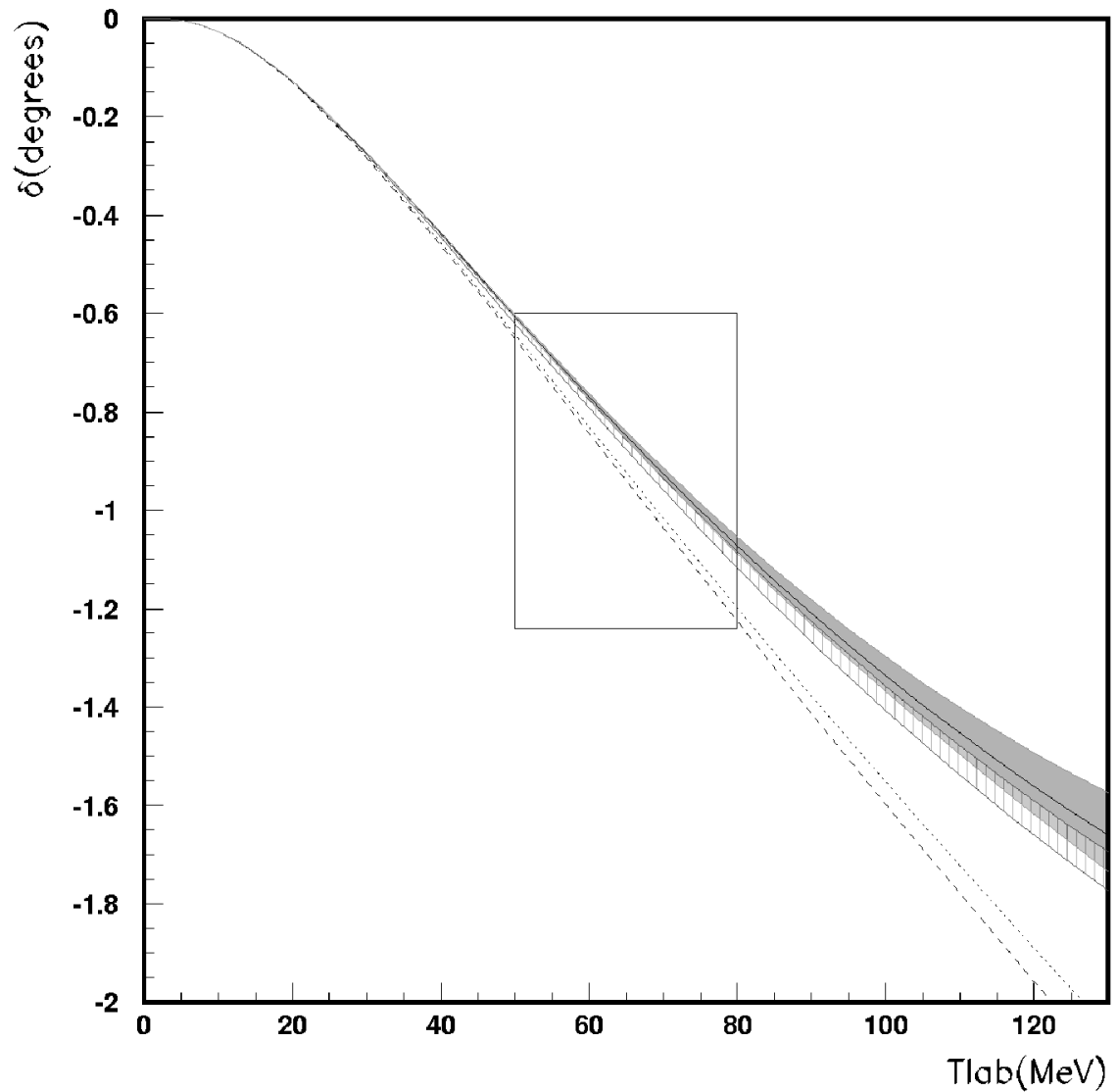


Figure 5.10: 3F_3 phase shifts near $\epsilon = 0$ for cut-off radius $R = 1.4$ fm. The dashed line is iterated OPE, the dotted line includes leading order TPE ($\epsilon = 2$) perturbatively, and the solid line is the full calculation to order $\epsilon = 3$ with TPE treated perturbatively. The shaded band shows variation of the $\epsilon = 3$ phase shifts for $0.5 < \epsilon < 0.5$. The boxed region is shown enlarged in Figure 5.11

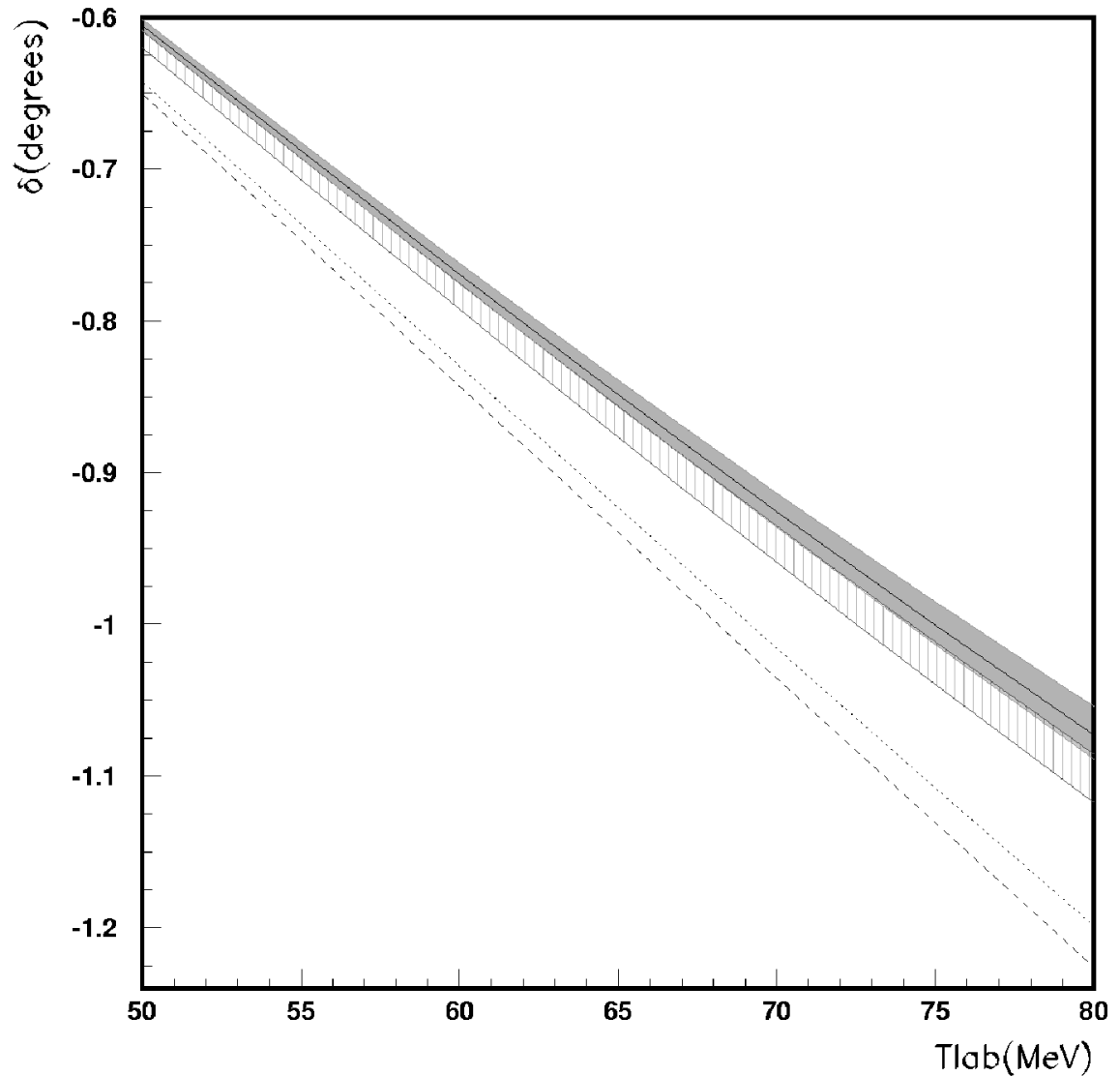


Figure 5.11: An enlarged section of the 3F_3 phase shift near $\eta = 0$ for $R = 1.4$ fm showing the effect of the full TPE calculation in a region where the phase shift is not sensitive to the cut-off or non-perturbative effects. The dashed line is iterated OPE, the dotted line is TPE to order $\eta = 2$ (DW BA), and the shaded band is the full $\eta = 3$ TPE (DW BA) calculation for $0.5 < \eta < 0.5$ with the solid line showing $\eta = 0$. The striped area shows the range of predictions of the three Nijmegen potentials [61] and 1993 partial wave analysis [62].

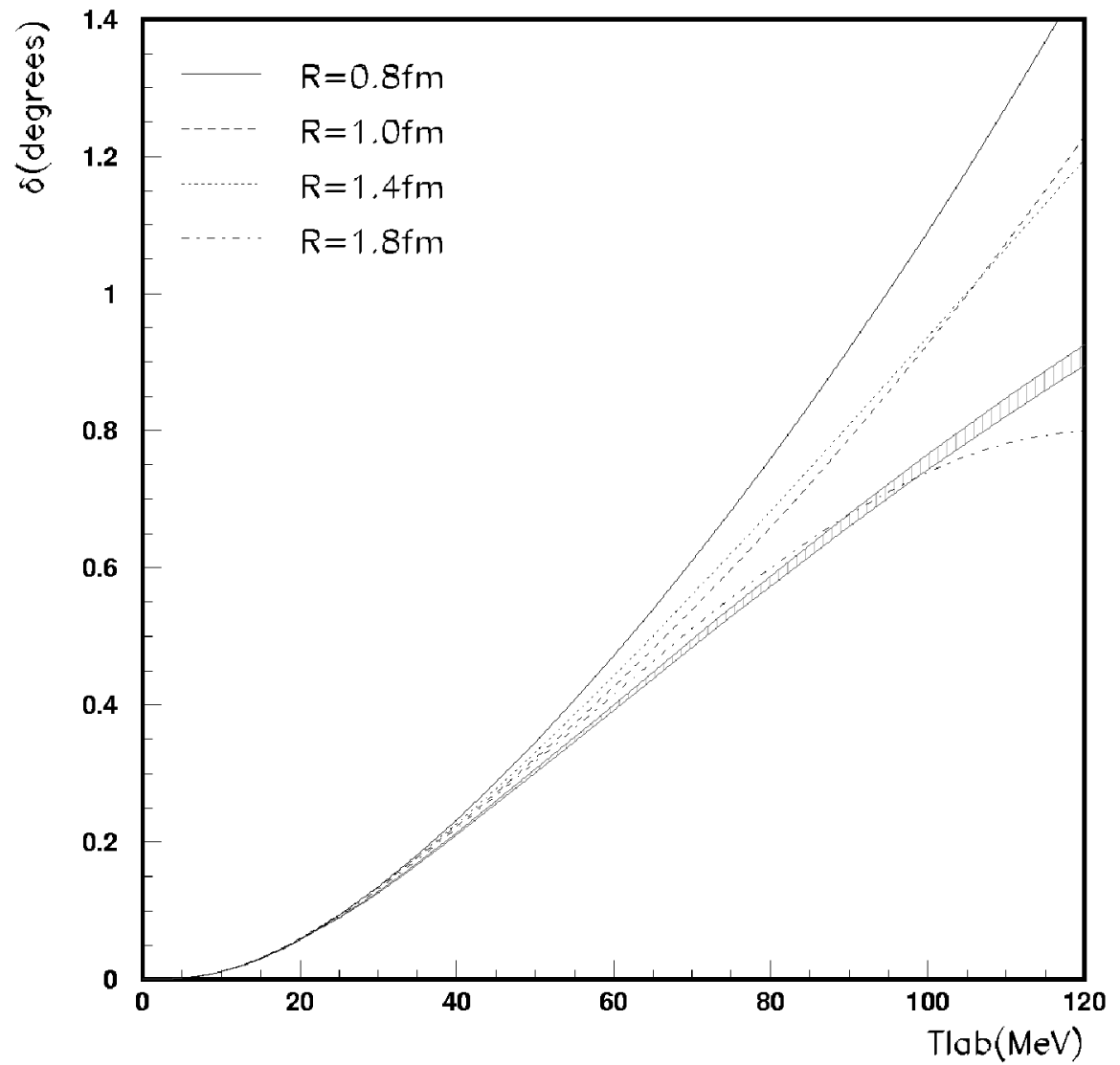


Figure 5.12: The 3F_2 phase shift at $A = 0$ for four cut-off radii. For each value of R , the result of including full OPE + TPE results non-perturbatively is shown.

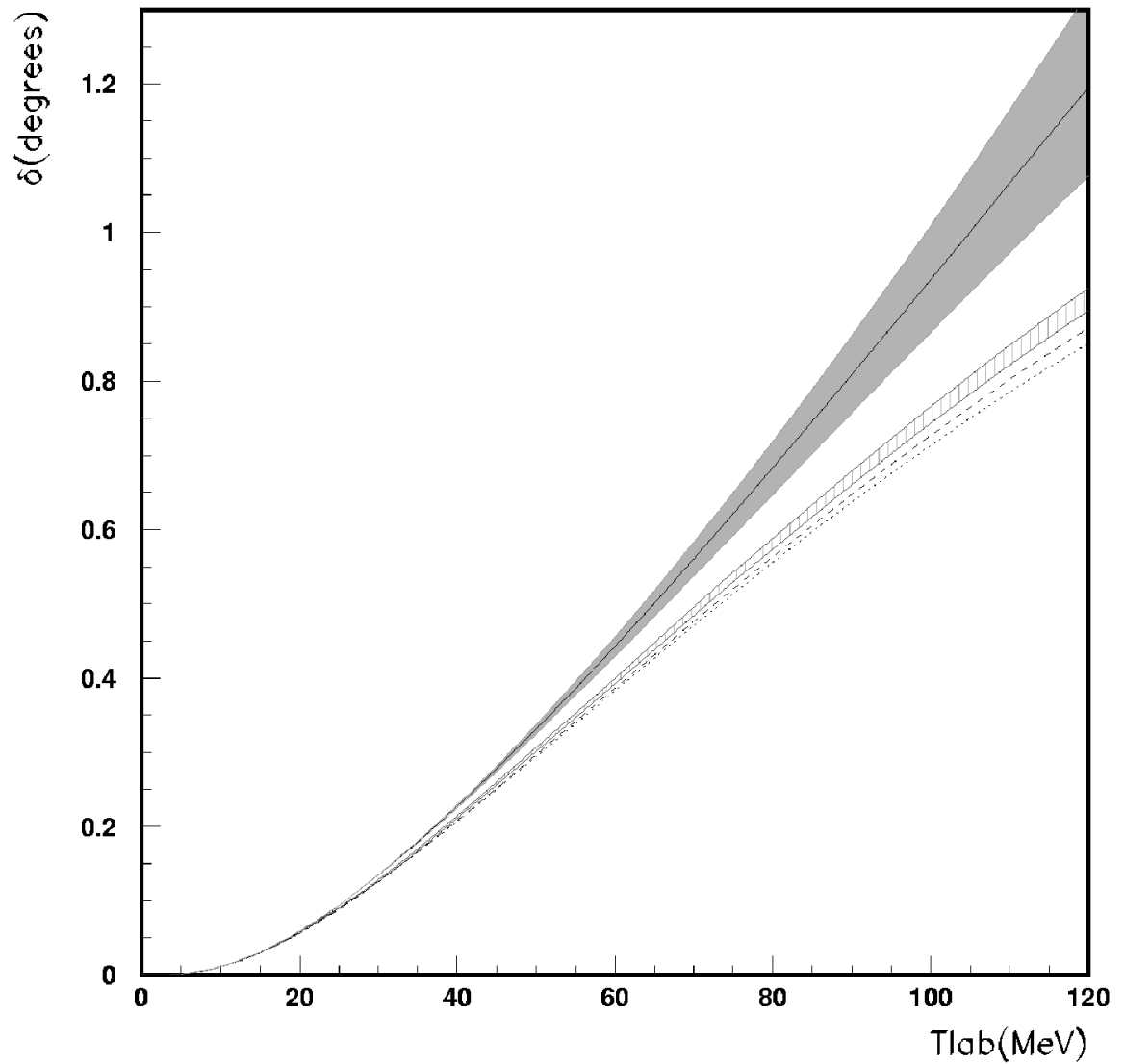


Figure 5.13: 3F_2 phase shifts near $A = 0$ for cut-off radius $R = 1.4$ fm. The dashed line is iterated OPE, the dotted line includes leading order TPE ($\ell = 2$) perturbatively, and the solid line is the full calculation to order $\ell = 3$ with TPE treated perturbatively. The shaded band corresponds to the $\ell = 3$ phase shifts, allowing each of the independent components of A to explore the range $-1/2 < A_{ij} < 1/2$.

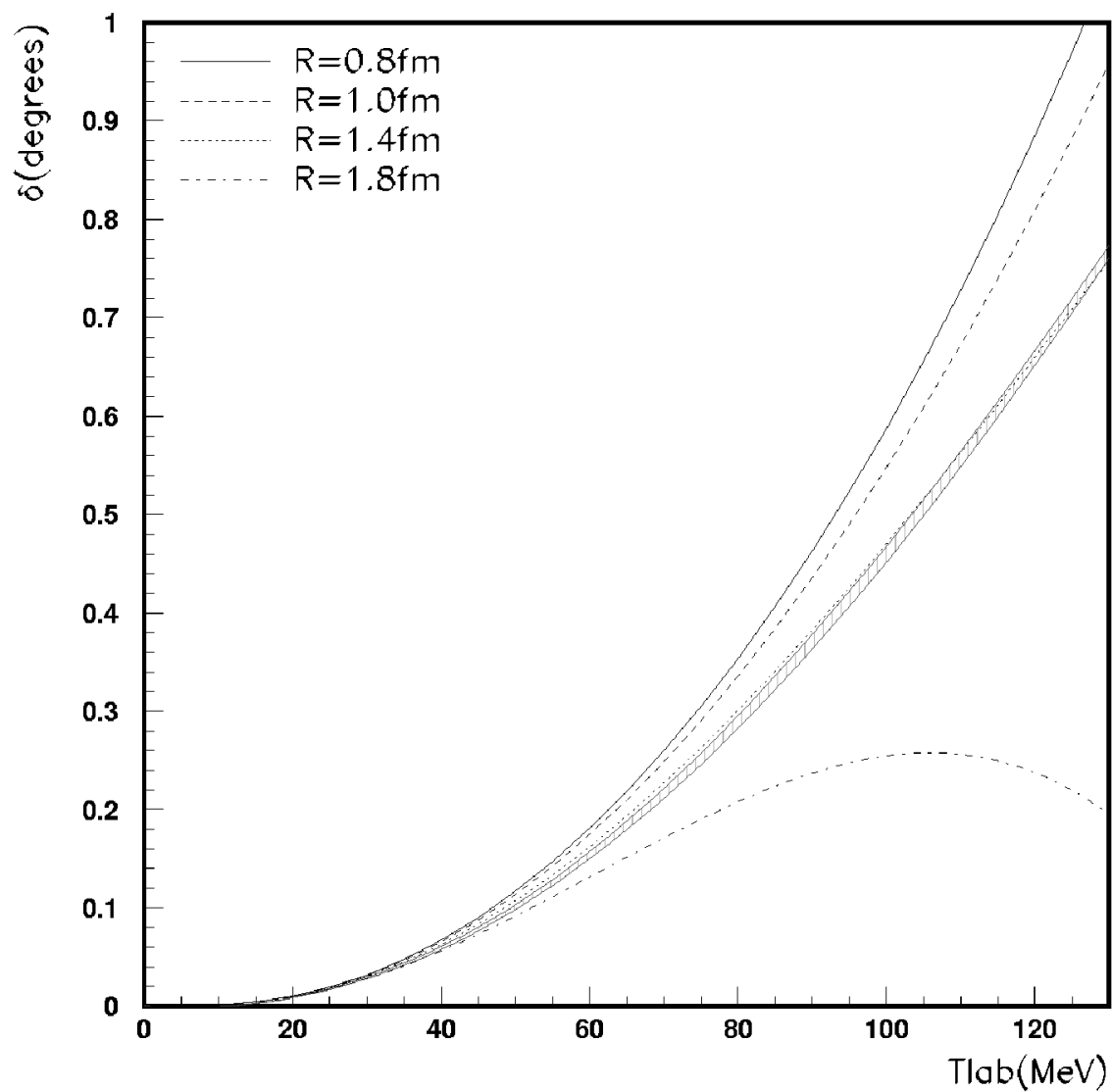


Figure 5.14: 3F_4 phase shift at $A = 0$ for four cut-off radii. For each value of R , the result of including full OPE + TPE results non-perturbatively is shown.

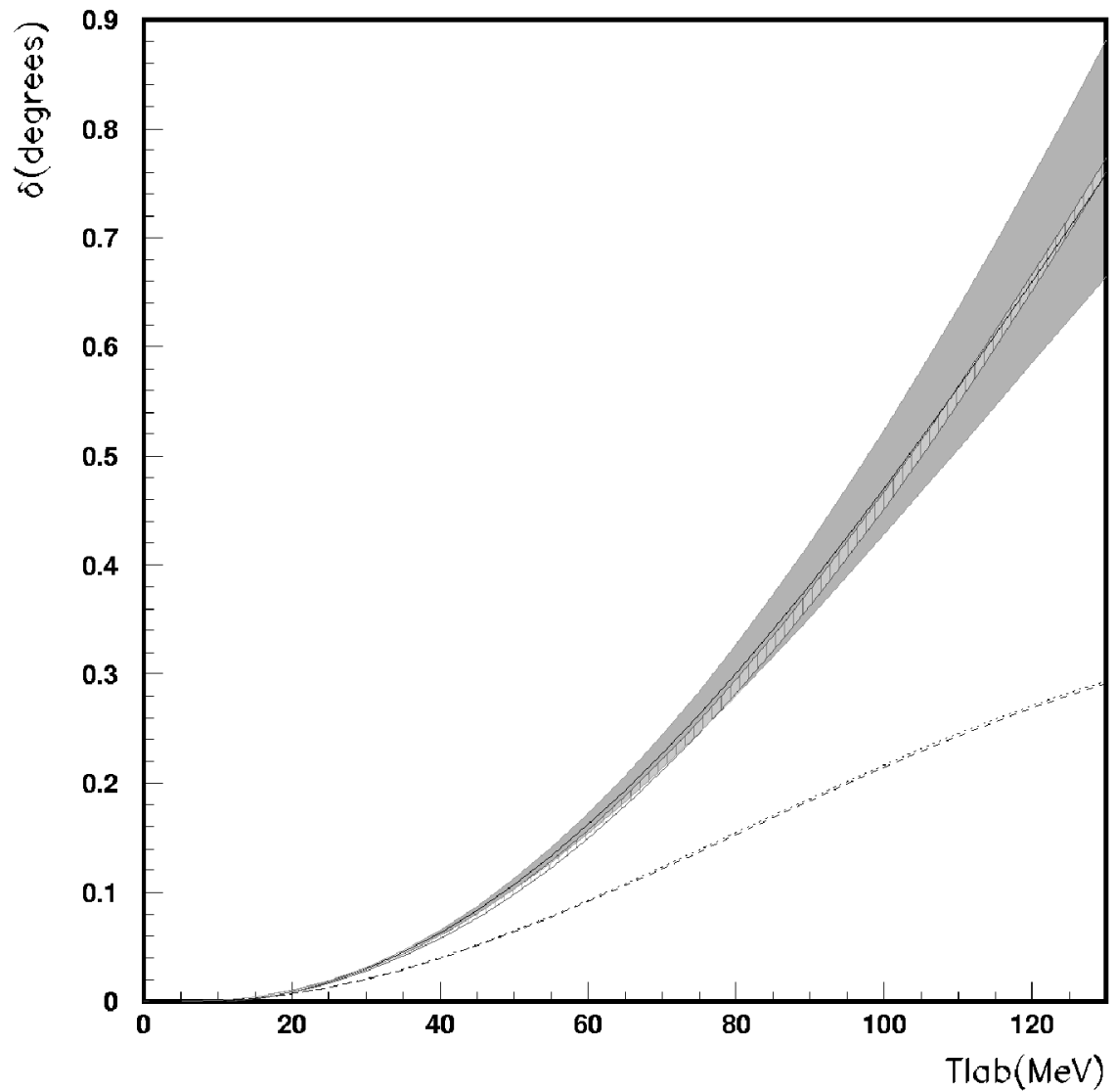


Figure 5.15: 3F_4 phase shifts near $A = 0$ for cut-off radius $R = 1.4$ fm. The dashed line is iterated OPE, the dotted line includes leading order TPE ($\ell = 2$) perturbatively, and the solid line is the full calculation to order $\ell = 3$ with TPE treated perturbatively. The shaded band corresponds to the $\ell = 3$ phase shifts, allowing each of the independent components of A to explore the range $-1/2 < A_{ij} < 1/2$.

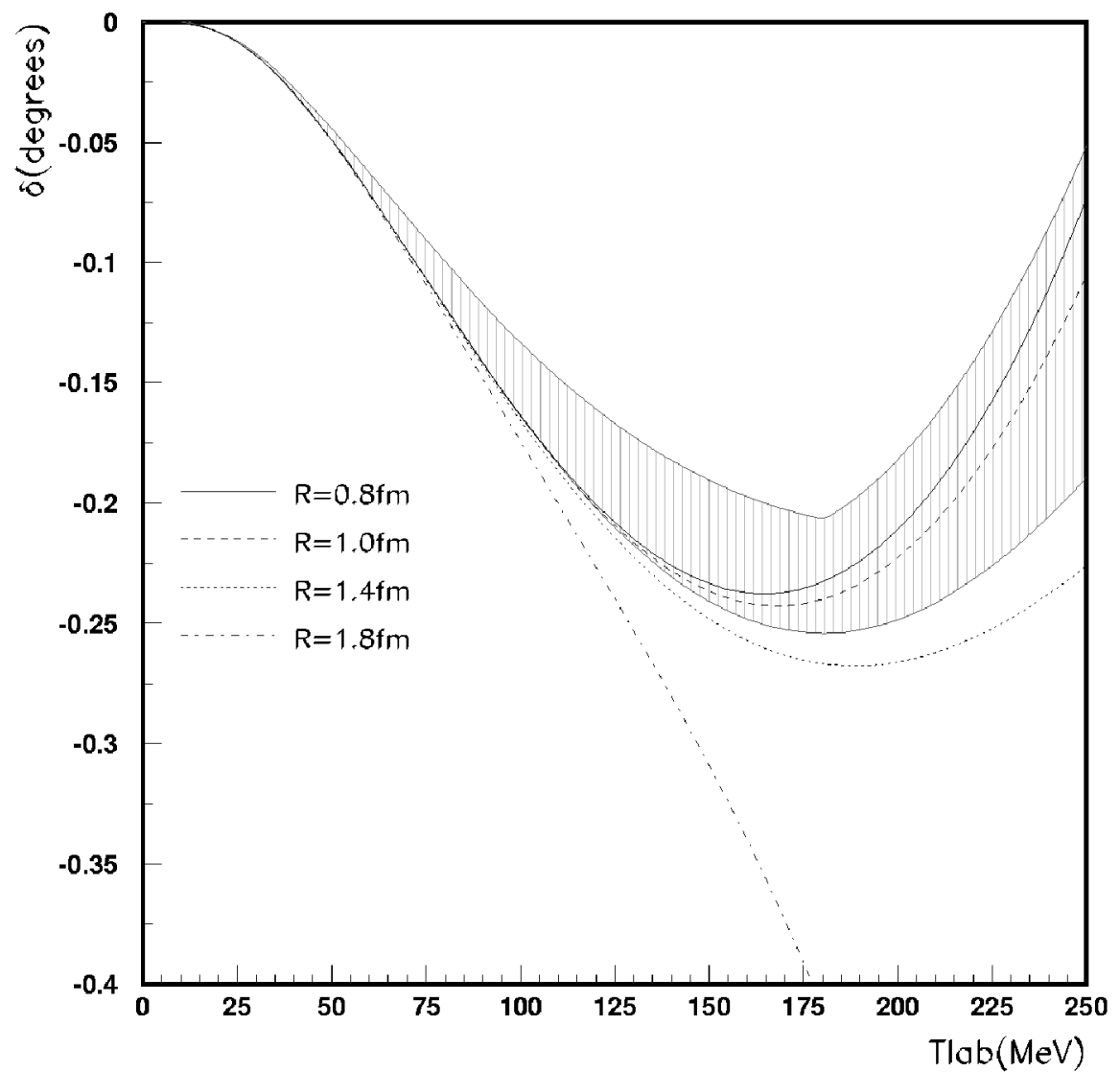


Figure 5.16: The 3G_5 phase shift at $A = 0$ for four cut-off radii. For each value of R , the result of including full OPE + TPE results non-perturbatively is shown.

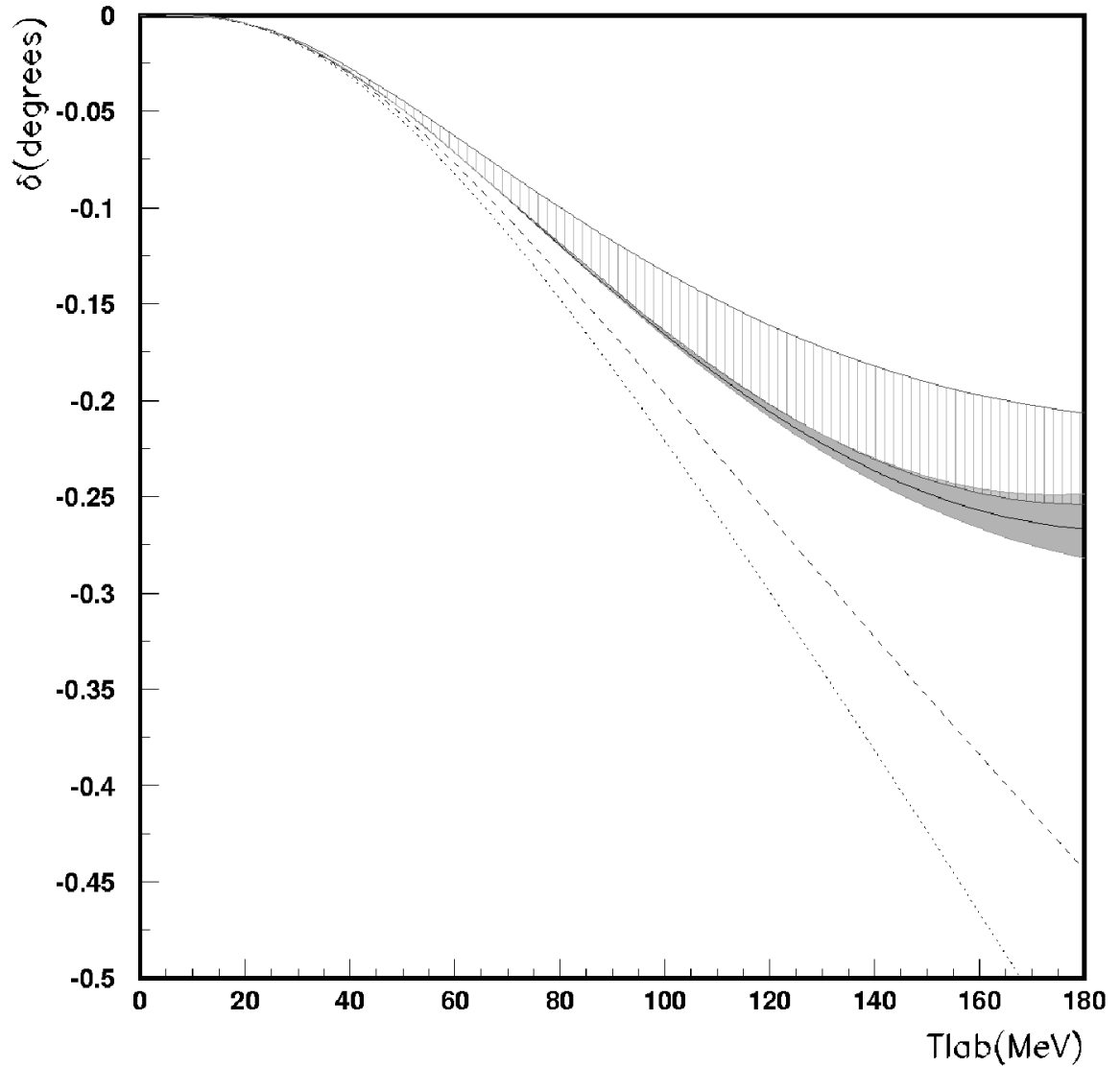


Figure 5.17: 3G_5 phase shifts near $A = 0$ for cut-off radius $R = 1.4$ fm. The dashed line is iterated OPE, the dotted line includes leading order TPE ($\ell = 2$) perturbatively, and the solid line is the full calculation to order $\ell = 3$ with TPE treated perturbatively. The shaded band corresponds to the $\ell = 3$ phase shifts, allowing each of the independent components of A to explore the range $-1=2 < A_{ij} < 1=2$.

Chapter 6

Conclusion

In this thesis, we have considered the application of effective field theory to the Nucleon-Nucleon interaction, with particular emphasis on the constraints imposed by chiral symmetry.

Consideration of the Wilson renormalisation group in a nucleon-only theory, which is valid at very low momenta, led us to identify two very different power counting schemes which are valid in different physical regimes.

A systematic power counting scheme for contributions to the reactance matrix K can be obtained in the case of weak scattering by expanding around the unique trivial RG fixed point. The power counting found here is straightforward, and was originally proposed by Weinberg.

For strong scattering at low energies, a useful expansion of $1=K$ can be obtained by expanding the potential around an unstable non-trivial fixed point corresponding to a bound state of two nucleons at threshold. This expansion can be ordered in such a way that it reproduces the familiar effective range expansion order by order.

The treatment of pions in the case of strong scattering remains problematic. We compared modified effective range expansions obtained by removing pions both perturbatively and non-perturbatively using a distorted wave treatment. In the perturbative treatment, the effective range decreased while non-perturbatively we found an increase of similar magnitude. The disagreement in these results suggests either that long-range physics other than OPE makes important contributions to the effective

range, or that unknown short distance physics with a complicated structure causes very slow convergence of the small momentum expansion.

In partial waves with angular momentum greater than one, coefficients of four-nucleon contact interactions do not contribute to NN scattering. Furthermore, scattering in these partial waves is weak, allowing us to use straightforward power counting corresponding to expansion of the potential around the trivial fixed point.

Iterating the Nucleon-Nucleon potential we obtained from HBCHPT in Chapter 4 produces all contributions to the interaction up to order Λ^{-3} .

We have found several partial waves in which the EFT predictions can be isolated to order Λ^{-3} in a parameter-free way. Of these, the 1F_3 and 3G_5 are isoscalar, and the 1G_4 , 3F_2 , 3F_3 and 3F_4 are isovector. In these phase shifts, there is a range of energies and cut-off radii for which sensitivity to the regularisation procedure and higher order effects generated by iterating the potential are small. Since the above list includes spin singlet and triplet waves, we have tested both the central and tensor parts of the potential.

In the partial waves mentioned above, with the exception of 1G_4 and 3F_2 , the Λ^{-3} potential is an improvement over both OPE and leading order TPE. In the 1G_4 partial wave, adjusting the single number Λ allows a satisfactory global fit to the Nijmegen PWA's up to about 300 MeV. This is not possible for OPE or leading order TPE.

The highest order, Λ^{-3} , contribution tends to be much larger than the leading order, Λ^{-2} , correction, so convergence of the small momentum expansion has not been established. On the other hand, the Λ^{-3} potential is the first in which important contributions, such as the π -like contribution can appear. The calculation to order Λ^{-4} involves no new counterterms for F-waves and above, and may offer a fairer test of convergence.

A trend which seems to emerge from the results is a tendency for the full TPE potential to provide slightly too little attraction in isoscalar partial waves, and too much attraction in isovector partial waves (especially for $R < 1.4$ fm). Isovector contributions which occur at next order may improve this situation. One example is

the two loop graph with a three-pion nucleon vertex from $L_N^{(1)}$ in which the three-pion lines terminate on the other nucleon.

Appendix A

The Nijmegen OPE Potential.

In the Nijmegen PWA's [62, 61] described in Chapter 2, the distinction between neutral-pion and charged-pion exchange is explicitly taken into account. Since we are looking for signals of shorter range physics, it is helpful to use their form of the OPE potential. Defining,

$$V(m) = \frac{m^2}{m} \gamma_1 \gamma_2 + \frac{3 + 3x + x^2}{x^2} S_{12} \frac{e^{-x}}{3x} \quad (\text{A } 1)$$

where $x = m r$, the Nijmegen OPE in the case of neutron-proton scattering may then be written as:

$$V(r) = f^2 V(m_0) \pm 2f^2 V(m_{\pm}); \quad (\text{A } 2)$$

where m_0 and m_{\pm} are the neutral and charged pion masses. The plus sign applies in the case of total isospin $I = 1$, and the minus sign is used when $I = 0$.

References

- [1] R. Machleidt and G. Q. Li, *Phys. Rept.* 242 5 (1994).
- [2] M. C. Birse, *Prog. Part. Nucl. Phys.* 25 1 (1990).
- [3] R. K. Bhaduri *Models of the Nucleon*, (Addison-Wesley, 1988).
- [4] A. Pich, hep-ph/9806303.
- [5] M. C. Birse, *J. Phys. G : Nucl. Part. Phys.* 20, 1537 (1994).
- [6] V. Bernard, N. Kaiser and Ulf-G. Meißner *Int. J. Mod. Phys. E* 4, No.2 193-344 (1995).
- [7] C. Caso et al, *The European Physical Journal C* 3,1 (1998) and 1999 α -year partial update for the 2000 edition available on the PDG WWW pages (URL: <http://pdg.lbl.gov/>).
- [8] M. K. Banerjee, *Prog. Part. Nucl. Phys* 31, 77 (1993).
- [9] S. Weinberg, *The Quantum Theory of Fields*, (Cambridge University Press, 1996).
- [10] J. Goldstone, *Nuovo Cimento* 19, 154 (1961).
- [11] M. Gell-Mann, R. Oakes and B. Renner, *Phys. Rev.* 175, 2195 (1968).
- [12] S. Weinberg *Physica* 96A, 327-340 (1979).
- [13] J. F. Donoghue, E. Golowich and B. R. Holstein, *Dynamics of the Standard Model*, (Cambridge University Press, Cambridge, 1992).

-
- [14] E. Jenkins and A. V. Manohar, *Phys. Lett.* 255, 558 (1991).
- [15] S. Weinberg, *Phys. Lett. B* 251, 288 (1990); S. Weinberg, *Nucl. Phys. B* 363, 3 (1991).
- [16] C. Ordóñez, L. Ray and U. van Kolck *Phys. Rev. C* 53, 2086 (1996).
- [17] S. Weinberg *Phys. Rev. Lett.* 17, (1966).
- [18] T. Ericson and W. Weise, *Pions and Nuclei* (Clarendon Press, Oxford, 1988).
- [19] P. Buttiker and Ulf-G. Meißner, hep-ph/9908247.
- [20] V. Bernard, N. Kaiser and Ulf-G. Meißner *Nucl. Phys. A* 615, 483 (1997).
- [21] V. Bernard, N. Kaiser and Ulf-G. Meißner, *Phys. Rev. C* 52, 2185 (1995).
- [22] S. K. Adhikari and T. Frederico, *Phys. Rev. Lett.* 74, 4572 (1995); S. K. Adhikari and A. Ghosh, *J. Phys. A: Math. Gen.* 30, 6553 (1997).
- [23] D. B. Kaplan, M. J. Savage and M. B. Wise, *Nucl. Phys. B* 478, 629 (1996).
- [24] T. D. Cohen, *Phys. Rev. C* 55, 67 (1997); D. R. Phillips and T. D. Cohen, *Phys. Lett. B* 390, 7 (1997).
- [25] S. R. Beane, T. D. Cohen and D. R. Phillips, *Nucl. Phys. A* 632, 445 (1998).
- [26] G. P. Lepage, nucl-th/9706029.
- [27] K. G. Richardson, M. C. Birse and J. A. McGovern, hep-ph/9708435.
- [28] P. F. Bedaque and U. van Kolck, *Phys. Lett. B* 428, 221 (1998); P. F. Bedaque, H. W. Hammer and U. van Kolck, *Phys. Rev. C* 58, R641 (1998).
- [29] T.-S. Park, K. Kubodera, D.-P. Min and M. Rho, *Phys. Rev. C* 58, 637 (1998).
- [30] D. B. Kaplan, M. J. Savage, and M. B. Wise, *Phys. Lett. B* 424, 390 (1998); *Nucl. Phys. B* 534, 329 (1998); *Phys. Rev. C* 59, 617 (1999).
- [31] J. Gegelia, nucl-th/9802038; *J. Phys. G: Nucl. Part. Phys.* 25, 1 (1999).
-

- [32] U. van Kolck, Talk given at the Joint Caltech/INT Workshop on Nuclear Physics with Effective Field Theory, KRL preprint MAP-228 (1998); U. van Kolck, Nucl. Phys. B 645, 273 (1999).
- [33] T. D. Cohen and J. M. Hansen, Phys. Rev. Lett. 440, 233 (1998).
- [34] D. R. Phillips, nucl-th/9804040.
- [35] M. C. Birse, nucl-th/9804028.
- [36] K. G. Wilson and J. G. Kogut, Phys. Rep. 12, 75 (1974); J. Polchinski, Nucl. Phys. B 231, 269 (1984); R. D. Ball and R. S. Thorne, Ann. Phys. 236, 117 (1994); T. R. Morris, Prog. Theor. Phys. Suppl. 131 395 (1998).
- [37] M. C. Birse, J. A. McGovern and K. G. Richardson, hep-ph/9807302.
- [38] D. R. Phillips, S. R. Beane and M. C. Birse, J. Phys. A 32 3397 (1999).
- [39] J. M. Blatt and J. D. Jackson, Phys. Rev. 76, 18 (1949); H. A. Bethe, Phys. Rev. 76, 38 (1949).
- [40] H. A. Bethe and C. Longmire, Phys. Rev. 77, 647 (1950).
- [41] M. Lacombe, B. Loiseau, J. M. Richard, R. Vinh Mau, J. Cote, P. Pires and R. de Tournell, Phys. Rev. C 21, 861 (1980)
- [42] G. E. Brown and A. D. Jackson, The Nucleon-Nucleon Interaction (North-Holland, Amsterdam 1976).
- [43] N. Kaiser, R. Brockmann and W. Weise, Nucl. Phys. B 624, 527 (1997).
- [44] E. L. Lomon and H. Feshbach, Ann. Phys. 48, 94-172 (1968).
- [45] R. G. Newton, Scattering Theory of Waves and Particles, (Springer-Verlag, New York, 1982).
- [46] E. Epelbaum, Ulf-G. Meiner, nucl-th/9903046.
- [47] E. Epelbaum, W. Glockle, Ulf-G. Meiner Nucl. Phys. A 637, 107 (1998).

-
- [48] M. Taketani, S. Machida and S. Ohnuma, *Prog. Theor. Phys. (Kyoto)* 7, 45 (1952).
- [49] K. A. Brueckner and K. M. Watson, *Phys. Rev.* 92, 1023 (1953).
- [50] S. A. Coon and J. L. Friar, *Phys. Rev. C* 34, 1060 (1986).
- [51] J. L. Friar and S. A. Coon, *Phys. Rev. C* 49, 1272 (1994).
- [52] J. L. Friar, *nucl-th/9901082*.
- [53] M. C. M. Rentmeester, R. G. E. Timmermans, J. L. Friar, J. J. de Swart, *nucl-th/9901054*.
- [54] J. V. Steele and R. J. Furnstahl, *Nucl. Phys. B* 645, 439 (1999).
- [55] D. B. Kaplan and J. V. Steele, *nucl-th/9905027*.
- [56] H. van Haeringen and L. P. Kok, *Phys. Rev. A* 26, 1218 (1982).
- [57] R. A. Amdt, J. S. Hyslop and L. D. Roper *Phys. Rev. D* 35, 121 (1987).
- [58] <http://NN-Online.scikun.nl/>.
- [59] N. Kaiser, S. Gerstendorfer and W. Weise, *Nucl. Phys. B* 637, 395 (1998).
- [60] Ulf-G. Meiner, *nucl-th/9909011*.
- [61] V. G. J. Stoks, R. A. M. Klomp, C. P. F. Terheggen and J. J. de Swart, *Phys. Rev. C* 49, 2950 (1994).
- [62] V. G. J. Stoks, R. A. M. Klomp, M. C. M. Rentmeester and J. J. de Swart, *Phys. Rev. C* 48, 792 (1993).
- [63] R. V. Reid, Jr., *Ann Phys. (NY)* 50, 411 (1968).
- [64] M. M. Nagels, T. A. Rijken and J. J. de Swart, *Phys. Rev. D* 17, 768 (1978).
-